Author's response

Dear Editor,
Prof. Urs Baltensperger,

Thank you and thank to the staff of ACP for the deadline extension given to our final revision paper. We are glad to notice that both referees appreciated the experimental efforts and the potential high relevance of the results presented in our paper.
Furthermore, both referees focused their attention on several issues, asking for elucidation of a number of technical points, which we are glad to focus on in the following responses to the referees. All the raised criticisms and relative answers have been addressed in the revised manuscript. Accordingly to the referees' concerns, a list (not exhaustive) of the most important changes made to the manuscript is the following:

- the paper was substantially changed and improved to make it more readable and easier to follow. We rearranged the sections to improve readability,
- the method section was improved both simplifying the heating rate measurements methodology (moving the demonstration of the radiative transfer concepts to the supplemental material) and clarifying the cloud classification algorithm; the non-core part of "average photon energy" was also moved to the supplemental material,
- a thorough validation of cloud classification was carried out and described at length in Appendix B,
- we fully re-organized the Results and discussion section following the referees' suggestions in order to improve the full manuscript and to clarify the logic behind the results presentation,
- Figures were improved accordingly to referees' comments and to make the data presentation more effective,
- a comprehensive list of acronyms was added in Appendix A

Finally, the whole text was proofread and edited to emendate the typos and to improve the language. We are pleased that this discussion based on the constructive criticisms of both referees has helped us to improve the scientific quality of the work done. A tracked version of the manuscript changes is present at the bottom of the answers.

With our best regards,

Yours sincerely,

Dr. Luca Ferrero

<u>Response to Reviewer#1</u>

We thank the reviewer for his or her helpful comments and insight. They allowed us to improve the scientific quality and presentation of the work done. We respond to the general and to the specific points below. All the comments are addressed in the revised manuscript. A tracked version of the manuscript changes is present at the bottom of the answers.

GENERAL COMMENTS

<u>General Comment 1 (C1P1)</u>: The manuscript by Ferrero et al. acp-2020-264 titled "The impact of cloudiness and cloud type on the atmospheric heating rate of black and brown carbon" presents heating rate measurements of the atmosphere over the Po Valley, Italy.
The measurements are valuable as they are relatively rare in the community. The work is incremental on Ferrero et al. 2018, with the main incremental improvement being the automated separation of clouds into cloud types using radiometer measurements combined with Lidar-Ceilometer measurements. The introduction of lidar information into the automated cloud classification is novel and may be valuable to other work, yet was not thoroughly validated. I recommend that the authors describe this cloud classification algorithm in detail in a separate paper and include more detailed validation work. If the authors do not follow this recommendation, they must provide a clear argument for why in the review responses and in the manuscript.

<u>Answer to General Comment 1 (C1P1):</u> We thank the reviewer for the comment on the experimental results, their relevance and implications reported in this work. Indeed, as underlined in the review, the present work represents an important incremental step of Ferrero et al. (2018).
We carefully considered the suggestion to split the paper in two. However, the cloud classification is only one of the incremental improvements. The main goal of our study is to experimentally unravel the relative and synergic role of cloudiness and of different cloud types on the heating rate (HR) of light absorbing aerosol (LAA) in general and that of BC and BrC in particular. As we state at the end of the introduction (revised version of the manuscript) we aim to:

1. describe the interaction between cloudiness and light-absorbing aerosol, to aerosol HR as a function of cloudiness, and in turn to estimate the systematic bias introduced by incorrectly assuming clear-sky conditions in radiative transfer models;
2. introduce an original cloud type classification to investigate the impact of both cloudiness and cloud types on the total HR;
3. separate the contributions of BC and BrC carbonaceous fractions to HR and investigate their relative impact on the total HR as a function of sky conditions.

The results we present in this study add an important piece of information to the influence of the two most important LAA species (i.e. BC and BrC) in different sky conditions. Therefore, the manuscript was planned from the beginning as a whole, with the main focus on the environmental influence of LAA on the climate.
Immediately after our submission (20 Mar 2020), Ylivinkka et al. submitted to Atmospheric Measurement Technique (03 Apr 2020) a paper titled “Clouds over Hyytiälä, Finland: an algorithm to classify clouds based on solar radiation and cloud base height measurements”(

https://doi.org/10.5194/amt-13-5595-2020) which was accepted and published (22 Oct 2020). The paper discusses a cloud classification technique very similar to ours. This is a clear coincidence of an interesting scientific development.

Taking into account the reasons above, due to the fact that the concerns were mostly related to one section (2.3.2, cloud classification section), and due to Reviewer#2, asking for a technical simplification of the paper, we have decided (previously asking the opinion of the handling editor) to not split the paper into two, but rather to improve the present manuscript. We have rewritten large part of the manuscript main body, and moved material to the Appendix and the now modified Supplemental material. We have additionally taken into account the publication of Ylivinkka et al. (2020) and included this and other references related to the lidar-ceilometer capabilities at detecting cloud base and cloud classification. To answer this reviewer comment, a validation of the classification scheme was carried out in in two steps.

The first validation step was carried out comparing the automatized cloud classification (based on Duchon and O'Malley, 1999, and additionally lidar cloud base height) with a visual cloud classification based on sky images collected during 1 month of the field campaign. The second validation step involved the recent published method discussed by Ylivinkka et al. (2020). Their method is based on the same logical approach followed in our work: the application of Duchon and O'Malley (1999) classification improved by the knowledge of the cloud base height. The aim of the second step was to determine the degree of consistency between the two approaches which were developed simultaneously and independently in two completely different European regions.

The complete validation is reported in Appendix B ("Cloud type validation"). This was performed not to interrupt the flow of the manuscript, as requested in the Specific Comment 25 (C6P1-C7P1). The overall balanced accuracy was 80% for the visual validation and 90% for the intercomparison with Ylivinkka et al. (2020) (please see answer to your specific question 23, C6P1, for further details). This shows the reliability of the classification algorithm, allowing us to study the impact of clouds on LAA HR with a sufficient degree of certainty.

General comment 2 (C2P1). The actual presentation of the results in this manuscript is incredibly poor. Here I present 200 lines of comments which I had to make simply in order to understand the results. The discussion is long, dense, and disorganized. Most of these comments are on presentation and organization, at the level which is normally given to an author's first draft of a first manuscript. After I finally understood what was done and what the results were, I see a valuable data set. However, the scientific interpretation is on a similar level to the writing.

I fear that my scientific feedback has been drowned by the poor writing, manuscript organization, and figure presentation in this work. To emphasize my main scientific comments I have used boldface text in the following. The authors should streamline their manuscript by referring to Ferrero et al. 2018 whenever possible, by separating their cloud analysis from their light-absorbing aerosol analysis, and by clearly demonstrating whether or not there is any value to the different levels of information available here. Those levels are: 1) heating rate resolved in time, 2) heating rate resolved by time and cloud height, 3) heating rate resolved by time, cloud height, and cloud type.

My recommendation to the authors is to completely rewrite this manuscript and reinterpret the results. Since this work is incremental to earlier, well-presented work (Ferrero et al., 2018), and

since the results are well supported if poorly presented and interpreted, I do not recommend rejection but major revisions to the Editor.
(NB: I have not numbered my feedback below. When the authors respond, please refer to my comments as "C1P2" for page C1, paragraph 2, etc. Please also copy and paste the comment before responding.)

Answer to General Comment 2 (C2P1)*:* We have considerably rewritten the manuscript as suggested in the comment.
We started with the suggestion "to separate the cloud analysis from the light-absorbing aerosol analysis". As reported in the answer to General Comment 1, we cannot split the manuscript in two manuscripts, as a similar cloud classification scheme was just published. The strength and the innovation of the present paper is the synergy between the automatic classification of cloudiness and quantifying the effect of the light-absorbing aerosols on the climate. Thus, we fully re-organized the Results and discussion section following the suggestion in order to improve the full manuscript, to clarify the logic behind the methodology, and to more specifically discuss the different aspects (levels) of the results. Now, following the suggestion on the three different levels of information, the Results and discussion section features the following arrangement of the subsections:

- Section 3.1 introduces the environmental context of the measurement campaign and the magnitude of the observed parameters (eBC, irradiance, HR and cloud data). We have incorporated here the suggestion "to separate the cloud analysis from the light-absorbing aerosol analysis". All cloud analysis is presented here. The validation of the cloud classification was moved to the Appendix B.
- Old sections 3.2 and 3.3 were re-written in line with the changes performed in section 3.1 and merged in a new section 3.2 with three sub-sections. The first discusses the influence of clouds in term of cloudiness, the second the influence of cloudiness on the diurnal pattern of the HR while the third the cloud type effect on the total HR only (sections 3.2.1, 3.2.2 and 3.2.3, respectively).
- The old section 3.4 (now section 3.3) was completely re-written merging and shortening the two original sub-sections 3.4.1 and 3.4.2. We discuss the role of cloudiness, cloud type and their effect on the HR apportioned with respect to BC and BrC fractions. The discussion concerning the role of average photon energy was moved to the supplemental material.

This gradual approach streamlines the manuscript, making it easier to read. We improved the Results and Discussions outline at the beginning of section 3 describing this approach. Moreover, all the manuscript was revised simplifying all the sections and making them more concise and easier to follow. We did not use the acronyms for the concepts which did not appear too often and also added an Appendix explaining all the remaining acronyms and symbols present in the paper.
To address the suggestions about the data analysis and the most relevant results, we moved the Figure S5 (time resolved heating rate) to the main body of the manuscript (now Figure 5 in the manuscript; here below as Figure A1) adding a proper description. We first improved the new Figure 5 adding both the cloudiness (expressed in oktas) and the cloud base height. The same was also done for Figure S6 (now Figure S4).
Then we focused on the reviewer's suggestions concerning the relationship between 1) the heating rate and cloud height and 2) the heating rate, cloud height and cloud type. This helped us to enrich the explanation of the interaction between the clouds and light-absorbing aerosols. We prepared Figures A2a-c, A3 and A4a-d which are discussed here below.

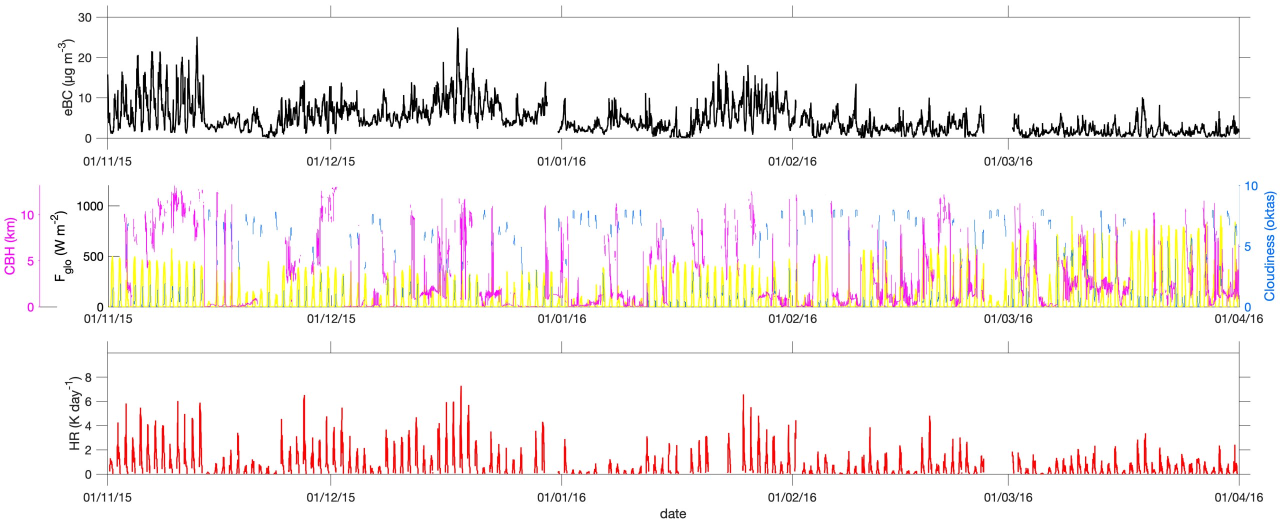

Figure A1 (Figure 5 in the revised version of the paper). High time resolution data (5-min) for eBC, global irradiance ($Fglo$), cloud base height (CBH), coldness (oktas), and the related heating rate (HR) from 1 November 2015 to 1 April 2016.

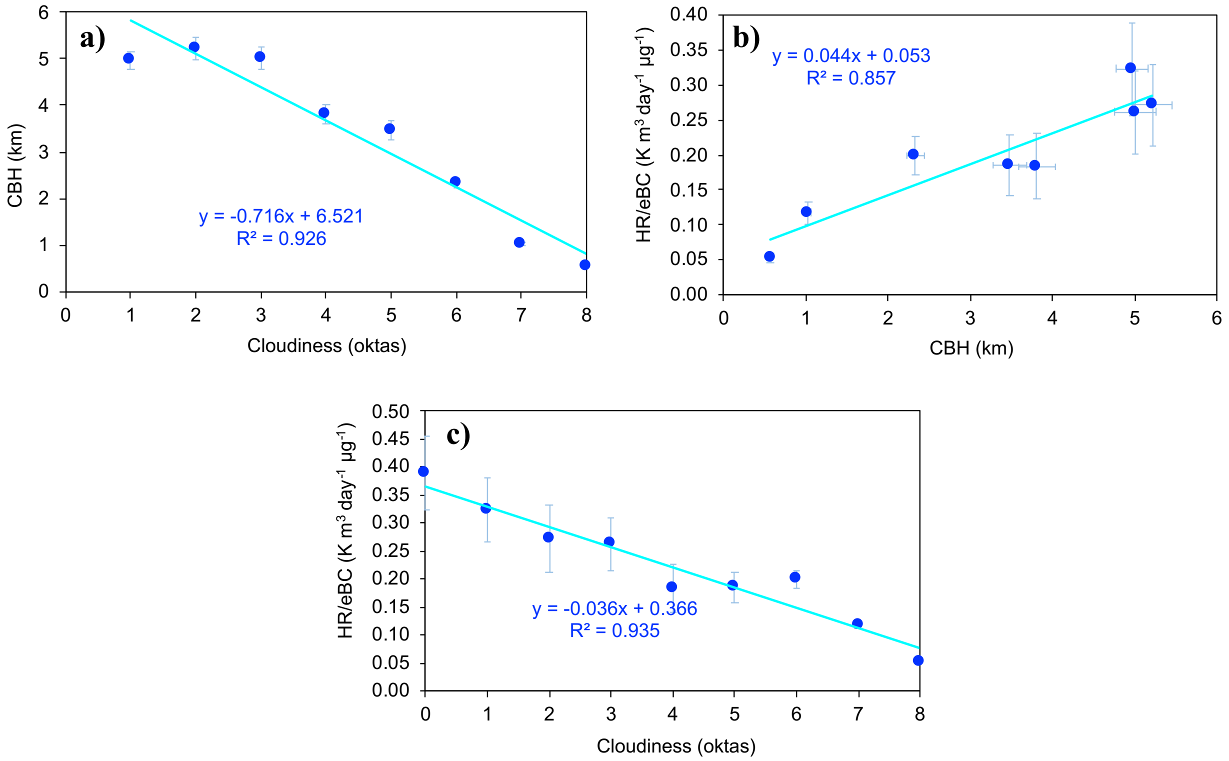

Figure A2. Relationship between a) cloud base height (CBH) and cloudiness (oktas), b) HR/eBC and CBH and c) HR/eBC and cloudiness (oktas).

Figure A2a shows a clear relationship between the cloud base height (averaged for each okta) and cloudiness. This is not surprising, considering the contribution of each cloud type to the cloudiness reported in the manuscript (section 3.3, page 12, lines 440-445): “the contribution (expressed in oktas) of the cloud type is reported in Figure 7b. This clearly shows that, while Stratus clouds were mostly responsible of overcast situations (oktas=7-8, frequency: 87 and 96%), Stratocumulus clouds dominated the intermediate cloudiness conditions (oktas=5-6, frequency: 47 and 66%); moderate cloudiness (oktas=3-4) were mostly due to a transition from Cirrocumulus and Cirrostratus to Stratocumulus while low cloudiness (oktas=1-2) were mostly dominated by Cirrus and Cumulus (frequency: 59 and 40%, respectively)."

In section 2.3.2 and Figure 4 we reported that low level clouds (<2 km) include Stratus (St), Cumulus (Cu) and Stratocumulus (Sc), mid-altitude clouds (2-7 km) include Altostratus (As), and Altocumulus (Ac) and high-altitude clouds (>7 km) include Cirrus (Ci), Cirrocumulus and Cirrostratus (Cc-Cs). Combining these cloud altitudes with the overcast situation statistics above, it appears that the higher cloudiness (higher oktas) was due to a higher frequency in low-mid altitude clouds. We described this point better in the manuscript text (section 3.1): we included the whole Figure A2 to the Supplemental material and modified Figure 7b by adding the average cloud base height for each okta (below as Figure A3). Moreover, as cloud base height was related with cloudiness, a good linear relationship can be derived between the HR/eBC and cloud base height (Figure A2b; R^2=0.857), but this relationship is weaker than that between HR/eBC and cloudiness (Figure A2c; R^2=0.935). The cloudiness, describing the fraction of sky covered by clouds, is a better predictor of the capability to suppress the incoming radiation and thus lower the HR of BC and BrC, because the relationship between cloudiness and cloud base height – shown on Figure A2a, is weaker at higher cloud base heights. Addressing also the specific question 33(C8P1), we can add that the relationship shown in Figure A2a between cloud base height and cloudiness should be also investigated in other monitoring sites around the world to see whether the cloud base height can be used as a promising prognostic variable for the HR of light absorbing aerosols (see also answer to specific comment 33).

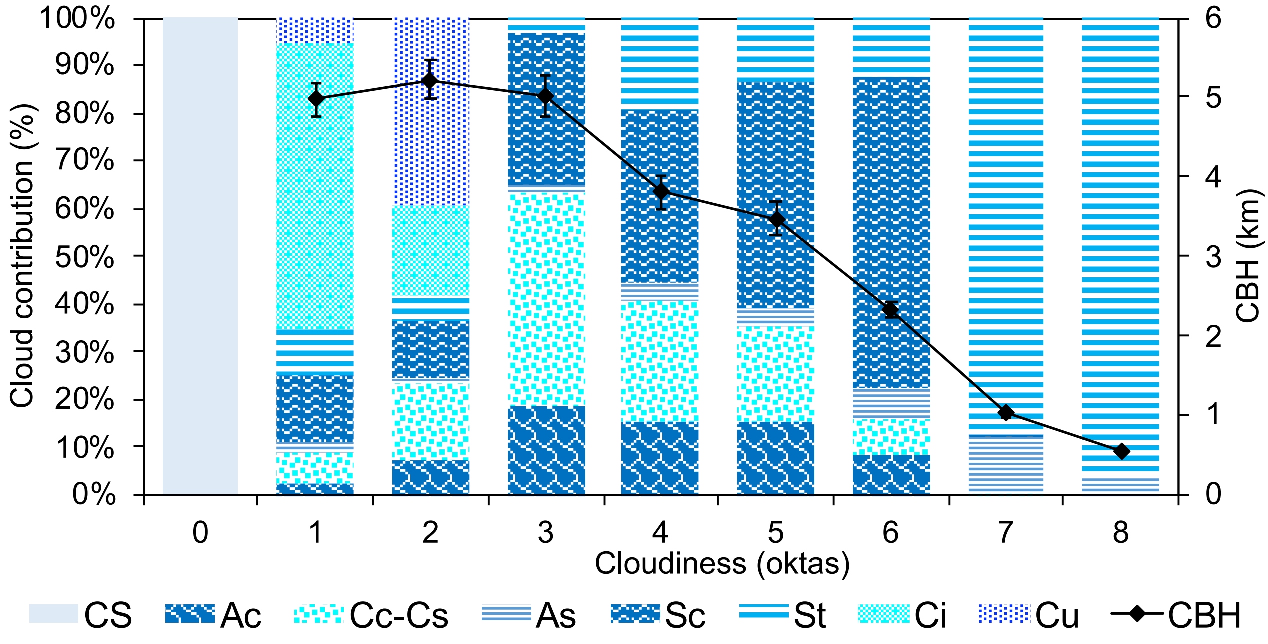

Figure A3 (Figure 7b, revised). Contribution (%) of each cloud type to the oktas measured over the U9 site, and averaged (±95% confidence interval) cloud base height (CBH) for each okta. CS=clear sky,; Ac=AltoCumulus; Cc-Cst=CirroCumulus-CirroStratus; As=AltoStratus; Sc=StratoCumulus; St=Stratus; Ci=Cirrus; Cu=Cumulus.

Figure A4 (heating rate, cloud height and cloud type) shows the absence of any relationship between HR/eBC (and each of its components) under different cloud types and the cloud base height (averaged in this case for each cloud type). This is reasonable, since, as reported in the manuscript (section 2.3.3, Figures 3 and 4), the cloud base height is a prognostic variable needed for the cloud classification and does not account for the amount of clouds present in the sky. We stress again that in Figure A4 the cloud base height is averaged for each cloud type thus reflecting mostly a property of the different cloud types above the measuring site.

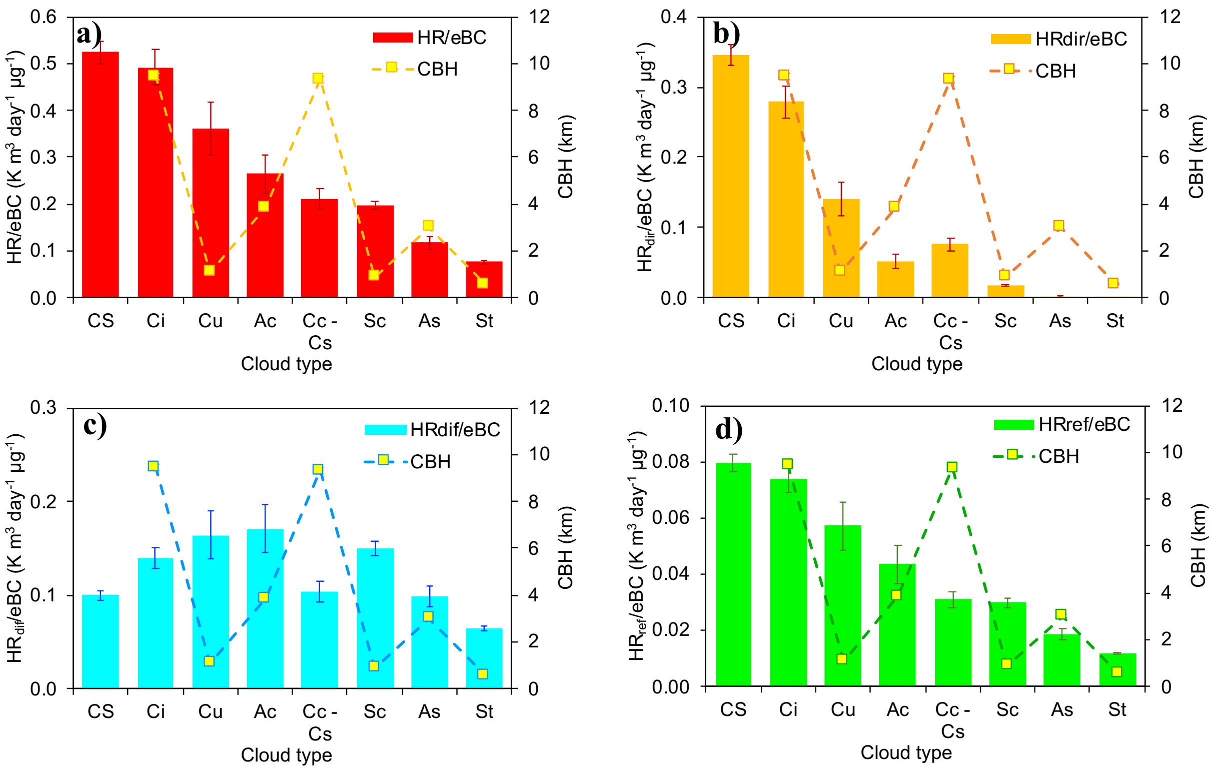

Figure A4. Impact of each cloud type on: HR/eBC (a), HR_{dir}/eBC (b), HR_{dif}/eBC (c), HR_{ref}/eBC. The cloud base height (CBH) is reported in each panel. CBH is not present in clear sky conditions (CS).

<u>General comment 3 (C3P1)</u>. The Introduction provides a strong motivation for the importance of HR and cloudiness, but the final 2 paragraphs are poorly structured. Please emphasize more the importance of cloudiness, including common levels to be expected (i.e. expand the discussion around Crock et al.) and feedbacks (i.e. expand the discussion around Perlwitz and Miller 2010, which is central to this work's motivation)

<u>Answer to General Comment 3 (C3P1):</u> We thank the reviewer for these comments. The work of Perlwitz and Miller (2010) was introduced in the original manuscript at lines 118-120 as they reported a counterintuitive feedback linking the atmospheric heating induced by tropospheric absorbing aerosol to a cloud cover increase. Particularly, they observed this change for low level clouds as a response to relative humidity due to opposite changes in specific humidity and temperature. Furthermore, Perlwitz and Miller (2010) concluded that higher levels of absorption by aerosols were responsible for two counter-acting processes: a larger diabatic heating warming of the atmospheric column (decreasing relative humidity), and a corresponding increase in the specific humidity, counteracting the drop on the relative humidity and resulting in more low cloud cover with increasing aerosol absorption.

This was an important result, given the fact that the traditional semi-direct effect relates the atmospheric heating induced by absorbing aerosol to a decreasing relative humidity and less cloud cover. This can further increase the amount of the incoming solar radiation that reaches Earth’s surface and is absorbed, leading to positive feedback characterized by additional warming and a decrease in the cloud amount (e.g. Koren et al., 2004). Thus, the aim of introducing the work of Perlwitz and Miller (2010) was to point the readers’ attention to the fact, that measuring the atmospheric heating rate in cloudy conditions is needed as constrain and/or input for more comprehensive climate model, to shed light on the sign and magnitude on the related feedbacks on cloud dynamics.
For the reason above we extended the introduction section by adding these considerations. At the same time, results were discussed with the above cited study in mind, recapping this also in the conclusions.

<u>General comment 4 (C3P1)</u>. In many places in this manuscript the authors say that "Fλ is the radiation" when they seem to mean "spectral irradiance" (W/m2/nm). The word "radiation" is not accurate. On line 351 they suddenly use "irradiance". Be consistent. Avoid confusing your readers.
It appears that all reported quantities are strongly corelated for direct and reflected irradiance. If this is correct then please sum these two quantities in all figures. The presentation is too confusing.
The preceding work (Ferrero et al. 2018) included diurnal trends in irradiance, which would be valuable here. Why were they not included?

<u>Answer to General Comment 4 (C3P1):</u> We thank the reviewer for addressing the terminology question. In many parts of the manuscript the term “radiation” was used as a general synonymous of different more specific terms under the assumption that it was easier to identify the specific object of the sentence (e.g. spectral irradiance) from its context. We understand from the comment that this can lead to some confusion, therefore we changed the generic word “radiation” with the appropriate term everywhere in the manuscript. We left the term “radiation” when a generic reference to it was needed (e.g. introduction).
The observation that “all reported quantities are strongly correlated for direct and reflected irradiance” is right. However, a sum of the two quantities is wrong from a methodological point of view. Also, we need to first show that they are correlated. In fact, the relationship that appears in the present work is due to the simple coincidence that measurements were collected upon Milan were the surface albedo is quite stable in time. For any other application (e.g. in the Arctic and Antarctic or other regions featuring extreme changes between snow cover and bare ground, over a steppes or other grassed regions, measurements from ships, drones) the reflected spectral irradiance can change with sky conditions, leading to a nonlinear relationship with the direct spectral irradiance. For these reasons we decided to maintain them separated, and, in agreement with the specific comment 31 (C8P1), we rigorously reported direct, diffuse and reflected spectral irradiance contribution to the HR in every Figure of the manuscript.
Finally, the diurnal variation in irradiance was not reported in this work, since they were presented earlier (Ferrero et al. 2018). However, we agree with the suggestion that they would be valuable in the present manuscript, especially when reporting the diurnal pattern of the HR averaged for clear sky conditions and cloudy conditions – old Figure 11 (now Figure 10 in the revised version of the

manuscript). We added to Figure 11 (now Figure 10a-d) the global irradiance and eBC, together with wind speed. The new Figure 10a-d is reported here below as Figure A5.

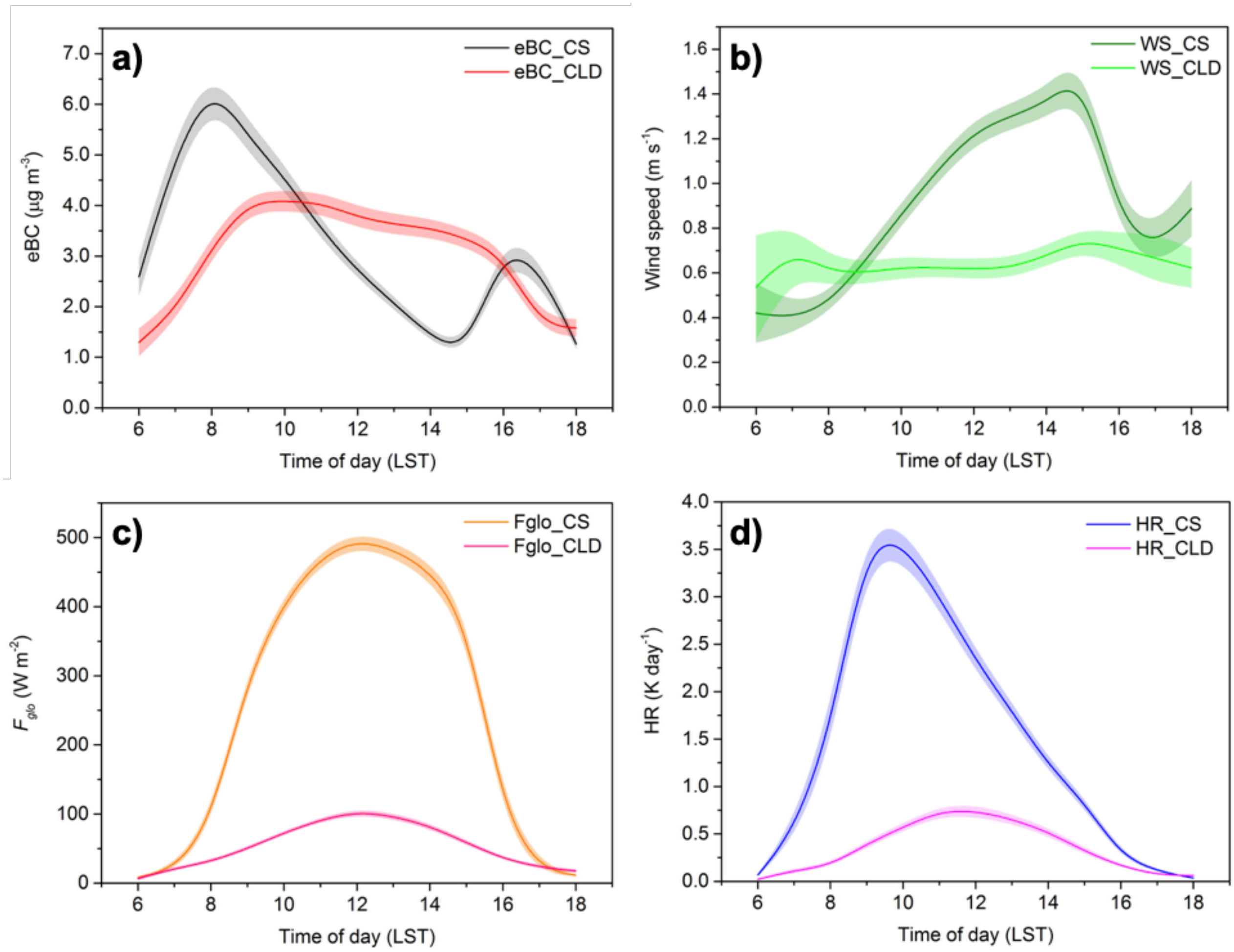

Figure A5 (Figure 10 in the revised version of the manuscript). Diurnal pattern of eBC (a), wind speed (b), global irradiance (F_{glo}) (c) and HR (d). Data are averaged for clear sky conditions (CS, oktas=0) and cloudy conditions (CLD, oktas=7-8).

SPECIFIC COMMENTS

Specific Comment 1 (C3P1): I would require that the authors add a glossary table (defining abbreviations) before publication due to the large number of symbols in the figures. Moreover, please improve the legends (e.g. 6b)
I will suggest that the authors change Fig 8, 9 axis labels from "Ci" to "cirrus" etc for all cloud types.

Answer to Specific Comment 1 (C3P1): We fully agree with you that a glossary table is needed and we added it in the manuscript as a new section "Appendix A".
Figure 6b (now Figure 9b in the revised version of the paper) required a legend improving in order to better separate the clear sky case with respect to cloudy ones. The same is also valid for Figure 11 (now Figure 10 in the revised version of the paper). At this purpose we used the term "CLD" in each legend for cloudy conditions (oktas=7-8) and "CS" for clear sky. After considering the comment

about the cloud acronyms, we decided to maintain the acronyms and improve them using the nomenclature in the international abbreviations for cloud genera and species of the World Meteorological Organization (WMO, https://cloudatlas.wmo.int/en/home.html) for brevity, clarity and comparability with Figures 10 and 15 (now Figures 13 and 16 in the revised version of the paper). We are now using the nomenclature in the international abbreviations for cloud genera and species of the World Meteorological Organization. They were included in in the new section "Appendix A".

Specific Comment 2 (C4P1): Figure 10's axis label should include HR.

Answer to Specific Comment 2 (C4P1): We thank the reviewer for the suggestion. We changed Figure 10 y-axis (now Figure 13 in the revised version of the paper) accordingly and we did the same also with Figure 15 (now Figure 16 in the revised version of the paper). The x-axis was also improved in both Figures with a more rigorous label "Cloudiness (oktas)".

Specific Comment 3 (C4P1): 79 Higher than clear sky conditions in certain localized regions only, or?

Answer to Specific Comment 3 (C4P1): Line 79 summarizes results from the works of Mims and Frederick (1994) and Feister et al. (2015). Mims and Frederick (1994) determined that scattering from the sides of cumulus clouds can enhance the total (global) UV-B solar irradiance by 20% or more over the maximum solar noon value when cumulus clouds were just near the Sun (the cloud not blocking the solar disk). In a similar way, Feister et al. (2015) concluded that the scattering of solar radiation by clouds can enhance UV irradiance at the surface; for example, Cumulonimbus clouds with top heights close to the tropical tropopause layer have the potential to significantly enhance diffuse UV-B radiance over its clear sky value. We reported these findings as UV represents an important region for BrC absorption and future studies should investigate specific cases of UV enhancement (which is actually beyond the aims of the present work) with respect to the impact of BrC on the climate. We extended and improved this part of the Introduction.

Specific Comment 4 (C4P1): 110 'Conversely' is not appropriate here

Answer to Specific Comment 4 (C4P1): We agree and the sentence was rewritten as follows: "To our knowledge, there has been no experimental investigation of cloudiness and cloud type impact on the HR of aerosol layers below clouds, where most of the aerosol pollution typically resides".

Specific Comment 5 (C4P1): 110 Please start a new paragraph at "This study". End this paragraph instead with "This study aims to fill this gap" or similar.

Answer to Specific Comment 5 (C4P1): We thank the reviewer for the suggestion. We changed the text accordingly. Please note that we added about 15 lines as answer to your general comment 3 before this sentence, and that the end of the Introduction was reordered for clarity.

Specific Comment 6 (C4P1): Fig S2. Please add an "uncorrected" panel to give readers an idea of the magnitude of the correction (which is related to uncertainties).

Answer to Specific Comment 6 (C4P1): This figure (Figure A6) is attached below. Care needs to be taken when interpreting the meaning of this plot as it is not related to the Aethalometer measurement uncertainty.

First, we need to recall that in the Aethalometer AE31, the aerosol sample is continuously deposited on the filter tape. Seven light sources with different wavelengths (λ) illuminate the tape. Attenuation (ATN) of light is measured under the sample for each of the 7 wavelengths relative to an illuminated sample-free part of the tape acting as a reference. ATN is calculated as:

$$ATN = 100 * \ln (I_0/I) \tag{A1}$$

where I_0 and I are the intensity of light transmitted through the reference and aerosol blank spot of the filter respectively. The attenuation coefficient of the aerosol particles collected on the filter tape, $b_{ATN(\lambda)}$, is then defined as follows (Weingartner, et al., 2003):

$$b_{ATN(\lambda)} = \frac{A}{Q}\frac{\Delta ATN(\lambda)}{\Delta t} \tag{A2}$$

where A is the filter spot area, Q the flow rate and ΔATN is the change in attenuation during the time interval Δt.

It is noteworthy that b_{ATN} differs from the aerosol absorption coefficient of airborne particles because it is determined from the attenuation of light passing through a particle-laden filter. The filter is responsible for measurement artifacts. These artifacts can be corrected with different procedures to account for the so-called loading effect and multiple scattering inside the filter matrix (Weingartner, et al. 2003, Arnott, et al., 2005, Schmid, et al. 2006, Collaud Coen, et al. 2010; Drinovec et al., 2015). We used a known correction scheme (Weingartner et al., 2003). Parameters C and $R(ATN,\lambda)$, are introduced to convert Aethalometer attenuation measurements to absorption coefficients ($b_{abs(\lambda)}$):

$$b_{abs(\lambda)} = \frac{b_{ATN(\lambda)}}{C \cdot R(ATN,\lambda)} \tag{A3}$$

where C and $R(ATN,\lambda)$ are the filter multiple scattering enhancement parameter and the wavelength-dependent loading effect correction parameter, respectively. The parameter $R(ATN,\lambda)$ corrects for the loading effect due to the reduction in the optical path due to an increase of the sample collected on the filter over time (Weingartner, et al., 2003). $R(ATN,\lambda)$ was dynamically determined following the Sandradewi et al. (2008b) algorithm. This approach was recognised to be one of the best approaches as correction does not affect data in terms of the absorption Ångström exponent (AAE) (Collaud Coen et al., 2010), the parameter describing the dependence of the absorption coefficient on the wavelength. This scheme was previously applied to data collected at the investigated site (Ferrero et al., 2018), because the experimental assessment of HR must avoid any artificial perturbation of the AAE.

The parameter C corrects for the enhanced optical path through the filter caused by multiple scattering of light by the filter fibers and by the particles embedded in it. The multiple scattering coefficient C is determined by comparing the attenuation coefficient, that needs to be previously corrected for the loading effect (b_{ATN}/R; see equation A3), with the absorption coefficient measured simultaneously at the same wavelength with a reference instruments (b_{abs_ref}) (in our case, MAAP) as follows:

$$C = \frac{b_{ATN}/R}{b_{abs\_ref}} \tag{A4}$$

Thus, applying a non-corrected attenuation coefficient (raw data, not corrected for the loading effect; e.g. Figure A6) represents an erroneous application of the Aethalometer data, as it features a systematic error – the loading effect. Correcting for the loading effect increases the value of the parameter C. For the reason above we did not included Figure A6 (here below) to the Supplemental material.

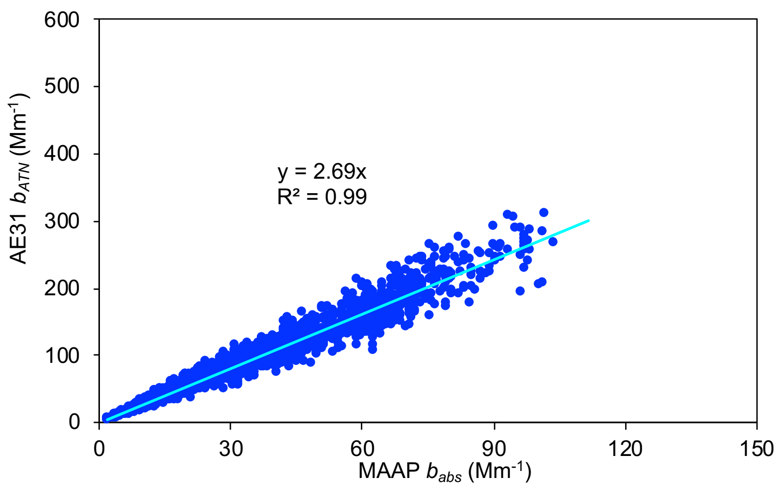

Figure A6. Linear correlation between the Aethalometer AE31 attenuation coefficient at 660 nm, not corrected for the loading effect ($b_{ATN,660nm}$ raw data), and the MAAP absorption coefficient at 637 nm.

However, the reviewer question posed the important issue of uncertainty. We describe it here below and we added the description to the method section 2.1 (Instruments), where the uncertainties of all the other instruments were already reported.
As mentioned above, absorption coefficient measurements are based on measurements of light transmission through the sample-laden filter, which needs to be compensated for different artifacts, like the multiple scattering effect and loading effect (Liousse et al., 1993; Petzold et al., 1997; Bond et al., 1999). In this respect, Collaud-Coen et al. (2010) tested different correction schemes on data from different sites and showed linear regression between the Aethalometer data corrected with the Weingartner et al. (2003) procedure and reference MAAP data, with slopes close to one and relative standard deviations on average of 23%. This is an estimation of the global uncertainty of Weingartner et al. (2003) procedure applied in the present work. Moreover, Drinovec et al. (2015) showed a good agreement between Aethalometer AE31 data (corrected using Weingartner et al., 2003) and that of the new Aethalometer AE33 with a slope close to one and R^2>0.90. We referred to the Collaud-Coen et al. (2010) uncertainty estimation in our work.

Specific Comment 7 (C4P1): Line 168 What is the physical meaning of the C value being close to the GAW value? (e.g.: The particle size and single scattering albedo were typical of atmospheric monitoring sites. Collaud Coen et al., 2010).

Answer to Specific Comment 7 (C4P1): We thank the reviewer for this question as it enabled us to improve the manuscript. The physical meaning of the similarity between the obtained C value (3.24) and the GAW ones implies that Milan (in the middle of the Po Valley) features aerosol with continental characteristics (e.g. Carbone et al., 2010) not far from the global ones. However, the question that emerges is the physical reliability of the C value given the findings reported in Collaud Coen et al. (2010). Collaud Coen et al. (2010) defined the reference value of C (C_{ref}) for the AE31 tape in the pristine atmosphere of Jungfraujoch and Hohenpeissenberg, where aerosol has a single scattering albedo of ~1; C_{ref} was equal to 2.81±0.11.

At the same time, Collaud Coen et al. (2010) took into account the cross-sensitivity to scattering of the filter measurements and its influence on the parameter C, starting from C_{ref} as follows:

$$C = C_{ref} + \alpha \frac{\omega_0}{1-\omega_0} \tag{A5}$$

where α is the parameter for the Arnott (2005) scattering correction (0.0713 at 660 nm) and ω_0 the single scattering albedo which, in wintertime in Milan, within the mixing layer, was found to be 0.846±0.011 at 675 nm by Ferrero et al. (2014). With respect to C interpretation, we need to underline first that the nominal AE31 660 nm channel is provided by a Kingbright light-emitting diode (APT 1608SRC PRV 1.6 x 0.8 mm SMD Chip LED Lamp; King bright, 2018) which is characterized by a 20 nm spectral full bandwidth at half maximum under 20mA of supplied current (information from manufacturer). This is in agreement with the absorption photometer intercomparison, reported by Muller et al. (2011), in which the nominal AEs red channel was found to have a 23 nm spectral full bandwidth at half maximum. Thus, for practical purposes, the single scattering albedo (0.846±0.011 at 675 nm) reported in Milan at a wavelength slightly different from the one featured in the AE31 by Ferrero et al. (2014) was applied to eq. A5.
Considering the variability for both C_{ref} (±0.11) and ω_0 (±0.011) the obtained C for Milan was 3.20±0.15. This lies within the experimental range obtained from the comparison of the AE31 with the MAAP: 3.24±0.03. Calculating in the opposite direction, the retrieval of ω_0 using the experimental C and C_{ref}, led to a value of 0.858±0.043 which is very close to the value reported by Ferrero et al. (2014), underling the reliability of the obtained results.
We added the aforementioned considerations in section 2.1 where the experimental C is presented while details on the AE31 led were added to the Supplemental material. Moreover section 2.1 was divided in two subsections (2.1.1 Light absorbing aerosol measurements and 2.2.2 Radiative and meteorological measurements) due to the requirements of the Specific Comment 8 below.

<u>Specific Comment 8 (C4P1):</u> **171 Was the MRI built by U Milano-Bicocca? Please add manufacturer, even if it is homebuilt.**

<u>Answer to Specific Comment 8 (C4P1):</u> We thank the reviewer for the suggestion which improves the instrument description. The MRI was developed at the University of Milano-Bicocca by PhD Sergio Cogliati using commercial-grade optoelectronics devices. The instrument uses an optical switch (MPM-2000-2x8-VIS, Ocean Optics Inc., USA) to sequentially select between different input fibers fixed to the upwards- and the downwards-looking entrance fore-optics. The configuration used in the present work connects each spectrometer to 3 input ports: 1) The CC-3 cosine-corrected irradiance probes to collect the down-welling irradiance; 2) the bare fiber optics with a 25° Field-of-View to measure the up-welling radiance from the terrestrial surface; 3) the blind port that is used to record the instrument dark-current. A 5 m long optical fiber with a bundle core with a 1 mm diameter is used to connect the entrance fore-optics to the multiplexer input, while the connection between the multiplexer output ports and the spectrometers is obtained with a 0.3 meters long optical fibers. The set-up allows to sequentially measure the dark-current and both up- and down-welling spectra simultaneously with the two spectrometers – High Resolution HR4000 holographic grating spectrometers (Ocean Optics Inc., USA). Finally, the MRI is equipped with a 3648-element linear CCD-array detector (Toshiba TCD1304AP, Japan) with a 14-bit A/D resolution.

We added this description to section 2.1, which was also divided in two subsections (2.1.1 Light absorbing aerosol measurements and 2.1.2 Radiative and meteorological measurements) due to the deepening also required by your previous Specific Comment 7.

<u>Specific Comment 9 (C4P1):</u> 200 What is the uncertainty or accuracy of the Nimbus 15k? In other words, please mention the limitations as well as the strengths of this system.

<u>Answer to Specific Comment 9 (C4P1):</u> The Lufft Nimbus CHM-15K is a high-performance lidar-ceilometer system operating at 1064 nm and capable of providing vertical profiles of aerosols and clouds in the bottom 15 km of the atmosphere with a temporal resolution of 30 seconds and a vertical resolution of 15 m.
In order to improve the signal to noise ratio of the backscatter signal, the signal is processed with temporal averages of 2 minutes. The full overlap is obtained at altitude of some hundred meters from the observation site and overlap correction functions are applied in the first layers. More technical information are provided by: Wiegner, M. and Geiß, A.: Aerosol profiling with the Jenoptik ceilometer CHM15kx, Atmos. Meas. Tech., 5, 1953–1964, doi:10.5194/amt-5-1953-2012, 2012, and Madonna, F., Amato, F., Vande Hey, J., and Pappalardo, G.: Ceilometer aerosol profiling versus Raman lidar in the frame of the INTERACT campaign of ACTRIS, Atmos. Meas. Tech., 8, 2207–2223, 2015.
We added the Madonna et al. (2015) reference to the manuscript, while the Wiegner and Geiß (2012) reference was already included.
We added the following sentence to section 2.1.2 Radiative and meteorological measurements: “Given the vertical resolution of the instrument, expected accuracy on the cloud base height derived by the lidar-ceilometer is < ±30 m”.

<u>Specific Comment 10 (C4P1):</u> 238 "This is due to the negligible ..." This sentence is not accurate. The authors may instead consider the simple harmonic oscillator (Moosmuller et al. 2011, doi:10.5194/acp-11-1217-2011) or energy gap (Sun 2007 doi:10.1029/2007GL029797) models here.

<u>Answer to Specific Comment 10 (C4P1):</u> We thank the reviewer for this comment. The sentence aimed simply at recalling the intrinsic property of BrC: it features an absorption spectrum that smoothly increases from the VIS to UV wavelengths, as recently described by Laskin et al. (2015; DOI: 10.1021/cr5006167 Chem. Rev. 2015, 115, 4335−4382) who pointed out that “light absorption by BrC at 440 nm is~40% of the light absorption by BC at this wavelength, while BrC contributes only 10% to the light absorption at 675 nm”. Similarly, Moosmueller et al. (2011) shows in their Fig. 7 that there are ~1.5 orders of magnitude between the mass absorption efficiencies for relevantly sized particles. However, we understood from your question that this sentence was poorly connected with the previous one: “Conversely, BrC absorption is spectrally more variable, with an AAE from 3 to 10 (Ferrero et al., 2018; Shamjad et al., 2015; Massabò et al., 2015; Bikkina et al., 2013; Yang et al., 2009; Kirchstetter et al., 2004).” leading to misinterpretations.
We fully agree with you that the lower absorption coefficient of BrC in the IR region (compared to UV) is a consequence of the large wavelength difference (IR) with respect to the resonance in the UV, as can be described by the simple harmonic oscillator reported in Moosmuller et al. (2011). The band-gap model with the Urbach tail (Sun et al., 2007; and referenced in Moosmuller et al., 2011),

where the key factor is the difference between the highest occupied and lowest unoccupied energy state of the molecules in the BrC ensemble, gives similar results.
We reworded the sentence as required adding this explanation.

Specific Comment 11 (C4P1): 243 change 'successfully' to 'previously'

Answer to Specific Comment 11 (C4P1): Done.

Specific Comment 12 (C4P1): 251 First use of LAA on this line was not defined. Please introduce the concept in the introduction. It is a nice and useful abbreviation.

Answer to Specific Comment 12 (C4P1): We thank the reviewer for addressing this. We modified the introduction accordingly.

Specific Comment 13 (C4P1): 350 Give limits of the integral in the equation.

Answer to Specific Comment 13 (C4P1): There is no equation at line 350. We interpreted your question as relating to Eq. 7 (now moved to the Supplemental material). We added the limits to the integral.

Specific Comment 14 (C5P1): 135 This information is redundant with lines 110-112, please shorten 110-112.

Answer to Specific Comment 14 (C5P1): We thank the reviewer for addressing this. We shortened lines 110-112 as required.

Specific Comment 15 (C5P1): 171-177 Please cite Cogliati immediately after introducing the MRI.

Answer to Specific Comment 15 (C5P1): We agree. Changed.

Specific Comment 16 (C5P1): 263 Change "N represents one of the possible 9 classes" to "N = 1,2,3, ..., 9, representing 9 classes of cloud fractions".

Answer to Specific Comment 16 (C5P1): We thank the reviewer for the question from which we understand that the sentence was poorly written. In the original version, we stated "where *N* represents one of the possible 9 classes of cloud fraction". The term "cloud fraction" was improperly used as the correct sentence would be "where *N* represents one of the possible 9 classes of sky conditions expressed in oktas (from 0, clear sky, to 8, complete overcast)". We rephrased the sentence as above.

Specific Comment 17 (C5P1): 3.1 Heating rate measurements – Equation 1,2, and 3 There is no need for all 3 equations here. Delete Eq 1. Start with Eq 2 to introduce and define ADRE first, then the reader will understand Equation 3 (new Eq 2) naturally. Remove μ and replace it with cos θ. There is no need to introduce μ because it is only used twice in the manuscript, and anyway cos θ is more easily understood.

Also, use the integral sign to specify "integral over the whole 2π" (line 209) instead of writing it only in words. Same for θ.

Answer to Specific Comment 17 (C5P1): Thanks for the suggestion. We modified the text according to the suggestion above. To simplify the radiative transfer concepts used in the HR assessment, we have reduced the number of equations in the text. Instead of Eqs. 1-3 we now present only 2 equations in the main body of the manuscript moving the demonstration to the supplemental material. The HR assessment is presented as follows:

"The heating rate is determined from the air density (ρ, kg m^{-3}), the isobaric specific heat of dry air (C_p, 1005 J kg^{-1} K^{-1}) and the radiative power absorbed by aerosol per unit volume of air (W m^{-3}) describing the interaction between the radiation (either direct from the sun, diffuse by atmosphere and clouds, and reflected from the ground) and the LAA (BC and BrC in Milan). The HR is determined as follows (Ferrero et al., 2018):

$$HR = \frac{1}{\rho C_p} \cdot \sum_{dir,dif,ref} \int_{\theta=0}^{\theta=\pi/2} \int_{\lambda=300}^{\lambda=3000} \frac{F_{dir,dif,ref}(\lambda,\theta)}{\cos(\theta)} b_{abs}(\lambda) d\lambda d\theta \quad \text{(A5)}$$

where the subscripts *dir*, *dif* and *ref* refer to the direct, diffuse and reflected components of the spectral irradiance F of wavelength λ impinging on the LAA with a zenith angle θ (from any azimuth).

Under the isotropic and Lambertian assumptions (as used in Ferrero et al., 2018) equation 2 can be solved becoming:

$$HR = HR_{dir} + HR_{dif} + HR_{ref} =$$

$$= \frac{1}{\rho C_p} \cdot \left[\frac{1}{\cos(\theta_z)} \int_\lambda F_{dir}(\lambda)\, b_{abs}(\lambda)\, d\lambda + 2 \int_\lambda F_{dif}(\lambda)\, b_{abs}(\lambda)\, d\lambda + 2 \int_\lambda F_{ref}(\lambda)\, b_{abs}(\lambda)\, d\lambda \right] \quad \text{(A6)}$$

where θ_z refers to the solar zenith angle, while $F_{dir}(\lambda)$, $F_{dif}(\lambda)$ and $F_{ref}(\lambda)$ are the spectral direct, diffuse and reflected irradiances. Eqs. 2 and 3 are related to the concept of actinic flux (Tian et al., 2020; Gao et al., 2008; Liu, 2007); an extended description, as well as its demonstration is detailed in the Supplement."

Specific Comment 18 (C5P1): Equations 4 and 5 use subscripts dir, dif, ref to specify direct, diffuse and reflected radiation. Equations 1, 2, 3 use "nth type of F" to do the same. Choose one and stick to it. The text subscript is better, and the authors obviously agree as they used it later in the manuscript.

Answer to Specific Comment 18 (C5P1):We agree indeed. We changed the manuscript accordingly by using the subscripts dir, dif, ref to specify direct, diffuse and reflected radiation to avoid unnecessary new symbols and make the work more readable (see answer to specific comment 17). This also goes in the direction asked by reviewer#2 which requires the use of less technical jargon.

Specific Comment 19 (C5P3.1): The term Fglo = Fdir + Fdif + Fref must be introduced already in the first equation of Section 2.2. Prepare the reader for Equation 6. I have to assume that this is the definition, the authors never gave it.

Answer to Specific Comment 19 (C5P3.1): We thank the reviewer for addressing this point. There is a misunderstanding that we have to clarify. This improved the methodology section. We need to start from the radiometric definition of the global downwelling irradiance which is as follows:

$$F_{glo} = F_{dir} + F_{dif} \quad \text{(A6)}$$

We added this definition in Appendix A. Equations 1-4 (now 2-3 in the revised version of the manuscript) could have caused the misinterpretation, as the calculation of the ADRE and the HR requires the sum of the total amount of radiative energy interacting with light-absorbing aerosol, also including the reflected irradiance in addition to the direct and diffuse components from the sun and sky. In fact, an alternative writing of the ADRE is:

$$ADRE = \int_{\lambda} AF_{(\lambda)} b_{abs(\lambda)} d\lambda \quad \text{(A7)}$$

where $AF_{(\lambda)}$ represents the actinic flux, that is the total spectral flux of photons per unit area and wavelength interval available to molecules/aerosol at a particular point in the atmosphere. The radiative flux from all directions onto a volume of air is called the actinic flux (Seinfeld and Pandis, 2006). We added this information in section 2.1.2.

The actinic flux consists of three components: direct solar radiation, diffuse radiation originating from scattering in the atmosphere, and diffuse radiation originating from reflection from the Earth's surface.

Thus, it is only for the AF that the following sum is valid:

$$AF_{tot} = AF_{dir} + AF_{dif} + AF_{ref} \quad \text{(A8)}$$

The actinic flux at a particular point in the atmosphere is calculated by integrating the spectral radiance over all directions of space. The actinic flux must be distinguished from spectral irradiance, which is the hemispherically integrated radiance weighted by the cosine of the angle of incidence, and represents the photon flux per unit area through a plane surface. Under the isotropic and Lambertian assumptions, the diffuse and reflected irradiances are related with the corresponding radiances by a factor π; the direct irradiance is related to the radiance as a function of the solar zenith angle.

From a physical point, given a generic monochromatic radiance $R(\lambda,\theta,\phi)$, the corresponding $AF(\lambda)$ and irradiance $F(\lambda)$ (Seinfeld and Pandis, 2006; Liu, 2007) are given by:

$$AF(\lambda) = \int_{\phi=0}^{\phi=2\pi} \int_{\theta=0}^{\theta=\pi/2} R(\lambda,\theta,\phi) \sin(\theta)\, d\theta d\phi \quad \text{(A9)}$$

$$F(\lambda) = \int_{\phi=0}^{\phi=2\pi} \int_{\theta=0}^{\theta=\pi/2} R(\lambda,\theta,\phi) \cos(\theta) \sin(\theta)\, d\theta d\phi \quad \text{(A10)}$$

For the direct component, the radiance comes only from the sun direction (the solar zenith angle, SZA), it can be assumed to be a collimated beam, essentially parallel, and originates from a very small solid angle and thus:

$$AF_{dir}(\lambda) = R_{dir}(\lambda) = F_{dir}(\lambda)/\cos(SZA) \quad \text{(A11)}$$

For the diffuse and reflected component (under the isotropic and Lambertian assumptions, respectively) the radiance comes homogeneously from each direction and thus:

$$AF_{dif,ref}(\lambda) = 2\pi R_{dif,ref}(\lambda) \quad \text{(A12)}$$

$$F_{dif,ref}(\lambda) = \pi R_{dif,ref}(\lambda) \quad \text{(A13)}$$

implying:

$$AF_{dif,ref}(\lambda) = 2F_{dif,ref}(\lambda) \quad \text{(A14)}$$

Now, as in section 2.2 we gave the following definition:

$$ADRE = ADRE_{dir} + ADRE_{dif} + ADRE_{ref} \quad \text{(A15)}$$

we can finally rewrite it (given eq. A7 and A8) as follows:

$$ADRE = \frac{1}{\cos(SZA)} \int_{\lambda} F_{dir}(\lambda)\, b_{abs}(\lambda)\, d\lambda + 2\int_{\lambda} F_{dif}(\lambda)\, b_{abs}(\lambda)\, d\lambda + 2\int_{\lambda} F_{ref}(\lambda)\, b_{abs}(\lambda)\, d\lambda \quad \text{(A16)}$$

With the heating rate being:

$$HR = \frac{1}{\rho C_p} \cdot ADRE \quad \text{(A17)}$$

We included this description in the supplemental material and changed the use of the word "radiation" in the manuscript text as already described in the answer to the general comment 4.

<u>Specific Comment 20 (C5P1):</u> The only real difference between HR and ADRE in Figure 5 is the air density ρ. So, the authors should plot ρ in the figure and emphasize this in the caption to avoid confusing readers who are not familiar with HR or ADRE (in other words, most readers).
Since the main contribution of this manuscript is to discuss heating rates, why discuss ADRE at all? Leave that to the SI. Or, of the authors disagree, then discuss only ADRE. HR appears more valuable as ρ is a meteorological variable.

<u>Answer to Specific Comment 20 (C5P1):</u> Thanks for this comment. The paper focuses on the HR which is the valuable parameter. ADRE was introduced in section 2.2 (Heating rate measurements) for methodological purposes). In keeping with the suggestion, we removed both ADRE terminology and values from sections 2.2 (Heating rate measurements) and 3 (results and discussions) and its plot from Figure S5 (now Figure 5 in the revised version of the manuscript); this avoids confusing readers and keeps them focused on the main target of the work (i.e. HR, cloudiness and cloud type).

<u>Specific Comment 21 (C6P1):</u> This section is a mess. Do not mix discussion and results in S 2.3.2. Review the literature first, then present your results. Present "failed analysis" in the SI, not in the main text. Use only 1 or 2 sentences in the main text for failed analysis.

<u>Answer to Specific Comment 21 (C6P1):</u> Indeed section 2.3.2 was differently structured in the first draft of the manuscript, underling first the literature methods and presenting the methodology. A shortening of the paper before submission probably resulted in the confusing section. We apologize for that. We completely restructured it following this comment.

<u>Specific Comment 22 (C6P1):</u> This reviewer spent several minutes studying Figure 2 and writing the following comments before learning that it is a "this did not work" figure. The writing should make this clear immediately. Restructure S2.3.2 to fix this.

<u>Answer to Specific Comment 22 (C6P1):</u> Thank for addressing it as we were able to fix a couple of inaccuracies. We improved the legend and we also fixed panels (g-h) by indicating with coloured dashed lines the time periods to which the dots reported in the SD-R plot of panel h refers to. The new Figure 2 is reported here below as Figure A7 and was extensively described in the revised version of the manuscript in section 2.3.2.

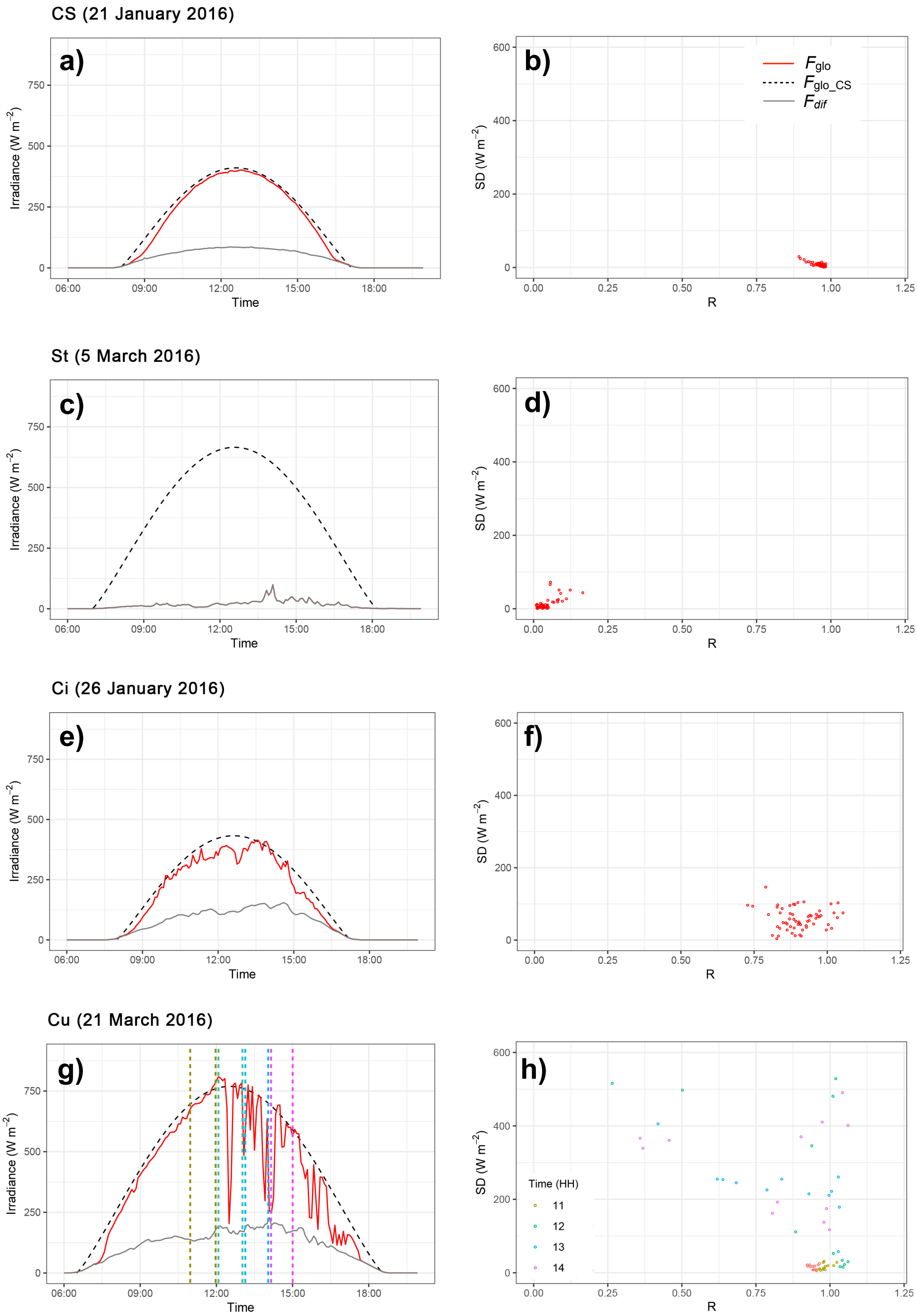

Figure A7 (new Figure 2 in the manuscript). Cloud classification based on broadband solar radiation following Duchon & O'Malley (1999). Each row represents a different clout type in a specific day as a case study. The left columns represent the time series of global and diffuse measured solar irradiance (F_{glo} and F_{dif}) and modelled clear sky irradiance (F_{glo_CS}), while the right column the scatter plot of the observed standard deviation of irradiance (SD) vs. the fraction of modelled clear sky irradiance (R). In the panel (h) different colors are related to different time (hours) of the day as reported in the legend.

<u>Specific Comment 23 (C6P1):</u> The section here concludes that the 2 literature methods discussed (Duchon 1999 and Harrison et al 2008) were not adequate, based on the conclusions of Harrison's work. So the authors introduce a new method, but with no validation of it. How can the reader trust this? I believe the author's work is valuable but the discussion needs to include validation.

<u>Answer to Specific Comment 23 (C6P1):</u> Thank you for remarking on the need for a validation. As reported in the answer to the general comment 1 (C1P1) a thorough validation was carried out and described at length in Appendix B ("Cloud type validation") resumed here below.

A resume of Appendix B: Cloud type validation

The validation was conducted in two subsequent steps.

The first validation step was carried out by comparing the automatized cloud classification (based on Duchon and O'Malley, 1999, and additionally lidar cloud base height) with a visual cloud classification based on sky images collected during 1 month of field campaign. We describe this in Appendix B1.

The second validation step involved the recently published method (Ylivinkka et al., 2020), based on the same approach followed in our work: the application of Duchon and O'Malley (1999) classification improved by the knowledge of the cloud base height. Thus, the aim of the second step was to determine the degree of consistency between the two approaches that were developed simultaneously and independently in two completely different European regions. We describe this in Appendix B2.

Both validations were evaluated by means of a confusion matrix, a special kind of contingency table, with two dimensions and identical sets of "classes" in both of them. From the confusion matrix, the balanced accuracy was computed as follows:

$$Balanced\ Accuracy = \frac{Sensitivity + Specificity}{2} \quad \text{(B1)}$$

where the *Sensitivity* describes the true positive rate (the number of correct positive predictions divided by the total number of positives), and the *Specificity* describes the true negative rate (the number of correct negative predictions divided by the total number of negatives). The balanced accuracy is especially useful when the investigated classes are imbalanced, i.e. one of the classes appears far more often than the other, a condition useful for cloud classification (García et al., 2009).

Appendix B1: visual cloud classification

Sky images were collected during 1 month of the campaign (13 February – 9 March 2017) using a sky view camera (GoPro Hero4 Session installed on the U9 roof) characterized by a field of view of 95x123°. The camera was oriented south with the same declination of the shadow band applied to DPA154 global radiometer for diffuse broadband irradiance measurements (section 2.1.2) manually each day. Sky images were taken with 1 minute time resolution. Visual classification of sky images, based on the principles of cloud classification published in Cloud Atlas (WMO, https://cloudatlas.wmo.int/en/home.html).

To test the performance, 869 sky images were analyzed, and the cloud type was determined through visual inspection. From the visual classification and our automatized classification, the following confusion matrix (Table B1) was created. The highest balanced accuracy was found for stratus (St) data (95%) while the lowest (50%) for mixed cloud types Cirrocumulus and Cirrostratus (Cc-Cs) whose absolute number of cases, however, was ~0.6% of the total, probably biasing the obtained accuracy; the same happened for Cumulus (Cu) and Altocumulus (Ac). Overall, five classes over eight were above 68% of balanced accuracy while the overall balanced accuracy was 80%, underlying the reliability of the classification algorithm allowing to study the impact of clouds on light-absorbing aerosols HR with a sufficient grade of certainty.

	Cloud type	Visual classification (reference)								Balanced
		Cu	St	Sc	Ac	As	Ci	Cc-Cs	CS	accuracy
Cloud classification algorithm	Cu	**6**	2	7	1		2		9	59%
	St	1	**259**	25		10				95%
	Sc	7	9	**61**	1				15	81%
	Ac				**1**	4				62%
	As		3			**23**				81%
	Ci						**45**	4	10	70%
	Cc-Cs						3	**0**		50%
	CS	16			1		56	1	**287**	89%

Table B1. Confusion matrix and balanced accuracy for each cloud type classified visually and following the algorithm reported in Table 1 within the present work. Stratus (St), Cumulus (Cu), Stratocumulus (Sc), Altostratus (As), Altocumulus (Ac), Cirrus (Ci), Cirrocumulus and Cirrostratus (Cc-Cs).

Appendix B2: intercomparison with Ylivinkka et al. (2020)

The second validation step involved the recently published method (Ylivinkka et al. 2020), which is based on the same approach followed in our work: the application of Duchon and O'Malley (1999) classification improved by the knowledge of the cloud base height. The classification scheme of Ylivinkka et al. (2020) is summed up in Table B2, following the nomenclature used in our present work. It is necessary to underline that the cloud classes determined in the work Ylivinkka et al. (2020) differ from those reported in our present work. Particularly, while both approaches enabled the Cu, St, Sc classification, some of the cloud classes were merged in the Ylivinkka et al. (2020) study: CS and Ci (CS+Ci), Ac and As (Ac+As) and mixed situation composed by Ci, Cc, Cs (Ci+Cc+Cs). In addition, they introduced the classes Cu+GRE and Ci+GRE to account for global radiation enhancement (GRE) due to this cloud types. We interpret these differences to be due to different conditions at the different latitudes at which the two algorithms were developed, especially due to the solar zenith angle and hence the sunlight interaction with clouds. A detailed investigation of this difference is beyond the aim of the present work. However, it is necessary to account for the classification differences in order to properly merge cloud classes with similar features to perform a comparison between the two methods. The cloud classes homogenization is summarized in Table B3, while the final intercomparison is reported in Table B4. The confusion matrix (Table B4) revealed a global balanced accuracy of 90%, showing that the two methods are comparable. The highest accuracy (100%) was obtained for CS followed by Ac+As (99%); Cu, St and Sc reached values of 94, 93 and 86%, respectively. The lowest performance was reached for Ns whose presence cannot be detected in the present study generating a false positive signal in the Ac+As class; however, due to the very low number of Ns cases (1.8%), its impact on the cloud classification can be neglected.

Overall, also the second validation step pointed out the reliability of the results obtained in the present work.

Cloud type	CBH (m)	R	SD (W/m2)	N of cloud layers
Cu	< 2000	0.6 – 0.85 & Rmax > 1	>= 200	1
	< 2000	> 0.85 & Rmax > 1	0 – 200	1
St	< 2000	< 0.6	< 100	1
Sc	< 2000	0.1 – 0.6	>= 100	1
Ns	2000 - 3000	< 0.3	< 100	1
Ac+As	2000 - 5000	>=0.3	< 500	1
Ci+Cc+Cs	>= 4000	0.85 – 1.1	50 - 400	1
	>= 4000	0.5 – 0.85	< 400	1
CS+Ci	NaN	0.85 – 1.05	< 50	1
Cu+GRE	< 2000	> 1 & Rmax > 1	>= 200	1
Ci+GRE	>=4000	> 1	< 400	1

Table B2. Final criteria adopted for cloud classification in Ylivinkka et al. (2020). Ns here represents Nimbostratus while GRE global enhancement radiation. Stratus (St), Cumulus (Cu), Stratocumulus (Sc), Altostratus (As), Altocumulus (Ac), Cirrus (Ci), Cirrocumulus (Cc) and Cirrostratus (Cs), Nimbostratus (Ns) and global radiation enhancement (GRE).

This study	Cu	St	Sc	/	Ac, As	Ci Cc-Cs	CS
Ylivinkka et al., 2020	Cu, Cu+GRE	St	Sc	Ns	Ac+As	Ci+Cc+Cs Ci+GRE	CS+Ci
Merged Cloud type	Cu	St	Sc	Ns	Ac+As	Ci+Cc+Cs	CS+Ci

Table B3. Cloud classes homogenization adopted for comparison purposes between the present study cloud classification and the one reported in Ylivinkka et al. (2020).

Cloud type classification		Ylivinkka et al. (2020)							Balanced accuracy
		Cu	St	Sc	Ns	Ac+As	Ci+Cc+Cs	CS+Ci	
This study	Cu	**80**							94%
	St		**3853**	58		1			93%
	Sc	11	596	**231**					86%
	Ns				**0**				50%
	Ac+As				153	**383**	51		99%
	Ci+Cc+Cs						**846**		97%
	CS+Ci							**2142**	100%

Table B4. Confusion matrix and balanced accuracy for each cloud type classified using the algorithm reported in the present study and the one reported in Ylivinkka et al. (2020).

<u>Specific Comment 24 (C6P1):</u> Line 308 how many cases (%) were analyzed after this limitation?? The authors should not discard cases of multiple cloud layers. Simply include a category "Multiple layers" or "Complex cloud layers" or similar.

<u>Answer to Specific Comment 24 (C6P1):</u> Thanks. We analysed 8405 one single layer cases, 61% of the total. The single layer choice is related to the aim of the paper: "to experimentally measure for the first time the impact of different cloudiness and cloud types on the HR exerted by light-absorbing aerosol" as stated in the introduction section. In this respect it was also clarified in section 2.3.2 "Finally, to avoid misclassification cases due to the presence of multiple cloud layers, we limited the

analysis to those cases where only one cloud layer was detected by ceilometer. This choice was also done given the main goal of this work: to quantify the effects of different cloudiness and cloud types on light-absorbing aerosol HR. "
We added the number of cases and their percentage to section 2.3.2.

<u>Specific Comment 25 (C6P1-C7P1):</u> **If I am to believe this section then the authors have contributed a numerical algorithm to the topic of automated cloud type analysis. Only 2 papers have been published on this topic, and most cloud type identification remains manual. This is the 3rd paper to contribute to this topic in 30 years, yet the authors did not include a solid analysis of the algorithm. Either the authors have used an unvalidated algorithm in their work, or the authors should write an entire manuscript describing their validation of what seems to be a valuable contribution. Separating the cloud algorithm work from the radiative heating work would mean removing Figures 2, 3, 4, 7, 14, and some SI figures from this to another manuscript. This would avoid breaking up the "BC+BrC" story.**
I note that the Harrison et al. 2008 work was missing from the reference list.

<u>Answer to Specific Comment 25 (C6P1-C7P1):</u> The cloud classification literature reports a huge quantity of papers and reviews aimed at classifying clouds (to avoid the limits of a simple manual human inspection) by means of different techniques and their integration. Some examples are reported in Singh and Glennen (2005), Ricciardelli et al. (2008), Calbó and Sabburg (2008), Tapakis and Charalambides (2013). Whith respect to the Po Valley, the Duchon and O'Malley (1999) was previously successfully applied by Galli et al. (2004). Moreover, the introduction of ceilometer data for cloud classification and cloud study purposes does not represent an absolute novelty in literature as demonstrated by Huertas-Tato et al. (2017) and Costa-Surós et al. (2013).
The novelty of the actual study is the combination of the Duchon and O'Malley (1999) with ceilometer cloud base height data. However, as reported in the answer to your General Comment 1, we have to underline that just after our submission of the present paper (20 Mar 2020), Ylivinkka et al. submitted to Atmospheric Measurement Technique (03 Apr 2020) a paper titled "Clouds over Hyytiälä, Finland: an algorithm to classify clouds based on solar radiation and cloud base height measurements"(https://doi.org/10.5194/amt-13-5595-2020) which was recently published. The paper discusses a cloud classification technique very similar to ours. This is a clear coincidence of an interesting scientific development. We therefore maintained the present paper as whole and improved it following reviewer suggestions by appropriately balancing the main body of the manuscript, Appendix, and the Supplemental material. For the validation we refer to the answer to the Specific Comment 23.
Finally, many thanks for finding that the Harrison et al. (2008) reference was missing. We added it the reference list together with the other aforementioned ones.

<u>Specific Comment 26 (C7P1):</u> **Make Fig S3 axis labels consistent with the language in S 2.3.2. Put R on the x axis.**

<u>Answer to Specific Comment 26 (C7P1):</u> We thank the reviewer for addressing it. It was done but the Figure was also removed in the revised final version to improve clarity and due to the extensive validation reported in Appendix B.

<u>Specific Comment 27 (C7P1):</u> The use of a 20 minute interval in calculating SD for the Duchon and O'Malley method means that wind speeds are included in the measurement of cloudiness fluctuations. This must be discussed. How do wind speeds compare with this 20 minute interval?

<u>Answer to Specific Comment 27 (C7P1):</u> The 20-minute interval reported in the Duchon and O'Malley (1999) considers the variability induced by cloud movement and evolution (e.g. cloud microphysical processes) on the global irradiance. The standard deviation changes in the global irradiance can therefore be due to the wind influence on the cloud dynamics. However, the wind influencing these processes is the wind at the cloud altitude, not the one at ground where we carried out measurements. It would be great to have a Doppler lidar able to measure wind speeds at these altitudes. Nevertheless, we investigated the ground wind behavior for the cloud type classified in the present work together with the SD parameter. Results are reported in Figure A7 below. As expected, there is no strong correlation between the two parameters, as the wind speed was measured at ground level and reflects the stagnant conditions typical of the Po Valley. The average wind speed during each cloud type and clear sky conditions was below 1 m s^{-1}. Despite this, it is clearly visible that low-level clouds (e.g. stratus) are present in the lowest wind speed conditions. Particularly, the average ground wind speed in stratus conditions was 0.64±0.02 m s^{-1}, lower than the 0.92±0.04-1.04±0.03 m s^{-1} found in cirrus-clear sky conditions.

We added Figure A7 in the Supplemental material (now Figure S6) and a resume of this discussion in the main body of the manuscript (extensively in the Supplemental material).

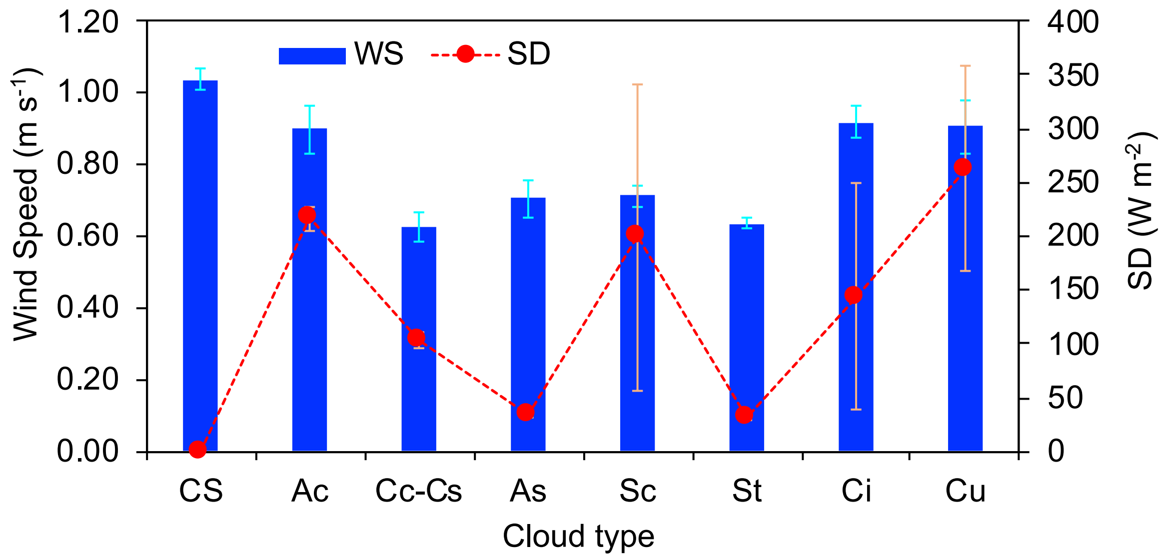

Figure A7. Wind speed (at ground) and SD for each cloud type.

<u>Specific Comment 28 (C7P1):</u> Lines 281-314 break up this huge paragraph.

<u>Answer to Specific Comment 28 (C7P1):</u> The section was rewritten (see answer to Specific Comments 21-25).

<u>Specific Comment 29 (C7P1):</u> Figure 2 comments: Fig 2's legend is inaccurate, there is no dashed line in the legend. In Fig 2g, colour the red line in the same way that the points in Fig 2h are coloured. Move the entire figure to the SI. Consider adding photographs to this figure.

Answer to Specific Comment 29 (C7P1): As reported in the answer to your Specific Comment 22, Figure 2 was improved by changing the legend: the nomenclature and assigning the coloured and dashed symbols to the proper lines. We also fixed panels (g) by indicating with coloured dashed lines the time periods to which the dots reported in the SD-R plot of panel (h) refer to. In Appendix B, a new Figure B1 shows the SD-R plot with the corresponding cloud pictures. Figure 2 instead has the aim to introduce the reader to Duchon and O'Malley (1999) method as required by the Specific comment 21.

Specific Comment 30 (C7P1): The results and discussion are too long, relative to the information content of the manuscript. The information is valuable but does not require extensive discussion.
As I mentioned above, the discussion is broken up by switching between the cloud analysis and the BC+BrC analysis. Start from the top and go down. Focus on the cloud effects before attributing HR to LAA afterwards and then to BC+BrC.

Answer to Specific Comment 30 (C7P1): We agree that the paper needs a shortening in the results and discussion with more concise and precise sentences. We also took care of the organization of the sections. We refer to the answer to the General Comment 2, which details all the changes reported in the manuscript.
We thank the reviewer for these comments which enabled us to improve the paper.

Specific Comment 31 (C8P1): The authors introduce direct, diffuse, and reflected irradiance yet do not present the data consistently. Some figures separate all 3. Some figures present direct, diffuse, and total (Fig 14). Some figures (Fig 13) present sums of 2, in various combinations. Some figures combine all 3 as "global irradiance" others combine all 3 as "total irradiance". Please, assess your data, choose one message, and present it clearly to your audience. Follow Harrison et al. 2008 in presenting the diffuse fraction unless your data support an alternative. Figure 9 is the only figure that suggests a difference between direct and reflected, but the impact on heating rate is unclear because Figure 13 changed the presentation strategy.

Answer to Specific Comment 31 (C8P1): We carefully read this comment. The rationale was to present the total HR behaviour and that of each of its components: HR_{dir}, HR_{dif}, HR_{ref}.
Thus, under this presentation strategy we have made the following changes:

- Figure 5a (now Figure 6a in the revised version of the manuscript) presents both the total HR (due to the contribution of direct, diffuse, and reflected irradiance to the actinic flux, see answer to your Specific Comment 19) and its components HR_{dir}, HR_{dif}, HR_{ref}. Figure 5b (now Figure 6b in the revised version of the manuscript) reports the irradiance measurements F_{glo}, F_{dir}, F_{dif}, F_{ref}. Please note that the global irradiance is related to the reflected one just via the surficial albedo effect. Please see also our reply to Specific Comment 19.
- Figure 6 (now Figure 9 in the revised version of the manuscript) was improved by adding to old Figure 6a the HR_{ref}/eBC and F_{ref}. Conversely, we added the total HR to Figure 6b. The figure is reported below as Figure A8.

- Figure 8a-d (now Figure 11a-d in the revised version of the manuscript) complies with the rationale of presenting the total HR/eBC behaviour and the each of its components: HR_{dir}/eBC, HR_{dif}/eBC, HR_{ref}/eBC. These are reported in panels a, b, c and d, respectively.
- Figure 9 (now Figure 12 in the revised version of the manuscript) presented only HR_{dir}, HR_{dif}, HR_{ref}. We also added the total HR. It is reported below as Figure A9.
- Figure 13a-d (now Figure 15a-d in the revised version of the manuscript) complies with the rationale of presenting the total HR behaviour and the each of its components: HR_{dir}, HR_{dif}, HR_{ref} for both BC and BrC. They are reported in panels a, b, c and d, respectively.

The diffuse fraction was introduced in Harrinson et al. (2008) mostly for cloud applications. In the present work, the splitting of the total HR in the each of its components (HR_{dir}, HR_{dif}, HR_{ref}) reflects not only a radiative behavior, but a synergy with the light-absorbing aerosol features. The contribution of the HR_{dif} to the total is discussed in the results and discussion sections.

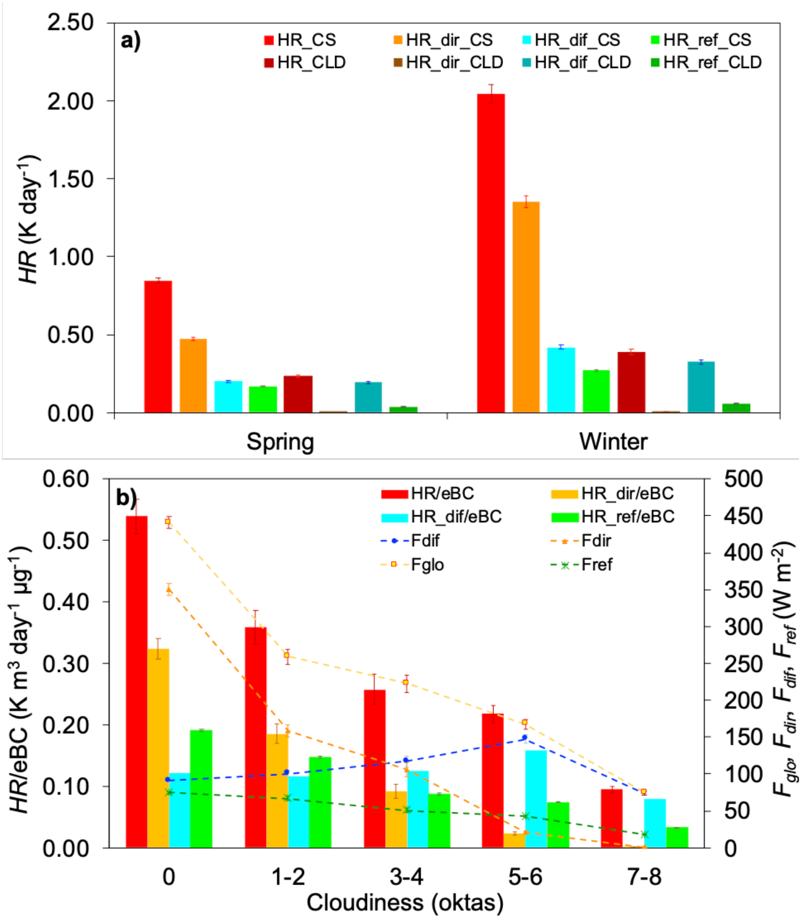

Figure A8 (Figure 9 in the revised version of the manuscript). Monthly averaged values of: a) HR values and their direct, diffuse and reflected components (HR_{dir}, HR_{dif} and HR_{ref}) during winter and spring both in clear sky (CS; oktas=0) and cloudy (CLD; oktas=7-8) conditions; b) HR/eBC values together with their direct, diffuse and reflected components (HR_{dir}/eBC, HR_{dif}/eBC and HR_{ref}/eBC), the direct, diffuse and reflected irradiance (F_{dir}, F_{dir} and F_{dif}) and the global one (F_{glo}).

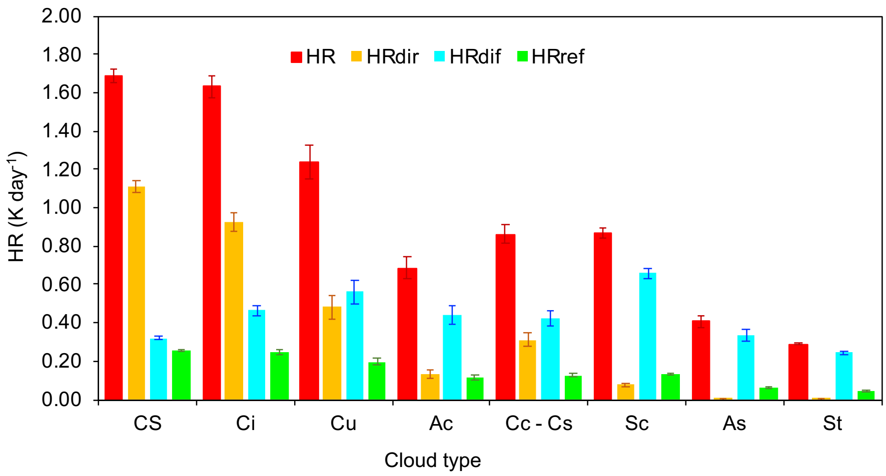

Figure A9 (Figure 12 in the revised version of the manuscript). Average values of total HR, HR_{dir}, HR_{dif} and HR_{ref} for different cloud types.

<u>Specific Comment 32 (C8P1):</u> The conclusions are similarly confused. Why are different cloud types discussed in detail when Figure 10 and 15 clearly show that the key predictor is oktas and not cloud type? Only high clouds (cirrus, cirrocumulus, and cirrostratus) do not follow this trend, presumably because they are well above the aerosol layers.

<u>Answer to Specific Comment 32 (C8P1):</u> Figure 10 and 15 relate the HR variation (compared to CS values) with respect to the oktas induced by a different cloud types. Figure A2c (in the answer to the General Comment 2) reports a linear relationship between HR and the cloudiness (expressed in oktas) without accounting for the cloud types responsible for such sky coverage. The linear relationship was very good (R^2=0.935) but slightly lower than the similar relationship reported in Figure 10 (R^2=0.963; now Figure 13 in the revised version of the paper). This strengthens the synergy between the fraction of sky covered by clouds and cloud type influencing the transmission of shortwave radiation. In addition to this, the cloudiness (oktas) is a non-linear function of the cloud type, as cloud types are related to the meteorological pattern: e.g. highly persistent stratiform clouds generate cloudy weather in conditions with lower wind. Figure A7 (answer to the Specific Comment 27) reports an average ground wind speed of 0.64±0.02 m s^{-1} in stratus conditions, lower than the 0.92±0.04-1.04±0.03 m s^{-1} in cirrus-clear sky conditions. As a result (Figure A10 added below and appearing as Figure 8 in the main body of the manuscript) the cloudiness associated with different cloud types starts at cirrus clouds (0.51±0.05 oktas) and increases to stratus clouds (7.20±0.04 oktas). This is in agreement with the recent work of Bartoszek et al. (2020) who associated higher cloudiness level with the presence of stratiform clouds. Moreover, they observed an increase in sunshine duration with a decrease in the incidence of low-level clouds, including mainly stratiform clouds underling the connection between cloudiness-cloud type and shortwave radiation.
We added this discussion to section 3.1 in the manuscript.
Finally, Figures 10 and 15 do not show any significant deviation of cirrus, cirrocumulus, and cirrostratus from the linear trend.

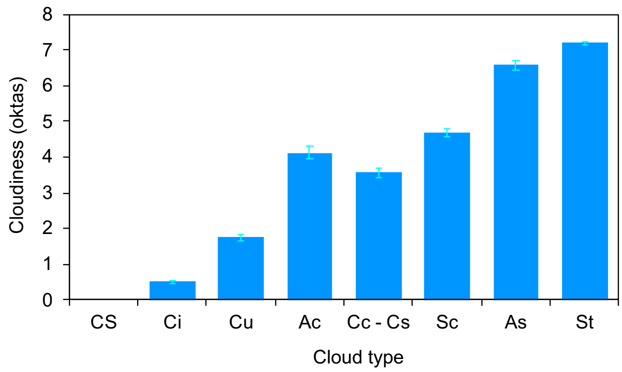

Figure A10 (now Figure 8 in the revised version of the manuscript). Cloudiness associated to each cloud type.

<u>Specific Comment 33 (C8P1):</u> I do not see any support for the final conclusion that the cloud impact affected HR of BC more than of BrC. The absolute value of the BC HR was higher initially, so it would naturally change more. My interpretation of the authors' results is that there is no need to attribute cloud types in future work, and that cloud height data combined with diffuse fraction (Harrison et al. 2008) may be sufficient. If this work is to be extended to other monitoring sites the authors must address this point explicitly. Simpler measurements are more likely to be adopted by others.

<u>Answer to Specific Comment 33 (C8P1):</u> We thank the reviewer for this comment which give us the opportunity to extend our previous answer, and to improve the conclusion of the present work. As answered to your Specific Comment 32, a relationship between cloud-type and cloudiness is present, moreover figure A2c showed that cloudiness alone is a good predictor of light-absorbing aerosol HR behaviour, but the association is closer when using cloud type (Figure 10, now Figure 13). In fact, as detailed in Tapakis and Charalambides (2013), in order to model the incoming irradiance, not only the effect of the cloudiness (in oktas) has to be taken into account, but also the cloud type, as not all clouds have the same effect on irradiance. There are different types of clouds with different dimensions, opacity and properties affecting the incoming irradiance differently. We added these considerations to section 3.2.2.

However, we agree that the cloudiness is a simpler parameter that can be likely adopted by others. Thus, we deepened the analysis concerning Figure 15 (now Figure 16) and concluded section 3.3 as follows:

"Overall, the derived linear regressions indicate a decrease of ~12% per oktas for both HR_{BC} and HR_{BrC} (with high R^2: 0.958 and 0.963, respectively). In details, the respective decreases of HR_{BC} and HR_{BrC} were -11.8±1.2% and -12.6±1.4% per okta, these values not being statistically different. We show that, while BC and BrC have different optical properties and wavelength dependence of absorption, their HR normalized to absorption, changed without any statistical difference as a function of cloudiness and cloud type. This simplifies the models and reduces the number of details needed to be considered: once HR_{BC} and HR_{BrC} are determined in clear sky conditions, their dependence on the cloudiness can be determined from the simple reduction of the HR normalized to the absorption coefficient (about 12% for both species, once dominant cloud type is known).

However, it noteworthy that normalized HR_{BrC} values in Figure 16 were always greater or equal to the corresponding ones of BC (even if 95% confidence interval bands overlapped). A possible explanation can be the synergic effect between the different spectral absorption of BC and BrC and the influence of clouds on the energy of the impinging radiation; this is detailed in the Supplement (section: The role of average photon energy on the HR of BC and BrC). This feature needs further investigation in other seasons and elsewhere the world where the prevailing clouds type and the light absorption by BrC might be different."

References

Arnott, W.P., Moosmueller, H., Rogers, C.F., Jin, T., Bruch, T.: Photoacoustic spectrometer for measuring light absorption by aerosol: instrument description, Atmospheric Environment, 33, 2845-2852, https://doi.org/10.1016/S1352-2310(98)00361-6, 1999,

Bartlett, J. S., Ciotti, Á. M., Davis, R. F. and Cullen, J. J.: The spectral effects of clouds on solar irradiance, Journal of Geophysical Research: Oceans, 103(C13), 31017–31031, doi:10.1029/1998jc900002, 1998.

Bartoszek, K., Matuszko, D. and Soroka, J.: Relationships between cloudiness, aerosol optical thickness, and sunshine duration in Poland, Atmospheric Research, 245(April), 105097, doi:10.1016/j.atmosres.2020.105097, 2020.

Bikkina, S., Sarin, M.M.: Light absorbing organic aerosols (brown carbon) over the tropical Indian Ocean: impact of biomass burning emissions. Environ. Res. Lett., 8 (4), 044042, 2013.

Bond, T. C., Anderson, T. L., Campbell, D.: Calibration and intercomparison of filter-based measurements of visible light absorption by aerosols. Aerosol Sci. Tech., 30(6), 582–600, 1999.

Calbó, J. and Sabburg, J.: Feature extraction from Whole-sky ground-based images for cloud-type recognition, Journal of Atmospheric and Oceanic Technology, 25(1), 3–14, doi:10.1175/2007JTECHA959.1, 2008.

Carbone, C., Decesari, S., Mircea, M., Giulianelli, L., Finessi, E., Rinaldi, M., Fuzzi, S., Marinoni, A., Duchi, R., Perrino, C., Sargolini, T., Vardè, M., Sprovieri, F., Gobbi, G. P., Angelini, F., and Facchini, M. C.: Size-resolved aerosol chemical composition over the Italian Peninsula during typical summer and winter conditions, Atmos. Environ., 44, 5269–5278, doi:10.1016/j.atmosenv.2010.08.008, 2010.

Cogliati, S., Rossini, M., Julitta, T., Meroni, M., Schickling, A., Burkart, A., Pinto, F., Rascher, U., Colombo, R.: Continuous and long-term measurements of reflectance and sun-induced chlorophyll fluorescence by using novel automated field spectroscopy systems. Remote Sensing of Environment, 164, 270–281, http://dx.doi.org/10.1016/j.rse.2015.03.027, 2015.

Collaud Coen M., Weingartner E., Apituley A., Ceburnis D., Fierz-Schmidhauser R., Flentje H., Henzing J.S., Jennings S.G., Moerman M., Petzold A., Schmid O., and Baltensperger U. Minimizing light absorption measurement artifacts of the Aethalometer: evaluation of five correction algorithms. Atmos. Meas. Tech., 3, 457–474, 2010.

Costa-Surós, M., Calbó, J., González, J. A. and Martin-Vide, J.: Behavior of cloud base height from ceilometer measurements, Atmospheric Research, 127, 64–76, doi:10.1016/j.atmosres.2013.02.005, 2013.

Drinovec, L., Mocnik, G., Zotter, P., Prevot, A. S. H., Ruckstuhl, C., Coz, E., Rupakheti, M., Sciare, J., Muller, T., Wiedensohler, A. and Hansen, A. D. A.: The "dual-spot" Aethalometer: An improved measurement of aerosol black carbon with real-time loading compensation, Atmospheric Measurement Techniques, 8(5), 1965–1979, doi:10.5194/amt-8-1965-2015, 2015.

Duchon, C.E., O'Malley, M.: Estimating Cloud Type from Pyranometer Observations. J. App. Meteorology, 38, 132–141, 1999.

Feister, U., Cabrol, N., and Häder, D.: UV Irradiance Enhancements by Scattering of Solar Radiation from Clouds, Atmosphere, 6, 1211-1228, 10.3390/atmos6081211, 2015.

Ferrero, L., Castelli, M., Ferrini, B.S., Moscatelli, M., Perrone, M.G., Sangiorgi, G., Rovelli, G., D'Angelo, L., Moroni, B., Scardazza, F., Mocnik, G., Bolzacchini, E., Petitta, M., Cappelletti, D.: Impact of Black Carbon Aerosol over Italian basin valleys: high resolution measurements along vertical profiles, radiative forcing and heating rate. Atmos. Chem. Phys., 14, 9641–9664, 2014.
Ferrero L., Močnik G., Cogliati S., Gregorič A., Colombo R., Bolzacchini E.: Heating Rate of Light Absorbing Aerosols: Time-Resolved Measurements, the Role of Clouds, and Source Identification. Environ. Sci. Tech., 52, 3546−3555, DOI: 10.1021/acs.est.7b04320, 2018.
Galli, C., Nardino, M., Levizzani, V., Rizzi, R. and Georgiadis, T.: Radiative energy partition and cloud radiative forcing at a Po valley site, Atmospheric Research, 72(1–4), 329–351, doi:10.1016/j.atmosres.2004.03.022, 2004.
Gao, R. S., Hall, S. R., Swartz, W. H., Schwarz, J. P., Spackman, J. R., Watts, L. A., Fahey, D. W., Aikin, K. C., Shetter, R. E. and Bui, T. P.: Calculations of solar shortwave heating rates due to black carbon and ozone absorption using in situ measurements, Journal of Geophysical Research Atmospheres, 113(14), 14–19, doi:10.1029/2007JD009358, 2008.
García V., Mollineda R.A., Sánchez J.S.: Index of Balanced Accuracy: A Performance Measure for Skewed Class Distributions. In: Araujo H., Mendonça A.M., Pinho A.J., Torres M.I. (eds) Pattern Recognition and Image Analysis. IbPRIA 2009. Lecture Notes in Computer Science, vol 5524. Springer, Berlin, Heidelberg. https://doi.org/10.1007/978-3-642-02172-5_57, 2009.
Harrison, R. G., Chalmers, N. and Hogan, R. J.: Retrospective cloud determinations from surface solar radiation measurements, Atmospheric Research, 90(1), 54–62, doi:10.1016/j.atmosres.2008.04.001, 2008.
Huertas-Tato, J., Rodríguez-Benítez, F. J., Arbizu-Barrena, C., Aler-Mur, R., Galvan-Leon, I. and Pozo-Vázquez, D.: Automatic Cloud-Type Classification Based On the Combined Use of a Sky Camera and a Ceilometer, Journal of Geophysical Research: Atmospheres, 122(20), 11,045-11,061, doi:10.1002/2017JD027131, 2017.
Kingbright: APT1608SRCPRV, 1.6 x 0.8 mm SMD Chip LED Lamp - Specifications, [online] Available from: https://www.kingbrightusa.com/images/catalog/SPEC/APT1608SRCPRV.pdf, (last access: 11 November 2020), 2018.
Koren, I., Kaufman, Y.J., Remer, L.A., Martins, J.V.: Measurments of the effect of amazon smoke on inhibition of cloud formation. Science, 303, 1342-1345, 2004.
Laskin, A., Laskin, J. and Nizkorodov, S. A.: Chemistry of Atmospheric Brown Carbon, Chemical Reviews, 115(10), 4335–4382, doi:10.1021/cr5006167, 2015.
Liou K.N.: An Introduction to Atmospheric Radiation, Second Edition. INTERNATIONAL GEOPHYSICS SERIES, Volume 84, Academic Press, 2007.
Liousse, C., Cachier, H., Jennings, S. G.: Optical and thermal measurements of black carbon aerosol content in different environments: Variation of the specific attenuation cross-section, sigma (σ). Atmospheric Environment, 27(8), 1203–1211, 1993.
Madonna, F., Amato, F., Vande Hey, J., and Pappalardo, G.: Ceilometer aerosol profiling versus Raman lidar in the frame of the INTERACT campaign of ACTRIS, Atmos. Meas. Tech., 8, 2207–2223, https://doi.org/10.5194/amt-8-2207-2015, 2015.
Massabò, D., Caponi, L., Bernardoni, V., Bove, M.C., Brotto, P., Calzolai,, G., Cassola, F., Chiari, M., Fedi, M.E., Fermo, P., Giannoni, M., Lucarelli, F., Nava, S., Piazzalunga, A., Valli, G., Vecchi, R., Prati, P.: Multi-wavelength optical determination of black and brown carbon in atmospheric aerosols, Atmos. Environ., 108, 1-12, 2015.
Mims, F. E., and Frederick, J. E.: Cumulus clouds and UV-B, Nature, 371, 291, 1994.
Moosmüller, H., Chakrabarty, R. K., Ehlers, K. M. and Arnott, W. P.: Absorption Ångström coefficient, brown carbon, and aerosols: Basic concepts, bulk matter, and spherical particles, Atmospheric Chemistry and Physics, 11(3), 1217–1225, doi:10.5194/acp-11-1217-2011, 2011.
Perlwitz, J. and Miller, R. L.: Cloud cover increase with increasing aerosol absorptivity: A counterexample to the conventional semidirect aerosol effect, Journal of Geophysical Research Atmospheres, 115(8), 1–23, doi:10.1029/2009JD012637, 2010.

Petzold, A., Ogren, J. A., Fiebig, M., Laj, P., Li, S.-M., Baltensperger, U., Holzer-Popp, T., Kinne, S., Pappalardo, G., Sugimoto, N., Wehrli, C., Wiedensohler, A., and Zhang, X.-Y.: Recommendations for reporting "black carbon" measurements, Atmos. Chem. Phys., 13, 8365–8379, https://doi.org/10.5194/acp-13-8365-2013, 2013.
Ricciardelli, E., Romano, F. and Cuomo, V.: Physical and statistical approaches for cloud identification using Meteosat Second Generation-Spinning Enhanced Visible and Infrared Imager Data, Remote Sensing of Environment, 112(6), 2741–2760, doi:10.1016/j.rse.2008.01.015, 2008.
Sandradewi, J., Prevot, A.S.H., Weingartner, E., Schmidhauser, R., Gysel, M., Baltensperger, U. A study of wood burning and traffic aerosols in an Alpine valley using a multi-wavelength Aethalometer. Atmos. Environ, 42, 101–112, 2008b.
Schmid, O., Artaxo, P., Arnott, W. P., Chand, D., Gatti, L. V., Frank, G. P., Hoffer, A., Schnaiter, M., and Andreae, M. O.: Spectral light absorption by ambient aerosols influenced by biomass burning in the Amazon Basin. I: Comparison and field calibration of absorption measurement techniques, Atmos. Chem. Phys., 6, 3443–3462, doi:10.5194/acp-6-3443-2006, 2006.
Seinfeld, J. H. and Pandis, S. N.: Atmos. Chem. Phys. – From air pollution to climate change. Wiley-Interscience edition, second edition, 2006.
Shamjad, P. M., Tripathi, S. N., Pathak, R., Hallquist, M., Arola, A., Bergin, M. H.: Contribution of Brown Carbon to Direct Radiative Forcing over the Indo-Gangetic Plain. Environ. Sci. Technol., 49 (17), 10474–10481, 2015.
Singh, M. and Glennen, M.: Automated ground-based cloud recognition, Pattern Analysis and Applications, 8(3), 258–271, doi:10.1007/s10044-005-0007-5, 2005.
Sun, H., Biedermann, L. and Bond, T. C.: Color of brown carbon: A model for ultraviolet and visible light absorption by organic carbon aerosol, Geophysical Research Letters, 34(17), 1–5, doi:10.1029/2007GL029797, 2007.
Tapakis, R. and Charalambides, A. G.: Equipment and methodologies for cloud detection and classification: A review, Solar Energy, 95, 392–430, doi:10.1016/j.solener.2012.11.015, 2013.
Tian, P., Liu, D., Zhao, D., Yu, C., Liu, Q., Huang, M., Deng, Z., Ran, L., Wu, Y., Ding, S., Hu, K., Zhao, G., Zhao, C. and Ding, D.: In-situ vertical characteristics of optical properties and heating rates of aerosol over Beijing, Atmospheric Chemistry and Physics Discussions, 1–33, doi:10.5194/acp-2019-780, 2019.
Wang, G. C., Urquhart, B. and Kleissl, J.: Cloud base height estimates from sky imagery and a network of pyranometers, Solar Energy, 184(March), 594–609, doi:10.1016/j.solener.2019.03.101, 2019.
Weingartner, E., Saathoff, H., Schnaiter, M., Streit, N., Bitnar, B., Baltensperger, U.: Absorption of light by soot particles: determination of the absorption coefficient by means of aethalometers. Journal of Aerosol Science, 34 (10), 1445–1463, 2003.
Wiegner, M. and Geiß, A.: Aerosol profiling with the Jenoptik ceilometer CHM15kx, Atmos. Meas. Tech., 5, 1953–1964, doi:10.5194/amt-5-1953-2012, 2012.
Yang, J., Min, Q., Lu, W., Yao, W., Ma, Y., Du, J., Lu, T. and Liu, G.: An automated cloud detection method based on the green channel of total-sky visible images, Atmospheric Measurement Techniques, 8(11), 4671–4679, doi:10.5194/amt-8-4671-2015, 2015.
Ylivinkka, I., Kaupinmäki, S., Virman, M., Peltola, M., Taipale, D., Petäjä, T., Kerminen, V. M., Kulmala, M. and Ezhova, E.: Clouds over Hyytiälä, Finland: An algorithm to classify clouds based on solar radiation and cloud base height measurements, Atmospheric Measurement Techniques, 13(10), 5595–5619, doi:10.5194/amt-13-5595-2020, 2020.

Response to Reviewer#2

We thank the reviewer for his or her helpful comments and insight. We respond to the general and specific points below. All the comments are addressed in the revised manuscript. A tracked version of the manuscript changes is present at the bottom of the answers.

GENERAL COMMENTS

General Comment 1: This study explores the effect of clouds on heating rates driven by absorbing aerosols. They do so using observations and measurements sorted per different cloud types and coverage, separating the effects of black vs. brown carbon.
The data is collected in U9 sampling site in Milan which is a superstation that contains instruments to measure radiation, filter collecting aerosols that are analysed for their optical properties, meteorological station and a Lidar.
The topic of the paper is important. Exploring heating rates for different aerosol types under different cloud conditions will provide a very important information for aerosol effect on climate, and clouds. As the authors pointed out direct measurements of heating rates in different cloud conditions are quite uncommon.
The basic cloud classification makes sense in particularly as they added Lidar information for the clouds base. The results clearly show how cloudiness can affect heating rates and the bland between the radiation types.

Answer to General Comment 1: We thank the reviewer for the comment which remarks on the big effort put in this work, and the quality of both the methodological approach and of the obtained experimental results.

General Comment 2: One drawback of the paper is that it is very technical and not always easy to follow. Even if one understands the radiative transfer concepts, the physical assumptions and results are buried in the technicalities. It contains many technical terms that may appeal only to the instrumentation experts. Being familiar with radiation transfer concepts, I'm sure that there is a better way to describe the measurements and analyses such that a non-expert in the instrumentation could better enjoy it. The concertation of acronyms is high. It is hard to remember all of them and some that appear again later in the text force the reader to look back for their meaning and it disturbs the reading. On the other hand, some basic concepts that are key in this study are not well explained. The authors send the reader to read many other references for the basic methods and the equations. I believe that such study could be more of a standalone in which the basic physics is explained in a better way using less technical jargon.

Answer to General Comment 2: Thank you very much for this comment which enabled us to improve the scientific quality and presentation of the paper. Reviewer#1 asked for a shortening of the results and discussion as well as an improvement of the logical steps in the methods sections. Thus, the paper was substantially changed and improved to make it more readable and easier to follow. We have rearranged the sections to improve readability, especially the results and discussion section in the manuscript:

- In section 3.1 we introduce the environmental context of the measurement campaign and the magnitude of the observed parameters ("eBC, irradiance, HR and cloud data"). We separated the cloud analysis from the light-absorbing aerosol analysis. All the cloud analysis is presented to the reader in this section.
- The old sections 3.2 and 3.3 were re-written in agreement with the changes performed in section 3.1, and merged in a new section 3.2 with three sub-sections. The first discusses the influence of clouds in term of cloudiness, the second the influence of cloudiness on the diurnal pattern of the HR while the third the cloud type effect on the total HR only (sections 3.2.1, 3.2.2 and 3.2.3, respectively).
- Finally, the old section 3.4 (now section 3.3) was completely re-written merging and shortening the two original sub-sections 3.4.1 and 3.4.2. We discuss the role of cloudiness, cloud type and their effect on the HR apportioned with respect to BC and BrC fractions. The discussion concerning the role of average photon energy was moved to the supplemental material.

To simplify the radiative transfer concepts used in the HR assessment, we have reduced the number of equations in the text. Instead of Eqs. 1-3 we now present only 2 equations in the main body of the manuscript moving the demonstration to the supplemental material. The HR assessment is presented as follows:
"The heating rate is determined from the air density (ρ, kg m^{-3}), the isobaric specific heat of dry air (C_p, 1005 J kg^{-1} K^{-1}) and the radiative power absorbed by aerosol per unit volume of air (W m^{-3}) describing the interaction between the radiation (either direct from the sun, diffuse by atmosphere and clouds, and reflected from the ground) and the LAA (BC and BrC in Milan). The HR is determined as follows (Ferrero et al., 2018):

$$HR = \frac{1}{\rho C_p} \cdot \sum_{dir,dif,ref} \int_{\theta=0}^{\theta=\pi/2} \int_{\lambda=300}^{\lambda=3000} \frac{F_{dir,dif,ref}(\lambda,\theta)}{\cos(\theta)} b_{abs}(\lambda) d\lambda d\theta \tag{A1}$$

where the subscripts *dir*, *dif* and *ref* refer to the direct, diffuse and reflected components of the spectral irradiance F of wavelength λ impinging on the LAA with a zenith angle θ (from any azimuth).
Under the isotropic and Lambertian assumptions (as used in Ferrero et al., 2018) equation 2 can be solved becoming:

$$HR = HR_{dir} + HR_{dif} + HR_{ref} =$$
$$= \frac{1}{\rho C_p} \cdot \left[\frac{1}{\cos(\theta_z)} \int_\lambda F_{dir}(\lambda)\, b_{abs}(\lambda)\, d\lambda + 2\int_\lambda F_{dif}(\lambda)\, b_{abs}(\lambda)\, d\lambda + 2\int_\lambda F_{ref}(\lambda)\, b_{abs}(\lambda)\, d\lambda \right] \tag{A2}$$

where θ_z refers to the solar zenith angle, while $F_{dir}(\lambda)$, $F_{dif}(\lambda)$ and $F_{ref}(\lambda)$ are the spectral direct, diffuse and reflected irradiances. Eqs. 2 and 3 are related to the concept of actinic flux (Tian et al., 2020; Gao et al., 2008; Liu, 2007); an extended description, as well as its demonstration is detailed in the Supplement."

We also introduced the indices *dir*, *dif*, *ref* to avoid the readers' confusion about the original "n" symbol which referred to each of the different kinds of impinging radiation.
In keeping with your suggestion, we removed many acronyms and technical terms whenever possible.
In agreement with a suggestion from reviewer#1, we prepared a list of acronyms and symbols (used in the manuscript) which was added in the new section Appendix A at the end of the paper.

In line with the suggestion to reference more papers, we added in the Supplemental Material the alternative notation of equations 1 as follows:

$$HR = \frac{1}{\rho C_p} \cdot \int_\lambda AF(\lambda) b_{abs(\lambda)} d\lambda \quad \text{(A3)}$$

where AF(λ) represents the actinic flux, that is the total spectral flux of photons per unit area and wavelength interval available to molecules/aerosol at a particular point in the atmosphere. The radiative flux from all directions onto a volume of air is called the actinic flux (Seinfeld and Pandis, 2006).
The actinic flux (actually a flux density) consists of three components: direct solar radiation, diffuse radiation originating from scattering in the atmosphere, and diffuse radiation originating from reflection at the earth's ground surface. Accordingly, the actinic flux at a particular point in the atmosphere is calculated by integrating the spectral radiance over all directions in space. The actinic flux must be distinguished from the spectral irradiance, which is the hemispherically integrated radiance weighted by the cosine of the angle of incidence, and represents the photon flux per unit area through a plane surface. A more exhaustive description can be found in Liou (2007), Tian et al. (2020) and Gao et al. (2008). We added these references to the method section 2.2 of the manuscript and deepened the topic in the Supplemental material.

SPECIFIC COMMENTS

<u>Specific Comment 1 (SC1)</u>: The aerosols that are collected at the station level serve as the only aerosol measurement and the basic assumption is that the filters collected at the station represent the whole boundary layer and therefore the heating rate is uniform for the layer below the clouds. I wonder how general this assumption is? This is always a key question of any work that try to link measurements near the surface to the atmospheric column. Is it always well mixed? Can the authors show that there is no dependency on the time of the day or the winds or the meteorology in general? Is it true for all seasons? For all cloud types? Moreover, if they have Lidar there can't they validate this assumption using the Lidar information. It would be nice to see uniform backscatter below the clouds to strengthen this basic assumption. The radiation measurements are collected in the station and are product of electromagnetic radiation interaction with the whole atmospheric column. What about the contribution of aerosols above the boundary layer. Is it assumed to be canceled by the proposed method? Or is it assumed to be negligible? If not, how such aerosols can affect the results?

<u>Answer to Specific Comment 1 (SC1):</u> Thank for all your questions. They are related to the methodology. In order to properly answer them it is necessary to address the following points: 1) the advantages and limitations of the applied methodology (relating to the measurements and derivation of the heating rate HR) and 2) the environmental context of the measuring site in the Po Valley (addressing the representativeness).

Methodology advantages and limitation

The most important advantages/limitations of the new method are resumed here. The first consideration is that the ADRE (and thus the HR) is the vertical derivative of the aerosol direct radiative effect (ADRE=dDRE/dz; see Ferrero et al. (2018)); we provide a detailed analysis at the end of the answer (*Methodology details and demonstration*). Thus, both the ADRE and the HR become independent from the thickness (Δz) of the investigated atmospheric layer as happens for routine atmospheric pollution measurements (i.e. BC, PM and particle number concentrations). The most important *advantages* in terms of HR measurements are:

- no radiative transfer assumptions are needed (i.e. clear sky situation), the input parameters into equations A1 and A2 are all measured,
- measurements of the spectral irradiance and the absorption coefficient are carried out at high time resolution, allowing to follow the HR dynamic with same temporal resolution,
- measurements of the spectral irradiance, the absorption coefficient and thus the HR are carried out in any sky conditions, enabling to investigate the impact by the cloud layers on the near-surface HR.

The most important *limitation* is the following:

- as both the ADRE and the HR are independent of the thickness (Δz) of the investigated atmospheric layer, they refer to the vertical location of the atmospheric layer in which both the ADRE and the HR are experimentally determined. In the present work, they are determined in the near-surface atmospheric layer.

It is noteworthy to consider the advantages that the new method allows to obtain: experimental measurement (not estimations) of ADRE and HR continuous in time with a high time resolution as a function of sources, species of light absorbing aerosol, and cloud cover. The use of the vertical derivative of the Direct Radiative Effect allows us to obtain a temporal continuity of ADRE and HR but "paying" it with the loss of vertical information.

Due to your question, we first clarified these points in the methodological section 2.2 expanding the sentence (lines 245-247 in the submitted version of the manuscript):

"As already pointed out in Ferrero et al. (2018), it is worth recalling that in the present method (equation 1), the HR is independent of the investigated atmospheric aerosol layer thickness."

and at lines 250-254:

"The main advantage of the new method to quantify the impact of clouds on the light-absorbing aerosol HR is that it allows to obtain experimental measurement (not estimations) of HR, which are continuous in time with a high time resolution, and resolved in terms of sources, species of light-absorbing aerosol, cloud cover, and cloud types."

Environmental context of HR measurements

In this section we address the representativeness of the HR determination at ground and answer the Reviewer's questions. As reported in the submitted version of the manuscript at lines 247-250: "BC and HR vertical profiles data previously collected both at the same site and in other basin valley sited (Ferrero et al., 2014) revealed that ADRE and HR were constant inside the mixing layer. The methodology is therefore believed to be valid for applications in atmospheric layers below clouds, assuming that near-surface measurements are representative of the whole mixing layer." This assumption is the core of your question.

The aim of the paper is the investigation of the impact of cloudiness and cloud-type on the HR induced by light absorbing aerosol. Ground-based highly time-resolved HR data are suitable to reach this goal – we need to introduce the representativeness shown in Ferrero et al. (2014) over Milan.

We performed combined in-situ and remote vertical profile measurements in Milan with tethered balloons and a lidar (in cooperation with the ISAC-CNR of Rome) since 2005. The collected data shows a homogeneous distribution of aerosol concentration within the mixing layer. Figure A1 reports averaged wintertime balloon profiles (PM concentrations and extinction coefficient) and lidar range corrected signal for Milan (Ferrero et al., 2019).

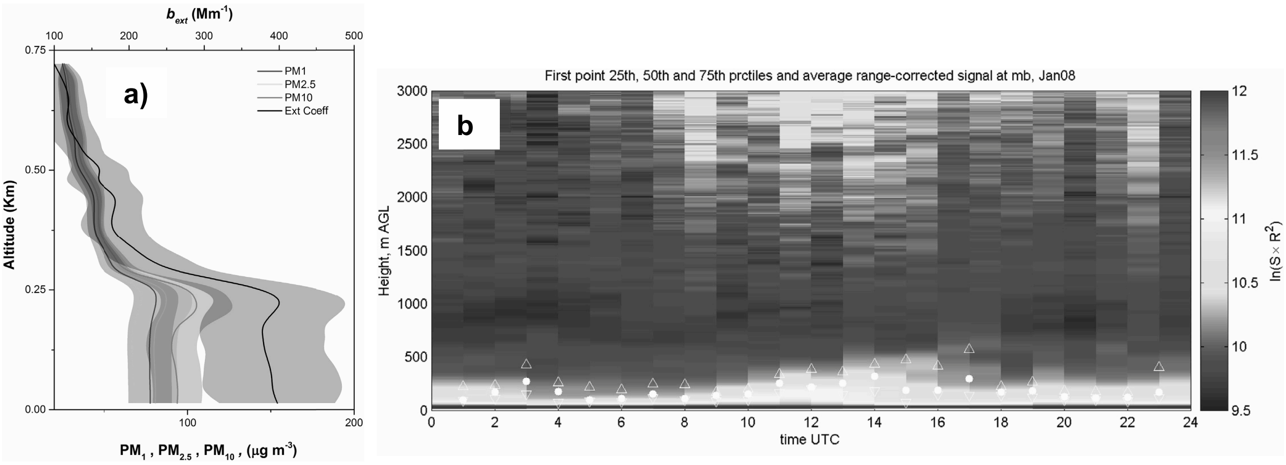

Figure A1. Milan averaged wintertime a) balloon profiles of PM_1, $PM_{2.5}$ and PM_{10} and extinction coefficient b) lidar range corrected signal. Data for the present figure are from Ferrero et al. (2019).

The same condition was verified by the lidar-ceilometer data collected during the present campaign (Figure A2, here below).

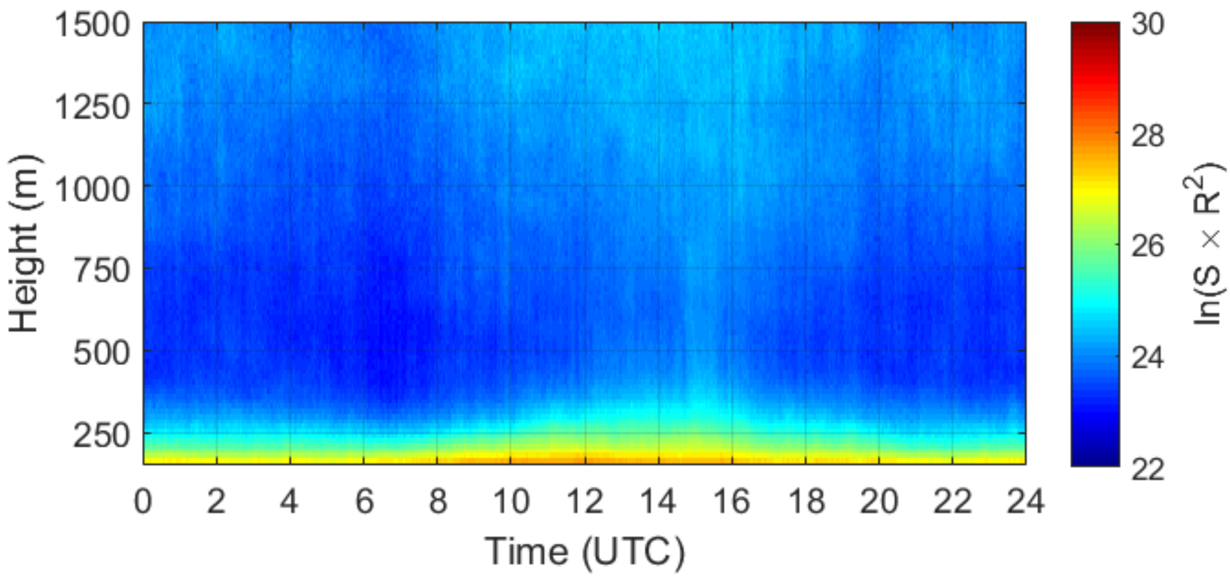

Figure A2. Milan averaged wintertime lidar range corrected signal (SxR^2) during the campaign presented in the manuscript.

Vertical profiles data reported in Figure A1 and A2 experimentally verify the assumption "that near-surface measurements are representative of the whole mixing layer" in wintertime in Milan.
Figures A1b and A2 show a typical mixing layer height diurnal behavior in wintertime conditions, with the mixing layer height not exceeding 500 m above ground. The same was previously retrieved from the vertical gradient of tethered balloon aerosol profiles (Ferrero et al., 2010; Figure A3). Within the mixing layer, aerosol concentrations were uniform (as reported in Figure A1) along each time of the day.

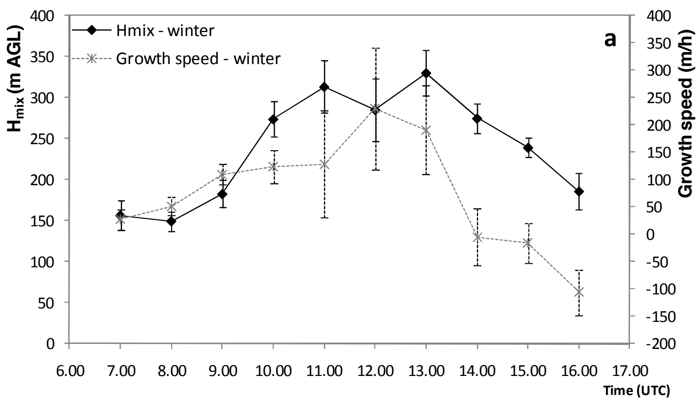

Figure A3. Diurnal variation of the mixing layer height. Plot taken from Figure 4, Ferrero et al. (2010).

Finally, in Ferrero et al. (2014), we explored the vertical behavior of the light absorbing aerosol HR. It is reported here below in Figure A4.

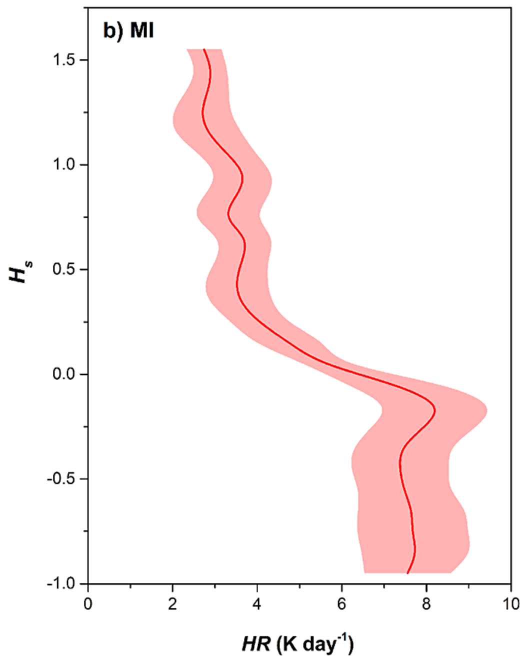

Figure A4. Heating rate (HR) vertical profile, with the normalized height H_s = -1 at ground level and 0 at the top of the mixing layer. Plot taken from Figure 10, Ferrero et al. (2014).

Figure A4 shows that the HR can be considered constant inside the mixing layer, making near-surface measurements representative of the mixing layer height.

Finally, as shown by both Figure A1 and A2 and as reported in Ferrero et al. (2019) the collected wintertime vertical data in Milan showed that 87.0% of AOD (aerosol optical depth) signal was contributed to within the mixing layer, 8.2% in the residual layer and 4.9% in the free troposphere. The impact of clouds on the incoming radiation reaching the mixing layer is therefore dominant.

We added Figure A2 in Supplemental Material and the aforementioned consideration in section 2.2. Here below, as written at the beginning of this answer, the method details and demonstration.

Methodology details and demonstration (Ferrero et al., 2018)

We start from the radiative transfer concept of the instantaneous aerosol Direct Radiative Effect (DRE; W m^{-2}) which can be quantified as the change in the net radiative flux between the atmospheric conditions with aerosols (*aer*) and without the aerosols ($Q_{aer}(z)$ and $Q_0(z)$, respectively) in the atmosphere across the surface at altitude z:

$$DRE(z) = Q_{aer}(z) - Q_0(z) \tag{A4}$$

Considering an atmospheric layer of thickness Δz, the difference between the *DRE* at the top and the bottom of this atmospheric layer represents the instantaneous radiative power density absorbed by the aerosol (ΔDRE; W m^{-2}):

$$\Delta DRE = DRE(z + \Delta z) - DRE(z) \tag{A5}$$

From ΔDRE, the instantaneous heating rate (*HR*; K day^{-1}) of the same atmospheric layer can be computed as follows:

$$HR = \frac{\partial T}{\partial t} = -\frac{g}{C_p}\frac{\Delta DRE}{\Delta p} \tag{A6}$$

where $\partial T/\partial t$ represents the instantaneous *HR*, g is the gravitational acceleration constant, C_p (1005 J kg^{-1} K^{-1}) is the isobaric specific heat of dry air, Δp is the pressure difference between the top and the bottom of the considered layer.

A more useful definition of the *HR* is based on the thickness of the atmospheric layer (Δz), and can be obtained introducing the hydrostatic equation ($dp = -\rho g dz$) into Eq. A6:

$$HR = \frac{\partial T}{\partial t} = \frac{1}{\rho C_p}\frac{\Delta DRE}{\Delta z} \tag{A7}$$

where ρ represents the air density (kg m^{-3}). The last term of Eq. A7 ($\Delta DRE/\Delta z$) represents the radiative power absorbed by the aerosol for unit volume of the atmosphere (W m^{-3}) and is defined as the absorptive direct radiative effect (*ADRE*) of light-absorbng aerosols. The *ADRE* is the vertical spatial derivative of the *DRE* (*dDRE/dz*). Hence, the *HR* becomes:

$$HR = \frac{1}{\rho C_p} \cdot ADRE \tag{A8}$$

Thus, any method able to determine the *ADRE* at high time resolution will produce continuous highly time-resolved time series of *HR*.

Let us consider a near-surface atmospheric layer of thickness Δz on which direct or diffuse or reflected monochromatic radiation ray $F_n(\lambda,\theta)$ of wavelength λ strikes with a zenith angle θ. We use the subscript n to denote the type of radiation: direct, diffuse or reflected. The amount of radiation absorbed by the aerosol within the present layer is as follows:

$$\Delta DRE_n(\lambda,\theta) = F_n(\lambda,\theta)(1-\omega(\lambda))\left(1-e^{-\tau(\lambda)/\cos\theta}\right) \quad \text{(A9)}$$

where $(1-\omega(\lambda))(1-e^{-\tau(\lambda)/\cos\theta})$ represents the fraction of light absorbed within the layer and is function of: $\omega(\lambda)$ – the single scattering albedo of the aerosol within the atmospheric layer, and $\tau(\lambda)$ – the aerosol optical depth. The $\omega(\lambda)$ and $\tau(\lambda)$ terms can be computed from the aerosol extinction, scattering and absorption coefficients ($b_{ext}(\lambda)$, $b_{sca}(\lambda)$ and $b_{abs}(\lambda)$):

$$\omega(\lambda) = \frac{b_{sca}(\lambda)}{b_{sca}(\lambda)+b_{abs}(\lambda)} \quad \text{(A10)}$$

$$\tau(\lambda) = \int_o^{\Delta z} b_{ext}(\lambda)\, dz \quad \text{(A11)}$$

Now, if the atmospheric layer is thin enough so that $\tau(\lambda) \ll 1$, the term $(1-e^{-\tau(\lambda)/\cos\theta})$ can be simplified introducing the Taylor series and the radiative power $\Delta DRE_{n(\lambda,\theta)}$ absorbed by the aerosol within that atmospheric layer can be computed from eq. A6 as follows:

$$\Delta DRE_n(\lambda,\theta) = F_n(\lambda,\theta)(1-\omega(\lambda))\,\frac{\tau(\lambda,\theta)}{\cos\theta} \quad \text{(A12)}$$

In this form, $\Delta DRE_n(\lambda,\theta)$ is not useful because it is a columnar quantity which again depends on $\tau(\lambda)$ that is integrated along the vertical direction.

Considering again an atmospheric layer thin enough so that $\tau(\lambda) \ll 1$ it is also possible to assume $F_n(\lambda,\theta) \approx$const and $\omega(\lambda) \approx$const through the whole Δz; thus, recalling the $ADRE$ definition ($ADRE=dDRE/dz$), and combining Eq. A10 with Eq. A11 and Eq. A12, it is possible now to write:

$$ADRE_n(\lambda,\theta) = \frac{dDRE_n(\lambda,\theta)}{dz} = F_n(\lambda,\theta)\frac{(1-\omega(\lambda))}{\cos\theta}\frac{d\tau_\lambda(\lambda)}{dz} = \frac{F_n(\lambda,\theta)}{\cos\theta} b_{abs}(\lambda) \quad \text{(A13)}$$

Equation A13 offers the opportunity to determine the $ADRE$, and thus the HR (eq. A5), just combining the absorption coefficient of light absorbing aerosols $b_{abs}(\lambda)$ and radiation measurements $F_n(\lambda,\theta)$. Thus, the resulting $ADRE$ and HR are only related to the light absorbing aerosols (and not to gases). Obviously, the atmospheric absorption and related HR can be obtained integrating Eq. A13 over the whole ensemble of shortwave wavelengths and incident angles:

$$ADRE_n = \int_\theta \int_\lambda \frac{F_n(\lambda,\theta)}{\cos\theta} b_{abs}(\lambda) d\lambda\, d\theta \quad \text{(A14)}$$

The shortwave radiation that can cross the atmospheric layer can be divided in three components, namely: the solar direct radiation ($F_{dir}(\lambda,\theta)$); the diffuse radiation from scattering on gases, aerosol and clouds in the sky ($F_{dif}(\lambda,\theta)$); and the radiation reflected backward from the ground ($F_{ref}(\lambda,\theta)$).

Equation A14 can be solved for all the three components allowing to determine both the total $ADRE$ and its components ($ADRE_{dir}$, $ADRE_{dif}$ and $ADRE_{ref}$) as follows:

$$ADRE = ADRE_{dir} + ADRE_{dif} + ADRE_{ref} \quad \text{(A15)}$$

Using Eq. A8 the same is valid for the HR:

$$HR = HR_{dir} + HR_{dif} + HR_{ref} \quad \text{(A16)}$$

so, the final equation for the *HR* can be written as follows:

$$HR = \frac{1}{\rho C_p} \cdot \sum_{n=1}^{3} \int_{\theta} \int_{\lambda} \frac{F_n(\lambda,\theta)}{\mu} b_{abs}(\lambda) d\lambda \, d\theta \quad \text{(A17)}$$

where n represents direct or diffuse or reflected radiation.

References

Ferrero et al. (2010): “Vertically-resolved particle size distribution within and above the mixing layer over the Milan metropolitan area”, Atmos. Chem. Phys., 10, 3915–3932, doi:10.5194/acp-10-3915-2010, 2010.

Ferrero et al. (2014): “Impact of Black Carbon Aerosol over Italian basin valleys: high resolution measurements along vertical profiles, radiative forcing and heating rate”. Atmos. Chem. Phys., 14, 9641–9664, 2014.

Ferrero L., Močnik G., Cogliati S., Gregorič A., Colombo R., Bolzacchini E.: Heating Rate of Light Absorbing Aerosols: Time-Resolved Measurements, the Role of Clouds, and Source Identification. Environ. Sci. Tech., 52, 3546−3555, DOI: 10.1021/acs.est.7b04320, 2018.

Ferrero et al. (2019): “Satellite AOD conversion into ground PM10, PM2.5 and PM1 over the Po valley (Milan, Italy) exploiting information on aerosol vertical profiles, chemistry, hygroscopicity and meteorology”, Atmospheric Pollution Research 10 (2019) 1895–1912, https://doi.org/10.1016/j.apr.2019.08.003.

Gao, R. S., Hall, S. R., Swartz, W. H., Schwarz, J. P., Spackman, J. R., Watts, L. A., Fahey, D. W., Aikin, K. C., Shetter, R. E. and Bui, T. P.: Calculations of solar shortwave heating rates due to black carbon and ozone absorption using in situ measurements, Journal of Geophysical Research Atmospheres, 113(14), 14–19, doi:10.1029/2007JD009358, 2008.

Liou K.N.: An Introduction to Atmospheric Radiation, Second Edition. INTERNATIONAL GEOPHYSICS SERIES, Volume 84, Academic Press, 2007.

Tian, P., Liu, D., Zhao, D., Yu, C., Liu, Q., Huang, M., Deng, Z., Ran, L., Wu, Y., Ding, S., Hu, K., Zhao, G., Zhao, C. and Ding, D.: In-situ vertical characteristics of optical properties and heating rates of aerosol over Beijing, Atmospheric Chemistry and Physics Discussions, 1–33, doi:10.5194/acp-2019-780, 2019.

The impact of cloudiness and cloud type on the atmospheric heating rate of black and brown carbon in the Po Valley

Luca Ferrero[1,*], Asta Gregorič[2,3], Grisa Močnik[3,4], Martin Rigler[2], Sergio Cogliati[1,5], Francesca Barnaba[6], Luca Di Liberto[6], Gian Paolo Gobbi[6], Niccolò Losi[1] and Ezio Bolzacchini[1]

[1]GEMMA and POLARIS Research Centers, Department of Earth and Environmental Sciences, University of Milano-Bicocca, Piazza della Scienza 1, 20126, Milan, Italy.

[2]Aerosol d.o.o., Kamniška 39A, SI-1000 Ljubljana, Slovenia.

[3]Center for Atmospheric Research, University of Nova Gorica, Vipavska 11c, SI-5270 Ajdovščina, Slovenia.

[4]Department of Condensed Matter Physics, Jozef Stefan Institute, SI-1000 Ljubljana, Slovenia.

[5]Remote Sensing of Environmental Dynamics Lab., DISAT, University of Milano-Bicocca, P.zza della Scienza 1, 20126, Milano, Italy

[6]ISAC -CNR, Roma - Tor Vergata, Via Fosso Del Cavaliere 100, 00133, Roma, Italy.

Correspondence to: Luca Ferrero (luca.ferrero@unimib.it)

Abstract.

We experimentally quantified the impact of cloud fraction and cloud type on the heating rates (HRs) of black and brown carbon (HR_{BC} and HR_{BrC}). In particular, we examined in more detail the cloud effect on HRs detected in a previous study (Ferrero et al., 2018). High time-resolution measurements of the aerosol absorption coefficient at multiple-wavelengths were coupled with spectral measurements of the direct, diffuse and surface reflected irradiance, and with lidar-ceilometer data during a field campaign in Milan, Po Valley (Italy). The experimental set-up allowed a direct determination of the total HR (and its speciation: HR_{BC} and HR_{BrC}) in all sky condition (from clear-sky to cloudy). The highest total HR values were found in the middle of winter (1.43±0.05 K day^{-1}) and the lowest in spring (0.54±0.02 K day^{-1}). Overall, the HR_{BrC} accounted for 13.7±0.2% of the total HR, the BrC being characterized by an absorption Angstrom exponent (AAE) of 3.49±0.01. To investigate the role of clouds, sky conditions were classified in terms of cloudiness (fraction of sky covered by clouds: oktas) and cloud types: stratus (St), cumulus (Cu), stratocumulus (Sc), altostratus (As), altocumulus (Ac), cirrus (Ci) and cirrocumulus-cirrostratus (Cc-Cs). During the campaign, clear sky conditions were present 23% of the time, the remaining time (77%) being characterized by cloudy conditions. Average cloudiness was 3.58±0.04 oktas (highest in February: 4.56±0.07 oktas, lowest in November: 2.91±0.06 oktas). St were mostly responsible of overcast situations (oktas=7-8, frequency: 87 and 96%), Sc dominated the intermediate cloudiness conditions (oktas=5-6, frequency: 47 and 66%) and the transition from Cc-Cs to Sc determined moderate cloudiness (oktas=3-4); finally, low cloudiness (oktas=1-2) were mostly dominated by Ci and Cu (frequency: 59 and 40%, respectively).

HR measurements showed a constant decrease with increasing cloudiness of the atmosphere enabling us to quantify for the first time the bias (in %) in the aerosol HR introduced by the simplified assumption of clear-sky conditions from radiative transfer model calculations. Our results showed that the HR of light absorbing aerosol

was ~20-30% lower in low cloudiness (oktas=1-2) and over 80% lower in complete overcast conditions (i.e., oktas=7-8), compared to clear sky ones. This means that, in the simplified assumption of clear-sky conditions, the HR of light absorbing aerosol can be largely overestimated (by 50% in low cloudiness, oktas=1-2 and up to 500% in complete overcast conditions, i.e., oktas=7-8).

The impact of different cloud types on the HR was also investigated. Cirrus were found to have a modest impact, decreasing the HR_{BC} and HR_{BrC} by -5% at most. Cumulus decreased the HR_{BC} and HR_{BrC} by -31±12 and -26±7%, respectively, while cirrocumulus-cirrostratus by -60±8 and -54±4%, which was comparable to the impact of altocumulus (-60±6 and -46±4%). A higher impact on HR_{BC} and HR_{BrC} was found for stratocumulus (-63±6 and -58±4%, respectively) and altostratus (-78±5 and -73±4%, respectively). The highest impact was associated to stratus suppressing the HR_{BC} and HR_{BrC} by -85±5 and -83±3%, respectively. The presence of clouds caused a decrease of both HR_{BC} and HR_{BrC} (normalized to the absorption coefficient of the respective species) by a factor of -11.8±1.2% and -12.6±1.4% per okta. This study highlights the need to take into account the role of both cloudiness and different cloud types when estimating the HR caused by both BC and BrC, and in turn decrease the uncertainties associated with the quantification of their impact on the climate.

~~We experimentally quantified the impact of cloud fraction and cloud type on the heating rates (HRs) of black and brown carbon (HR_{BC} and HR_{BrC}).In particular, in this work, we examine in more detail the average cloud effect (Ferrero et al., 2018) using high time-resolution measurements of aerosol absorption at multiple-wavelengths coupled with spectral measurements of the direct, diffuse and surface reflected radiation and lidar data in the Po Valley. The experimental set-up allowed a direct determination of HR_{BC} and HR_{BrC} in any sky condition. The highest values of total HR were found in the middle of the winter (1.43±0.05 K day^{-1}) while the lowest in spring (0.54±0.02 K day^{-1}) Overall the HR_{BrC} accounted for 13.7±0.2% of the total HR, the BrC being characterized by an AAE of 3.49±0.01.~~

~~Simultaneously, sky conditions were classified (from clear-sky to cloudy) in terms of fraction of sky covered by clouds (oktas) and cloud types. Cloud types were grouped as a function of altitude into the following classes: 1) low level (<2 km) stratus, cumulus and stratocumulus; 2) middle level (2-7 km) altostratus, altocumulus; 3) high level (> 7 km) cirrus, cirrocumulus-cirrostratus. Measurements carried out in different sky conditions at high-time resolution showed a constant decrease of HR with increasing cloudiness of the atmosphere enabling us to quantify for the first time the bias (in %) in the aerosol HR introduced by improperly assuming clear-sky conditions in radiative transfer calculations. In fact, during the campaign, clear sky conditions were only present 23% of the time while the remaining time (77%) was characterized by cloudy conditions. Our results show that, by incorrectly assuming clear-sky conditions, the HR of light absorbing aerosol can be largely overestimated (by 50% in low cloudiness, oktas=1-2), up to over 400% (in complete overcast conditions, i.e., oktas=7-8). The impact of different cloud types on the HR compared to a clear sky condition was also investigated. Cirrus were found to have a modest impact, decreasing the HR_{BC} and HR_{BrC} by -1 – -5%. Cumulus decreased the HR_{BC} and HR_{BrC} by -31±12 and -26±7%, respectively, while cirrocumulus-cirrostratus by -60±8 and -54±4%, which was comparable to the impact of altocumulus (-60±6 and -46±4%). A high impact on HR_{BC} and HR_{BrC} was found for stratocumulus (-63±6 and -58±4%, respectively) and altostratus (-78±5 and -73±4%, respectively), although the highest impact was found to be associated to stratus that suppressed the HR_{BC} and HR_{BrC} by -85±5 and -83±3%, respectively. Additionally, the cloud influence on the radiation spectrum that interacts with the absorbing aerosol was investigated. Black and brown carbon (BC and BrC) have different spectral responses (a different absorption Angstrom exponent, AAE)~~

~~and our results show that the presence of clouds causes a greater decrease for the HR_{BC} with respect to to HR_{BrC} going clear sky to complete overcast conditions; the observed the difference is 12±6%. This means that, compared to BC, BrC is more efficient in heating the surrounding atmosphere in cloudy conditions than in clear sky. Overall, this study extends the results of a previous work (Ferrero et al., 2018), highlighting the need to take into account both the role of cloudiness and of different cloud types to better estimate the HR associated to both BC and BrC, and in turn decrease the uncertainties associated to the quantification of the impact of these species on radiation and climate.~~

1 Introduction

The impact of aerosols on the climate is traditionally investigated ~~focusing on~~estimating their direct, indirect and semi-direct effects (Bond et al., 2013; IPCC, 2013; Ferrero et al., 2018, 2014; Bond et al., 2013; Ramanathan and Feng, 2009; Koren et al. 2008; Koren et al., 2004; Kaufman et al., 2002). Direct effects are related to the sunlight interaction with aerosols trough absorption and scattering;~~,~~ indirect effects are related to the ability of aerosol to act as cloud condensation nuclei affecting the clouds' formation and properties~~,~~ while semi-direct effects are those related to a feedback on cloud evolution affecting other atmospheric parameters (e.g. the thermal structure of the atmosphere) (IPCC, 2013; Ramanathan and Feng, 2009; Koren et al. 2008; ~~IPCC, 2013;~~ Koren et al., 2004; Kaufman et al., 2002).

Both ~~the~~ direct and indirect radiative effects ~~on the climate caused by~~of anthropogenic and natural aerosols on climate are still ~~represent~~ the major sources of ~~uncertainty~~ uncertainties (IPCC, 2013).~~;~~ Recent studies show, for example, that ~~for example~~ the aerosol direct radiative effect ~~(DRE)~~, on a global scale, may switch from positive to negative forcing on short (e.g. daily) time-scales (Lolli et al., 2018; Tosca et al., 2017; Campbell et al., 2016). This is due to the fact that aerosol is a heterogeneous complex mixture of particles characterized by different size, chemistry, and shape (e.g., Costabile et al., 2013), greatly varying in time and space both in the horizontal and vertical dimension (e.g., Ferrero et al., 2012). ~~On the~~At global scale,~~-~~ most of the values reported for the aerosol direct radiative effect~~DRE, used to quantify the aerosol impact on the climate,~~ were derived from models (Bond et al., 2013; Koch and Del Genio, 2010). This has the advantage of providing continuous direct radiative effect~~DRE~~ fields in space and time. However, inaccuracies related to simplified model assumptions on chemistry, shape, and the mixing state of ~~the~~ particles can affect the results (Nordmann et al., 2014; Koch et al., 2009), amplifying the uncertainties on the estimated global and regional aerosol climate effects (Andreae and Ramanathan, 2013). Another important issue is that the aerosol direct radiative effect~~DRE~~ ~~is~~ has been usually determined in clear-sky conditions both in model simulations and from measurements~~/approximations~~. Although ~~the~~ clear sky approximation is useful when comparing measurements to radiative transfer modelling outcomes during experimental campaigns performed in fair weather conditions (e.g., Ferrero et al., 2014; Ramana et al., 2007), in general this simplification cannot capture the complexity of the phenomenon in the majority of weather conditions (Myhre et al., 2013). In fact, clouds are one of the most important factors modulating the solar radiation ~~that reaches~~reaching the ground. By scattering and absorbing the radiation ~~passing through them,~~ clouds ~~strongly~~ can affect the radiation magnitude and ~~also~~ modify ~~the~~ its spectrum ~~of the short-wave radiation,~~ especially in the UV region~~-~~(López et al., 2009; Thiel et al., 2008; Calbó et al., 2005~~; López et al., 2009~~). Usually, during cloudy conditions the global irradiance is reduced, even though, sometimes, the presence of clouds results to short-term enhancement of global irradiance (Duchon and O'Malley, 1999). In fact, in~~In~~ some specific cases~~ (e.g. cirrus/cumulus clouds)~~, scattering of radiation from the sides of the cloud may enhance global irradiance in the UV to the levels higher than those in clear sky conditions (Mims and Frederick, 1994; Feister et al., 2015). In this respect, Mims and Frederick (1994) determined the that scattering from the sides of cumulus clouds can enhance the total (global) UV-B solar irradiance by 20% or more over the maximum solar noon value when cumulus clouds were just near the Sun (not when a cloud blocked the solar disk). In a similar way, Feister et al. (2015) concluded that the scattering of solar radiation by clouds can enhance UV irradiance at the surface; for example, Cumulonimbus clouds with top heights close to the tropical tropopause layer have the potential to significantly enhance diffuse UV-B radiance over its clear sky value. UV radiation also interacts with aerosols, and particularly with those exhibiting absorption properties in this spectral regions. UV represents an important region for BrC absorption with respect to other light absorbing aerosol (LAA) components (e.g. BC), thus the presence of clouds could influence in a different way its climatic impact.

Up to now, the role of cloudiness and ~~of ~~cloud type on the aerosol direct radiative effect~~DRE~~ was poorly investigated. Matus et al. (2015) recently used a complex combination of the CLOUDSAT's satellite multi-sensor radiative fluxes and heating rates (HR) products to infer both the direct radiative effect~~DRE~~ at the top-of-atmosphere ~~(TOA) ~~and HR profiles of aerosols that lie above the clouds. The study showed how results were affected by the cloudiness (e.g. cloud fraction) and, for example for the south eastern Atlantic, reported a direct radiative effect~~DRE~~ ranging from -3.1 to -0.6 W m^{-2} going from clear sky to cloudy conditions.

A further investigation by Myhre et al. (2013) reported results of modelling simulations during the AeroCom Project (Phase II): In all sky conditions (thus including the effect of clouds) they estimated an all-sky direct radiative effect~~DRE~~ for total anthropogenic aerosols of -0.27 W m^{-2} (range: -0.58 to -0.02 W m^{-2}), this being about half of the clear sky one. The most important factors responsible for the observed difference were the amount of aerosol absorption, the location of aerosol layers in relation to clouds (above or below), and the cloud distribution. In fact, the presence of ~~absorbing aerosols (~~LAA (mainly~~i.e.~~ Black Carbon, BC~~;~~, Brown Carbon, BrC~~;~~, ~~or ~~and mineral dust) might have important effects on the radiative balance. It is estimated that, due to its absorption of sunlight, BC is the second most important positive anthropogenic climate-forcing agent after CO_2 (Bond et al., 2013; Ramanathan and Carmichael, 2008), while BrC contributes ~10-30% to the total absorption on a global scale (Ferrero et al., 2018; Shamjad et al., 2015; Chung et al., 2012; Kumar et al., 2018). As a main difference compared to CO_2, absorbing aerosols are short-lived climate forcers, thus representing a potential global warming mitigation target. However, the real potential benefit of any mitigation strategy should also be based on observational measurements, possibly carried out in all sky conditions.

It also noteworthy that the HR induced by absorbing aerosol can trigger different atmospheric feedbacks. BC and mineral dust can alter the atmospheric thermal structure, thus affecting atmospheric stability, cloud distribution and even synoptic winds such as the monsoons (IPCC, 2013; Bond et al., 2013; Ramanathan and Feng, 2009; Koch et al., 2009; Ramanathan and Carmichael, 2008; Koren et al. 2008; Koren et al., 2004; Kaufman et al., 2002). Even in this case, the feedbacks should be quantified on the basis of HR measurements ~~carried out ~~in any sky conditions. In agreement with the aforementioned points, both Andreae and Ramanathan (2013) and Chung et al. (2012) called for model-independent, observation-based determination of the absorptive direct radiative ~~forcing ~~effect (ADRE) of aerosols. Since, similarly to aerosols, cloudiness and cloud type change on short time scales, long-term, highly time-resolved measurements covering different conditions, are necessary to unravel the role of ~~absorbing aerosol~~LAA on the HR.

As mentioned, s~~S~~ome satellite-based studies investigated the role of cloudiness and cloud type on the HR of aerosol layers above clouds (Matus et al., 2015). To our knowledge, there has been no experimental investigation on the impact aerosol layers laying below the clouds, where~~ conversely~~ most of the aerosol pollution typically resides. In addition to this, the cloud-aerosol forcing feedbacks can strongly depend on the HR magnitude in cloudy conditions. As a matter of fact, the atmospheric heating induced by absorbing aerosol is traditionally related to a decrease of atmospheric relative humidity and less cloud covering (semi-direct effect). This effect can further increase the amount of the incoming solar radiation that reaches Earth's surface (and the close-to-surface LAA layer), leading to positive feedback characterized by additional warming and a further decrease in the cloud amount (e.g. Koren et al., 2004). However a work carried out by Perlwitz and Miller (2010) reported a counterintuitive feedback linking the atmospheric heating induced by tropospheric absorbing aerosol to a cloud cover increase (especially low level clouds) due to a delicate balance between two opposite changes in specific humidity and temperature. That study concluded that high levels of absorption by aerosols were responsible for two counter-acting processes: a large diabatic heating warming of the atmospheric column, (thus decreasing relative humidity) and a corresponding increase in the specific humidity able to exceed the temperature effect on relative humidity with the net result of increasing low cloud cover with increasing aerosol absorption. This is an important result that underlines the importance of measuring the atmospheric HR in cloudy conditions as constrain and/or input for more comprehensive climatic model to shad a light on the sign and magnitude on the related feedbacks on cloud dynamics.

~~This study was performed in Milan (Italy), located in the middle of the Po Valley (section 2), this region representing a pollution hotspot in Europe due to the high emissions coupled to a complex topology of the landscape. In fact, similarly to a multitude of basin valleys surrounded by hills or mountains in Europe, low wind speeds and stable atmospheric conditions are common, thus promoting high concentrations of aerosol and BC (Zotter et al., 2017; Moroni et al., 2013; Moroni et al., 2012; Ferrero et al., 2011a ; Carbone et al., 2010; Rodriguez et al., 2007). At the same time, cloud presence cannot be neglected considering that in the last 50 years annual mean cloudiness, expressed in oktas, is estimated to be ~5.5 over Europe (Stjern et al., 2009) and ~4 over Italy (Maugeri et al., 2001). This is in agreement with 80 years of data of cloud cover in the United States (Crock et al., 1999). Moreover, recently, Perlwitz and Miller (2010) reported a counterintuitive feedback linking the atmospheric heating induced by tropospheric absorbing aerosol to a cloud cover increase.~~

~~Due to the aforementioned reasons~~In this context, this study attempts to ~~-~~experimentally ~~unravel~~ measure for the first time the impact of different cloudiness and cloud types on the HR exerted by ~~aerosol layers~~ specific LAA specied to fill the gap in this field of knowledge. The study was performed in Milan (Italy), located in the middle of the Po Valley (section 2), which is a pollution hot spot in Europe with meteorological characteristics similar to those of a multitude of basin valleys surrounded by hills or mountains (low wind speeds and stable atmospheric conditions promoting accumulation of aerosol and BC) (Zotter et al., 2017; Moroni et al., 2013; Moroni et al., 2012; Ferrero et al., 2011a ; Carbone et al., 2010; Rodriguez et al., 2007). At the same time, cloud presence cannot be neglected over the investigated area considering that in the last 50 years annual mean cloudiness, expressed in oktas, is estimated to be ~5.5 over Europe (Stjern et al., 2009) and ~4 over Italy (Maugeri et al., 2001). This is in agreement with 80 years of data of cloud cover in the United States (Crock et al., 1999). ~~. To this purpose~~ To determine the HR we use a methodology, previously developed in Ferrero et al. (2018), and further extended ~~the analysis~~here to explore the effects of different cloudiness and cloud types on ~~BC and BrC on~~ HR of BC and BrC.~~.~~ More ~~in detail~~specifically, with respect to the preliminary results by Ferrero et al. (2018), this work introduces the following novelties: 1) it describes the interaction between cloudiness and light-absorbing aerosol, presenting the aerosol HR as a function of cloudiness, and in turn estimates the systematic bias introduced by incorrectly assuming clear-sky conditions in radiative transfer models; 2) it introduces an original cloud type classification and investigates the impact of both cloudiness and cloud types on the total HR~~the~~; 3~~introduction of a cloud type classification; 2) the determination of the average photon energy impinging the absorbing aerosol; 3~~) it separates BC and BrC loads and investigates their relative impact on the total HR in function of sky conditions. ~~the determination of the impact of both cloudiness and cloud types on the HR of BC and BrC; 4) the investigation of the relative and synergic role of cloudiness and of different cloud types on HR of both BC and BrC~~. The results presented in this study ~~thus~~ could add an important piece of information in the general context of cloud~~-~~-absorbing aerosol~~-~~-HR interactions.

2 Methods

Aerosol clouds and spectral ~~radiation~~ irradiance measurements were carried in an experimental measurement station located in Milan (Italy) on the rooftop (10 m above the ground level) of the U9-building of the University of Milano-Bicocca (45°30’38”N, 9°12’42”E, Italy; Figure 1). The site is located in the midst of the Po Valley, ~~in the midst of~~ one of the most industrialized and heavily populated area in Europe. In the Po Valley, stable atmospheric conditions often occur causing a marked seasonal variation of aerosol concentrations within the mixing layer, well visible even from satellites (Ferrero et al., 2019; Di Nicolantonio et al., 2009; Barnaba and Gobbi 2004). A full description of the aerosol behavior in Milan at the University of Milano-Bicocca and the related aerosol properties (vertical profiles, chemistry, hygroscopicity, sources, and toxicity) are reported in previous studies (Diemoz et al., 2019; D’Angelo et al., 2016; Curci et al., 2015; Ferrero et al., 2015, 2010; Perrone et al., 2013; Sangiorgi et al., 2011). ~~Within~~ In the framework of the present work is important to underline that the U9 experimental site is particularly well suited for atmospheric radiation ~~transfer~~ measurements, in fact it is characterized by a full hemispherical sky-view equipped with the instruments described in Section 2.1. The measurements assembly allow the experimental determination of the instantaneous aerosol HR (K day^{-1}) induced by absorbing aerosol (e.g. BC and BrC) as detailed in Section 2.2. The methodological approach used to quantify the cloud fraction and to classify the cloud type is ~~instead~~ reported in Section 2.3.

2.1 Instruments

~~At the U9 sampling site in Milan, t~~The aerosol, cloud and radiation instrumentations instrumentations has been installed at the U9 sampling site in Milan since 2015. Site location is shown in Figure 1. The complete instrumental set up (Figure S1) is described hereafter.~~(Figure S1) needed to determine the HR (section 2.2), the cloud fraction and the cloud type (section 2.3) has been installed since 2015.~~

2.1.1 Light absorbing aerosol measurements and apportionment

Measurements of the wavelength dependent aerosol absorption coefficient $b_{abs(\lambda)}$ were obtained using the Magee Scientific Aethalometer AE-31. This allowed multi spectral measurements (7-λ: 370, 470, 520, 590, 660, 880 and

950 nm) in the wide UV-VIS-NIR region, not available from other instruments (e.g. MAAP, PSAP, photoacoustic) (Virkkula et al., 2010; Petzold et al., 2005). ~~In particular, measurements of the wavelength dependent aerosol absorption coefficient $b_{abs(\lambda)}$ in the UV-VIS-NIR region were obtained using the Magee Scientific Aethalometer AE-31. The reason of this choice (detailed in Ferrero et al., 2018) is related to the number and range of spectral channels (7 λ: 370, 470, 520, 590, 660, 880 and 950 nm) not available in other instruments (e.g. MAAP, PSAP, photoacoustic) (Virkkula et al., 2010; Petzold et al., 2005).~~ This spectral range is needed for the HR determination (section 2.2). ~~It noteworthy that the~~ The use of Aethalometers ~~take~~has also the advantage of global long-term data series (Ferrero et al., 2016; Eleftheriadis et al., 2009; Collaud-Coen et al., 2010; Junker et al., 2006) that ~~should~~ could allow ~~in the future~~ to derive historical data of the HR in the future.

To account for both the multiple scattering (the optical path enhancement induced by the filter fibers) and the loading effects (the non-linear optical path reduction induced by absorbing particles accumulating in the filter), the AE-31 data were corrected applying the Weingartner et al. (2003) procedure (Ferrero et al., 2018, 2014, 2011; Collaud-Coen et al., 2010). As detailed by Collaud Coen et al. (2010), the Weingartner et al. (2003) procedure compensates for all the Aethalometer artifacts (the backscattering is indirectly included within the multiple scattering correction), showing a good robustness (negative values are not generated and results in good agreement with other filter photometers) and, most importantly, it does not affect the derived aerosol Absorption Angstrom Exponent (AAE) (fundamental for HR determination, section 2.2).

Overall, the multiple scattering parameter *C* was 3.24±0.03 as obtained by comparing the AE31 data at 660 nm with a MAAP at the same wavelength (Figure S2). This value lies very close to that suggested by the Global Atmospheric Watch (GAW) program~~GAW~~ (2016), i.e. C=3.5. The physical meaning of the similarity between the obtained C value (3.24) and the GAW one implies that Milan (in the middle of the Po Valley) is characterized by continental type aerosols (e.g. Carbone et al., 2010) in keeping with global average. To verify the reliability of the obtained C value, it was also computed following Collaud Coen et al. (2010) procedure. They defined the reference value of C (C_{ref} = 2.81±0.11) for the AE31 tape based on data from pristine environments (Jungfraujoch and Hohenpeissenberg sites where aerosol has a single scattering albedo of ~1); at the same time, Collaud Coen et al. (2010) defined C for any kind of aerosol as follows:

$$C = C_{ref} + \alpha \frac{\omega_0}{1-\omega_0} \qquad (1)$$

where α is the parameter for the Arnott (2005) scattering correction (0.0713 at 660 nm) and ω_0 the single scattering albedo. In wintertime in Milan, within the mixing layer, the single scattering albedo was found to be 0.85±0.01 at 675 nm by Ferrero et al. (2014). From eq. 1 it follows that the expected C in Milan is 3.20±0.15; within its range the experimental 3.24±0.03 value lies. Details concerning wavelength differences are discussed in supplemental material.

The loading effects were dynamically determined following the Sandradewi et al. (2008b) approach while the final equivalent BC concentrations (eBC) were obtained applying the AE-31 apparent mass attenuation cross-section (16.6 $m^2 g^{-1}$ at 880 nm). The above mentioned compensation procedure introduce an uncertainty in the absorption coefficient measurements. Collaud-Coen et al. (2010) tested it in different sites and estimated as 23% the global accuracy of the Weingartner et al. (2003) correction applied in the present work. Moreover, Drinovec et al. (2015) showed a good agreement between Aethalometer AE31 data (corrected using Weingartner et al., 2003) and that of the new version AE33 with a slope close to one and R2>0.90. Thus the Collaud-Coen et al. (2010) accuracy estimation is considered here as the worst scenario.

As the spectral signature of $b_{abs(\lambda)}$ reflects the different nature of absorbing aerosol (BC and BrC), once $b_{abs(\lambda)}$ is obtained, it can be apportioned to determine the contributions of BC and BrC, respectively. This result can be achieved considering that BC aerosol absorption is characterized by an Absorption Angstrom Exponent, AAE ≈1 (Massabò et al., 2015; Sandradewi et al., 2008a; Bond and Bengstrom, 2006). Conversely, BrC absorption is spectrally more variable, with an AAE from 3 to 10 (Ferrero et al., 2018; Shamjad et al., 2015; Massabò et al., 2015; Bikkina et al., 2013; Yang et al., 2009; Kirchstetter et al., 2004). The lower absorption coefficient of BrC in the IR region (compared to UV) is a consequence of the wavelength distance (in the IR) with respect to the resonance one (in the UV) described by the simple harmonic oscillator reported in Moosmuller et al. (2011) which also yield to a decrease of AAE with increasing wavelengths. This is in keeping with the band-gap model with Urbach tail detailed in Sun et al. (2007) and recalled in Moosmuller et al. (2011) where the key factor is the difference between the highest occupied and lowest unoccupied energy state of the molecules included in the BrC ensemble. In this study we determined AAE_{BrC} following the innovative apportionment method proposed by Massabò et al. (2015). This allows to apportion $b_{abs(\lambda)}$ between BC and BrC and to determine, at the same time, the AAE_{BrC} assuming that the whole BrC is completely produced by biomass burning. The method by Massabò et al. (2015) was previously applied to the Milan U9 measurements leading to an average AAE_{BrC} (over a full solar year) of 3.66±0.03.

2.1.2 Radiative, meteorological and lidar measurements

~~Radiation~~ Spectral irradiance measurements ($F_{n(\lambda,\theta)}$) were collected using a Multiplexer-Radiometer-Irradiometer ~~(MRI)~~ (Figure S1; ~~D~~details ~~of the MRI are reported in~~ in Cogliati et al., ~~(~~2015).~~)~~. ~~The MRI~~which resolves the UV-VIS-NIR spectrum (350 - 1000 nm) in 3648 spectral bands (3648-element linear CCD-array detector (Toshiba TCD1304AP, Japan) for both the downwelling and the upwelling radiation fluxes. ~~The MRI~~ The instruments was developed at the University of Milano-Bicocca by using an optical switch (MPM-2000-2x8-VIS, Ocean Optics Inc., USA) to sequentially select between different input fiber optics fixed to the up-looking and the down-looking entrance fore-optics. The configuration used in the present work connects each spectrometer to 3 input ports: 1) The CC-3 cosine-corrected irradiance probes to collect the down-welling irradiance (up-looking channel); 2) the bare fiber optics with a 25° Field-of-View (down-looking channel) to measure the up-welling radiance from the terrestrial surface; 3) the blind port that is used to record the instrument dark-current. A 5 m long optical fiber with a bundle core of 1000 m of diameter is used to connect the entrance fore-optics to the multiplexer input, while the connection between the multiplexer output ports and the spectrometers is obtained with a 0.3 meters long optical fibers. The set-up allows to sequentially measurements of dark-current and and both up- and down-welling spectra simultaneously with the two spectrometers. The two spectrometers used are High Resolution HR4000 holographic grating spectrometers (Ocean Optics Inc., USA). Finally, the Multiplexer-Radiometer-Irradiometer was equipped with a rotating shadow-band enabling to measure separately the spectra of the direct, diffuse and reflected ~~radiation~~irradiance ($F_{dir}(\lambda)$, $F_{dif}(\lambda)$, $F_{ref}(\lambda)$). The reflected ~~radiation~~ irradiance originated from a~~the~~ Lambertian concrete surface (due to its flat and homogeneous characteristics which well represents the average spectral reflectance of the Milano urban area; Ferrero et al, 2018). ~~Details of the MRI are reported in Cogliati et al. (2015).~~

Broadband downwelling (global and diffuse) and upwelling (reflected) ~~radiation~~ irradiance measurements were also collected using LSI-Lastem radiometers (DPA154 and C201R, class1, ISO-9060, 3% accuracy; 300-3000 nm). Diffuse broadband irradiance~~radiation~~ was measured using the DPA154 global radiometer equipped with a shadow band whose effect was corrected (Ferrero et al., 2018) to determine the true amount of both diffuse and direct (obtained after subtraction from the global) ~~radiation~~irradiance.

In addition to radiation measurements, temperature, relative humidity, pressure and wind parameters were measured using the following LSI-Lastem sensors: DMA580 and DMA570 for thermo-hygrometric measurements (for T and RH: range -30 - +70 °C and 10% - 98%, accuracy of ± 0.1 °C and ± 2.5% sensibility of 0.025°C and 0.2%), the CX110P barometer model for pressure (range 800-1100 hPa, accuracy of 1 hPa) and the combiSD anemometer (range of 0 - 60 m/s and 0-360°) for wind.

The experimental station U9 is also equipped with an Automatic Lidar-Ceilometer ~~(ALC)~~ operated by ISAC-CNR in the framework of the Italian Automated LIdar-Ceilometers network (ALICENET, www.alice-net.eu) and contributing to the EUMETNET E-Profile ~~ALC~~ Network (https://www.eumetnet.eu/). It is a Jenoptik Nimbus 15k biaxial lidar-ceilometer operating 24 hours per day, 7 days per week. It is equipped with a Nd:YAG laser that emits light pulses at 1064 nm with an energy of 8 µJ per pulse and a repetition rate of 5 kHz. The backscattered light is detected by an avalanche photodiode in photon counting mode (Wiegner & Geiß, 2012; Madonna et al., 2015). The vertical and temporal resolution of the raw signals are 15 m and 15 seconds, respectively. Signals are recorded up to 15 km height, with a full~~n~~ overlap height < 1000 m. Vertical signals are averaged at 120 seconds to improve the signal to noise ratio. The Nimbus 15k lidar-ceilometer is able to determine cloud base height~~s~~ (CBH), penetration depth~~s~~, mixing layer height and, with specific processing, vertical profiles of aerosol optical and physical properties (e.g., Haeffelin et al., 2011, Dionisi et al., 2018; Diemoz et al., 2019a, 2019b). For the specific purpose of this study, exploitation of the U9 ~~ALC~~ ceilometer data has been limited to cloud layering and relevant cloud base height as the system can reliably detect multiple cloud layers and cirrus clouds (Boers et al., 2010; Martucci et al., 2010; Wiegner et al., 2014) within its operating vertical range (up to 15 km). Given the vertical resolution of the instrument, expected accuracy on the cloud base height derived by the lidar-ceilometer is < ±30 m.

Global and diffuse ~~radiation~~ irradiance measurements, coupled with the ~~ALC~~ ceilometer data were used to determine the sky cloud fraction and to classify the cloud types by following the methodology presented in the Section 2.3.

2.2 Heating rate measurements

The instantaneous aerosol HR (K day^{-1}) induced by absorbing aerosol is experimentally obtained using the methodology reported and validated in Ferrero et al. (2018). Here we briefly summarize the method and the reader is referred to the aforementioned publication for the physical demonstration of the approach.

The heating rate is determined from the knowledge of: the air density (ρ, kg m^{-3}), the isobaric specific heat of dry air (C_p, 1005 J kg^{-1} K^{-1}) and the radiative power absorbed by aerosol for unit volume of air (W m^{-3}) describing the interaction between the radiation (either direct from the sun, diffuse by atmosphere and clouds and reflected from the ground) and the LAA (BC and BrC in Milan). The HR is determined as follows (Ferrero et al., 2018):

$$HR = \frac{1}{\rho C_p} \cdot \sum_{dir,dif,ref} \int_{\theta=0}^{\theta=\pi/2} \int_{\lambda=300}^{\lambda=3000} \frac{F_{dir,dif,ref}(\lambda,\theta)}{\cos(\theta)} b_{abs}(\lambda) d\lambda d\theta \qquad (2)$$

where the subscripts *dir*, *dif* and *ref* refers to the direct, diffuse and reflected components of the spectral irradiance F of wavelength λ impinging the LAA with an zenithal angle θ (from any azimuth).

Under the isotropic and Lambertian assumptions (as used in Ferrero et al., 2018) equation 2 can be solved becoming:

$$HR = HR_{dir} + HR_{dif} + HR_{ref} =$$

$$= \frac{1}{\rho C_p} \cdot \left[\frac{1}{cos\,(\theta_z)} \int_\lambda F_{dir}(\lambda)\, b_{abs}(\lambda)\, d\lambda + 2 \int_\lambda F_{dif}(\lambda)\, b_{abs}(\lambda)\, d\lambda + 2 \int_\lambda F_{ref}(\lambda)\, b_{abs}(\lambda)\, d\lambda \right] \quad (3)$$

where θ_z refers to the solar zenith angle while $F_{dir}(\lambda)$, $F_{dif}(\lambda)$ and $F_{ref}(\lambda)$ are the spectral direct, diffuse and reflected irradiances. Eq. 2 and 3 represent a linkage with the concept of actinic flux (Tian et al., 2020; Gao et al., 2008; Liu, 2007); a deepening of this description, as well as its demonstration is detailed in Supplemental Material.

~~The instantaneous aerosol HR (K day^{-1}) induced by absorbing aerosol is experimentally obtained following Eq. 1 using the methodology reported and validated in Ferrero et al. (2018). Here we briefly summarize the method and the reader is referred to the aforementioned publication for the physical demonstration of the approach.~~

~~The integral over the whole shortwave solar spectrum and over the whole 2π hemispherical sky of the interaction between the radiation (either direct from the sun, diffuse by atmosphere and clouds and reflected from the ground) and the absorbing components of aerosol (BC and BrC in Milan, as detailed in Ferrero et al., 2018) gives the HR as:~~

~~*HR* =· (1)~~

~~where ρ represents the air density (kg m^{-3}), C_p (1005 J kg^{-1} K^{-1}) is the isobaric specific heat of dry air, n is the index indicating the nth type of radiation (direct, diffuse or reflected) impinging the absorbing aerosol, λ and θ represent the wavelength and zenith angle of the radiation, $F_{n(\lambda,\theta)}$ is the nth type (direct or diffuse or reflected) monochromatic radiation of wavelength λ that strikes with an angle θ the aerosol layer, μ is the cosine of θ (cosθ), $b_{abs(\lambda)}$ is the wavelength dependent aerosol absorption coefficient.~~

~~Considering that the absorptive DRE (ADRE), i.e. the radiative power absorbed by the aerosol for unit volume of the atmosphere (W m^{-3}), is equals to:~~

~~*ADRE* = (2)~~

~~Eq. 1 can be also re-written as:~~

~~*HR* =· *ADRE* (3)~~

~~Both Eq. 1 and 2 can also be solved for each of the three components of radiation (direct, diffuse, or reflected), i.e.: *ADRE* = + + (5)~~

~~*HR* = + + (4)~~

~~$ADRE = ADRE_{dir} + ADRE_{dif} + ADRE_{ref}$ (5)~~

~~where the subscript *dir*, *dif* and *ref* refers to the direct, diffuse and reflected radiation, respectively.~~

~~Eq. 4 and 5 allow to split the total ADRE and HR into the three components of radiation.~~ As the intensity of these ~~irradiance~~radiation components is a function of cloudiness and cloud type (section 2.3), ~~Eqs~~eq. 3~~4 and 5~~ enables to assess the impact of the latter components on the aerosol absorption of shortwave radiation and thus on the corresponding HR (sections 3.2 and 3.3).

The most important advantages and limitations of this measurement-based approach to derive HR are as follows.

Advantages:

- no radiative transfer assumptions needed (i.e. assumption of clear sky conditions), as the parameters input to equations 2 and 3 are all derived from measured quantities.
- possibility to investigate the HR temporal evolution, as measurements of spectral irradiance and absorption coefficient are carried out at high temporal resolution allowing to follow the rapid HR dynamic
- possibility to derive HR in all sky conditions, as measurements of spectral irradiance, absorption coefficient are independent from atmospheric conditions enabling to investigate the impact induced by the clouds

Limitation:

- the ADRE and the HR are independent from the thickness of the investigated atmospheric layer (as happens for routine atmospheric pollution measurements; i.e. BC, aerosol and particle number concentrations) and refers to the vertical location of the atmospheric layer in which both the ADRE and the HR are experimentally determined. In the present work they were applied to the near-surface atmospheric layer.

Despite this limitation, BC and HR vertical profiles data previously collected at the same site and in other basin valley sited revealed that the HR was constant inside the mixing layer (Ferrero et al., 2014). In fact, in our observational site, vertical profile measurements with tethered balloons and lidar-ceilometer were performed since 2005 mostly showing homogeneous concentrations of aerosol (and related extinction coefficient) within the mixing layer, particularly in daytime (Ferrero et al., 2019). The same condition was verified by the lidar-ceilometer data collected during the present campaign (Figure S3, supplemental material). The methodology is therefore believed to be also representative for the whole mixing layer if the aerosol vertical dispersion is homogeneous within it. This might not be the case for regions of the globe where the upper troposphere is impacted by high levels of BrC from biomass burning (Zhang et al, 2020). In addition, Ferrero et al. (2019) showed that in Milan 87.0% of aerosol optical depth signal was built up within the mixing layer, 8.2% in the residual layer and 4.9% in the free troposphere making the impact of cloud on radiation dominant with respect to that of aerosol (above the mixing layer) for the purpose of the present paper.

~~In addition, as the spectral signature of $b_{abs(\lambda)}$ reflects the different nature of absorbing aerosol (BC and BrC), $b_{abs(\lambda)}$ and thus the HR can be apportioned to determine the contributions of BC and BrC (HR_{BC} and HR_{BrC}), respectively. This result can be achieved considering that BC aerosol absorption is characterized by an Absorption Angstrom Exponent, AAE ≈1 (Massabò et al., 2015; Sandradewi et al., 2008a; Bond and Bengstrom, 2006). Conversely, BrC absorption is spectrally more variable, with an AAE from 3 to 10 (Ferrero et al., 2018; Shamjad et al., 2015; Massabò et al., 2015; Bikkina et al., 2013; Yang et al., 2009; Kirchstetter et al., 2004). This is due to the negligible BrC absorption in the infrared compared to UV. In this study we determined AAE_{BrC} following the innovative apportionment method proposed by Massabò et al. (2015). This allows to apportion $b_{abs(\lambda)}$ from BC and BrC at the same time and to determine the AAE_{BrC} assuming that the whole BrC is completely produced by biomass burning. The method by Massabò et al. (2015) was successfully applied to the Milan U9 measurements leading to an average AAE_{BrC} (over a full solar year) of 3.66±0.03, and to an associated HR_{BrC} explaining 13±1% of the total HR (Ferrero et al., 2018). The apportionment of absorption coefficient also enables to investigate the role of clouds on different absorbing aerosol species. As already pointed out in Ferrero et al. (2018), it is worth recalling that in the present method (equation 1), both the ADRE and the HR are independent from the thickness (Δz) of the investigated atmospheric aerosol layer. At the same time, BC and HR vertical profiles data previously collected both at the same site and in other basin valley sited (Ferrero et al., 2014) revealed that ADRE and HR were constant~~

~~inside the mixing layer, The methodology is therefore believed to be valid for applications in atmospheric layers below clouds, assuming that near-surface measurements are representative of the whole mixing layer. Main advantage of the new method to quantify the impact of clouds on the LAA HR is that it allows to obtain experimental measurement (not estimations) of ADRE and HR, which are continuous in time and resolved in terms of sources, species of LAA, cloud cover, and cloud types.~~

2.3 Cloud fraction, cloud classification and average photon energy

2.3.1 Cloud fraction

The cloudiness~~ fraction~~ was determined following the approach reported in Ehnberg and Bollen (2005) that~~. In particular, radiometer measurements were used~~ enables to calculate the fraction of the sky covered by cloud in terms of oktas (*N*), overall leading to 9 classes, corresponding to values of *N* ranging from 0 (clear sky) to 8 (complete overcast situation). As reported ~~in~~ by Ehnberg and Bollen (2005), the amount of global ~~radiation~~ irradiance (F_{glo}) ~~can be~~is related to the solar elevation angle (π/2-θ) and to the cloudiness ~~condition~~ following the Nielsen et al. (1981) equation:

$$F_{glo-(N)} = \left[\frac{a_0(N) + a_1(N)\sin\left(\frac{\pi}{2}-\theta\right) + a_3(N)\sin^3\left(\frac{\pi}{2}-\theta\right) - L(N)}{a(N)}\right] \qquad (\cancel{6}4)$$

where *N* represents one of the possible 9 classes of sky conditions expressed in oktas (from 0, clear sky, to 8, complete overcast)~~where *N* represents one of the possible 9 classes of cloud fraction~~ and a, a_0, a_1, a_3 and *L* are empirical coefficients that enable to compute the expected global ~~radiation~~ irradiance for each oktas class ($F_{glo-(N)}$), at a fixed solar elevation angle (π/2-θ). Their values, extracted from the original work of Ehnberg and Bollen (2005), are summarized in Table S1. Overall, ~~Eq~~eq. 6 allows to determine the unique oktas value *N* by comparing the measured global ~~radiation~~ irradiance (F_{glo}) with $F_{glo-(N)}$ at any given time.

With this approach ~~Still~~, the ~~so-derived cloud fraction~~cloudiness can be used to evaluate the interaction between incoming radiation and ~~light absorbing aerosol~~LAA in cloudy conditions but but does not provide the opportunity to ~~without the possibility~~ to discriminate between cloud type.~~-~~ The following section~~s (2.3.2 and 2.3.3)~~ describe the methods applied to overcome this limitation by implementing a cloud classification scheme.

2.3.2 Cloud classification

Identification of cloud ~~Cloud~~ classes ~~and cloud cover~~ is by common practice still largely ~~determined~~ performed by human observations based on the reference standard defined by the World Meteorological Organization ~~(WMO)~~. However, these observations lack the required time resolution which is needed by the present work to couple highly time resolved HR data with cloud type. ~~Due to high spatial and temporal variability of clouds, determination of cloud classes can be improved by measurements, adding highly temporally resolved and observer-independent information~~ Cloud classification literature reports a huge quantity of papers and reviews aimed at classify clouds avoiding the limits of a simple human inspection by means of different techniques and their integration; they ~~the , which~~ rely on different ensemble of instruments: 1) ground based, 2) remote sensing/satellite based or 3) installed on meteorological balloons (Tapakis and Charalambides, 2013). ~~many studies and review papers on the topic of cloud classification were published aiming to overcomeintegrating~~Some examples are reported in Singh and Glennen (2005), Ricciardelli et al. (2008), Calbó and Sabburg (2008), Tapakis and Charalambides (2013). Galli et al. (2004) successfully applied the Duchon and O'Malley (1999) approach to the Po Valley.

To exploit the full potential of our measurements, we needed a cloud type classification method able to follow the high temporal resolution of the observations, also considering the high spatial and temporal variability of clouds. Among the above mentioned instrumental ensembles, ground based instruments provide measurement of the incident solar irradiance to detect the effect of clouds along the path from the sun to the sensor (Calbò et al., 2001). The concept of using irradiance measurements to estimate cloud types was first introduced in the milestone work of Duchon & O'Malley (1999) which ~~used. T~~is based on the fact that clouds with different velocities and optical depth cross the slowly changing path of the solar beam over different time durations. Given the available irradiance data (section 2.1), in the present work, the cloud classification starts from the Duchon & O'Malley (1999) method which was previously applied in the geographical context of the Po Valley (Galli et al., 2004). In particular, we used irradiance measurements (F_{glo}) to compute two parameters R_t and SD_t as follows:

$$R_t = \frac{1}{20}\sum_{i=t-10}^{i=t+10} \frac{F_{glo(i)}}{F_{glo\_CS(i)}} \qquad (5)$$

$$SD_t = \sigma_{t\pm10}\left(F_{glo(t\pm10)} \cdot Sf_{t\pm10}\right) \qquad (6)$$

R_t is the 20 minutes running average ratio between the observed global irradiance (F_{glo}) and the modelled clear sky irradiance (Robledo and Soler, 2000) expected at the same place (F_{glo_CS}) at the time t; R_t describes the time-dependent cloud efficiency in reducing the incoming solar radiation (R_t=1 in perfect clear sky while R_t~0 in complete overcast conditions). SD_t instead represents the 20 minutes standard deviation (SD) of the scaled global irradiance ($F_{glo} \cdot Sf$) centered at the time t; SD_t describe the temporal stability of clouds in the atmosphere (e.g. persistent stratus clouds will be characterized by a SD_t~0 while cumulus of good weather will be characterized by higher values of SD_t) while Sf_t represent the so-called scaling factor (Duchon & O'Malley, 1999) that equals to:

$$Sf_t = \frac{1400\ W\ m^{-2}}{F_{glo\_CS(t)}} \qquad (7)$$

Visualization of the SD-R results thus represents a first tool in distinguishing different cloud categories as a function of their efficiency in reducing the incoming solar radiation (R) and their persistency (SD). ~~the~~The potential of the SD-R plot is presented in Figure 2a-h; it shows~~which presents~~ four example of the temporal evolution of the observed F_{glo}, F_{glo_CS} and F_{dif} (left column) ~~and GHI, together with~~and the corresponding SD-R diagrams (right column). More in detail:

1- in the first case (Figure 2a) ~~for the aforementioned 4 cloud classes identified by Duchon & O'Malley (1999). In a CS case (Figure 2a), F_{glo} approaches~~~~line~~ follows F_{glo_CS}~~GHI~~ without any significant temporal deviation, thus leading to a cluster of data in the SD-R diagram (Figure 2b) characterized by R~~~close to~~ 1 and SD~~~close to~~ 0 W m^{-2}. These conditions are those associated to clear sky (CS) by Duchon & O'Malley (1999) ~~(Figure 2b).~~

2- ~~Conversely,~~ the second case (Figure 2c) shows F_{glo} completely due to the diffuse irradiance (F_{dif}) along the whole day (note that in Figure 2c F_{dif} is superimposed on F_{glo}); this condition completely differ from the CS case as both R and SD approach 0 (Figure 2d). Duchon & O'Malley (1999) associate these conditions to the presence of persistent stratiform clouds.

3- the third case (Figure 2e) reports F_{glo} approaching F_{glo_CS} being at the same time characterized by small amplitude oscillations. In this case R ranges between 0.75 and 1 and SD from 0 to ~100 W m^{-2} (Figure

2f). The cluster of data is thus more dispersed than that of the CS case an placed slightly above it. Duchon & O'Malley (1999) attributed this situation to the presence of Cirrus (Ci) clouds without avoiding to underline that in some borderline cases a misclassification between CS and Ci (just based on SD-R plot) could be possible

4- the last case (Figure 2g) represents a transition from a CS situation (before midday) to cloudy conditions (after midday) characterized by a significant scatter of F_{glo}. Figure 2h clearly shows that the sky condition evolves from the CS toward cloudy sky, shifting the R data from ~1 down till ~0.25 and increasing SD from ~100 up to ~500 W m^{-2}. According to Duchon & O'Malley (1999), the arrival of Cumulus of good weather could be the reason of such behavior (Cu clouds movement in the sky result in fast sun/shadows transitions). Also in this case, the SD-R plot alone cannot exclude the presence of other kind of clouds responsible for a similar behavior (e.g. Altocumulus, Ac; Cirrocumulus, Cc; Cirrostratus, Cs). Note that in order to show the spread of data in the SD-R diagram (Figure 2h) in function of time, an hourly specific color code was assigned to the data points; the corresponding regions in Figure 2g were delimited by dashed lines with the same color code.

~~St clouds suppress the incoming radiation (Figure 2c) for all the time related to their presence resulting in R and SD both approaching 0 (Figure 2d) allowing a complete separation from the CS case. Ci clouds (Figure 2e) moderately suppress F_{glo} with smoothed fluctuations in time leading to a R between 0.75 and 1 and a SD ranging from 0 to ~100 W m^{-2} (Figure 2f); Ci clouds region thus lies adjacent but separated from the CS one. Finally the last case study (Figure 2g) shows a transition from CS (before midday) to Cu clouds in the afternoon; the arrival of Cu clouds in the sky first scattered R around 1 (Figure 2h; both below and slightly above it in keeping with Mims and Frederick (1994) and Feister et al. (2015)) and, most important, SD increased from 100 up to 500 W m^{-2} due to the Cu clouds movement in the sky which results in fast sun/shadows transitions. As a consequence, the Cu clouds regions is wider and above the one of Ci clouds.~~Overall, Figure 2a-h shows the potential (and limits) of the SD-R plots for a preliminary broad sky/cloud classification. ~~More recently, Harrison et al. (2008), went deeper showing that the SD-R differentiates between St and stratocumulus (StCu) clouds as StCu clouds are characterized by R values mostly moving from 0.4 to 0.8 and SD between 0 and 200 W m^{-2}. In this respect, StCu clouds can be found in the middle region of the SD-R space, with different levels of SD, depending on the cumuliform condition.~~ the SD-R diagram alone leaves margins of misclassification, especially because it is impossible to retrieve information in cases of simultaneous presence of different cloud types at different levels.

For this reason, in the present work we attempted a further refinement of cloud classification including the information of the cloud base height (CBH) and the number of cloud layers obtained from the automated Lidar-Ceilometer measurements. The CBH is a key parameter in the characterization of clouds (Hirsch et al., 2011), since its estimation limits the number of potential cloud classes that the SD-R classifier has to compare with, and thus maximizing the efficiency of the Duchon & O'Malley (1999) classification algorithm. In fact ceilometer instruments were firstly developed and are commonly used in airports to operationally detect cloud layers, and their use for aerosol–related studies is more recent. Furthermore, the use of ceilometer data for cloud classification and cloud study purposes does not represent an absolute novelty in the scientific literature as demonstrated by recent works by Huertas-Tato et al. (2017) and Costa-Surós et al. (2013). The availability of CBH information allows to divide cloud type in three fundamental categories (Tapakis and Charalambides, 2013): low level clouds (<2 km), mid-altitude clouds (2-7 km) and high-altitude clouds (>7 km). From a general perspective high level clouds includes Cirrus (Ci), Cirrocumulus (Cc) and Cirrostratus (Cs); Mid-level clouds includes Altocumulus (Ac), Altostratus (As), and Nimbostratus (Ns) and finally, Low level clouds includes Cumulus (Cu), Stratocumulus (Sc), Stratus (St), and Cumulonimbus (Cb) (Tapakis and Charalambides, 2013; Ahrens, 2009; Cotton et al., 2011).

The ceilometer-based information on cloud altitude of each analyzed data is added as color code to the SD-R diagram in Figure 3. It shows that, on average, low level clouds are located on the left side of the SD-R diagram (stratiform clouds), high-altitude clouds are conversely on the opposite side (this being the region of Ci and Cu clouds); finally, mid-altitudes clouds mostly cover the central part describing all the possible transitions/combinations from St to Cu and Ci, e.g. altostratus (As), altocumulus (Ac).

~~on the cloud base height and the magnitude of solar radiation.~~

~~In this study, clouds were classified coupling measurements of broadband solar radiation (global irradiance,~~ ~~F_{glo})~~ ~~and lidar-ceilometer measurements. The full methodology is described below.~~

~~As first introduced in the study by Duchon & O'Malley (1999), measurements of the magnitude of global solar irradiance and its deviation in 20-minute intervals can be used for cloud classification. Irradiance is used to calculate two quantities: 1) the ratio (R) between observed global irradiance (~~~~F_{glo}~~~~) and the modelled clear sky irradiance (GHI) (Robledo and Soler, 2000) expected at the same time and place (also referred to as scaled irradiance) and 2) the standard deviation (SD) of the measured global irradiance in 20 minute time intervals. Following the work of Duchon & O'Malley (1999), the SD-R plot enables to distinguish different cloud categories: clear sky conditions (CS), Stratus (St), Cirrus clouds (Ci) and cumulus (Cu).~~ Figure 2a-h shows ~~an example of the temporal evolution of the observed~~ ~~F_{glo}, F_{dif}~~ ~~and GHI, together with the corresponding SD-R diagrams for the aforementioned 4 cloud classes identified by Duchon & O'Malley (1999). In a CS case (Figure 2a),~~ ~~F_{glo}~~ ~~approaches GHI without any significant temporal variation, thus leading to a R close to 1 and SD close to 0 W m~~~~$^{-2}$~~ ~~(Figure 2b). Conversely, St clouds suppress the incoming radiation (Figure 2c) for all the time related to their presence resulting in R and SD both approaching 0 (Figure 2d) allowing a complete separation from the CS case. Ci clouds (Figure 2e) moderately suppress~~ ~~F_{glo}~~ ~~with smoothed fluctuations in time leading to a R between 0.75 and 1 and a SD ranging from 0 to ~100 W m~~~~$^{-2}$~~ ~~(Figure 2f); Ci clouds region thus lies adjacent but separated from the CS one. Finally the last case study (Figure 2g) shows a transition from CS (before midday) to Cu clouds in the afternoon; the arrival of Cu clouds in the sky first scattered R around 1 (Figure 2h; both below and slightly above it in keeping with Mims and Frederick (1994) and Feister et al. (2015)) and, most important, SD increased from 100 up to 500 W m~~~~$^{-2}$~~ ~~due to the Cu clouds movement in the sky which results in fast sun/shadows transitions. As a consequence, the Cu clouds regions is wider and above the one of Ci clouds. More recently, Harrison et al. (2008), went deeper showing that the SD-R differentiates between St and stratocumulus (StCu) clouds as StCu clouds are characterized by R values mostly moving from 0.4 to 0.8 and SD between 0 and 200 W m~~~~$^{-2}$~~~~. In this respect, StCu clouds can be found in the middle region of the SD-R space, with different levels of SD, depending on the cumuliform condition. As a consequence, despite the promising classification introduced by Duchon & O'Malley (1999) and Harrison et al. (2008), by using the SD-R diagram alone it is possible to encounter episodes of misclassification, especially because it is impossible to retrieve information concerning the contemporary presence of different cloud levels from the SD-R diagram alone. Therefore, the cloud classification was further improved in this study by including information from the automated Lidar-Ceilometer measurements on the cloud base height and the number of cloud layers. First of all, to avoid misclassification cases due to the presence of multiple cloud layers, we limited the analysis to those cases where only one cloud layer was detected by ceilometer (ALC). In this respect, the ALC-~~

~~derived cloud base height information allowed us to cluster clouds according to their altitude and distinguishing between low level clouds (<2 km), mid-altitude clouds (2-7 km) and high-altitude clouds (>7 km). The cloud altitude of each analyzed data is reported in Figure 3 within the SD-R diagram. It shows that, on average, low level clouds are located on the left side of the SD-R diagram(stratiform clouds), high-altitude clouds are conversely on the opposite side (this being the the region of Ci and Cu clouds); finally, mid-altitudes clouds density in the diagram mostly cover its the central part describing all the possible transitions/combinations from St to Cu and Ci, e.g. altostratus (AlSt) altocumulus (AlCu). Figure 3~~

~~further shows that use of the clouds base height as a third source of information (in addition to R and SD) allows to better separate overlapping cases in the bi-dimensional, SD-R diagram alone.~~

Overall, adding the CBH information to the SD-R plot enabled us to identify eight cloud types :~~Overall, coupling the SD-R plot and cloud base height, enabled us to identify seven classes~~: St (stratus), Cu (cumulus) and Sc~~tCu~~ (stratocumulus) as low level clouds; ~~ass;~~ As~~lSt~~ (altostratus) and Ac~~lCu~~ (altocumulus) as mid-altitude clouds; ~~s;~~ ~~and~~ Ci (cirrus) and Cc~~iCu~~-Cs~~iSt~~ (cirrocumulus and cirrostratus merged in one single class) as high-altitude clouds. A summary of the threshold values of R, SD, and cloud level used here to the final cloud classification is given in Table 1, the R and SD limits being based on the works of Duchon & O'Malley (1999) and Harrison et al. (2008) and those of CBH being derived considering the cloud properties at midlatitudes.

Finally, to avoid misclassification due to the presence of multiple cloud layers, the analysis was limited to those cases where only one cloud layer was detected by the ceilometer. Another reason for limiting the analyses to one cloud layer is due to the main aim of this work: to quantify the effects of different cloudiness and cloud types on LAA HR. Any multiple-layers cloudy conditions would result in a confounding information for the purpose of the present study. In this respect, 10855 single layer cases were analysed, representing 61% of all measurements.

~~. The final overview of the parameters (R, SD, cloud level) and their threshold values used for cloud classification is presented in Table 1.~~

Figure 4 shows the SD-R diagram of all data (grey) with superimposed R and SD mean value and 99% confidence interval of each of the eight identified cloud classes, plus the clear sky (CS) one. ~~The final SD-R diagram with presentation of mean value and 99% confidence interval for R and SD of each cloud class, plus the clear sky (CS) case, is presented on Figure 4 while the same SD-R diagram with presentation of mean value and the standard deviation of each cloud classes, plus the clear sky (CS) case, is presented on Figure S3~~. ~~Note in particular that the overlapping in the standard deviation of each classes shown in the SD-R plot in Figure S3 are solved by the introduction of the cloud base height from lidar data underling the reliability of the performed cloud classification.~~

Final cloud classification was obtained for the period from November 2015 - March 2016, during which all necessary parameters were available (section 3).

Since this methodology is applied for the first time in the Po Valley, a complete validation of the aforementioned approach is reported in Appendix B ("Cloud type validation"); it also includes a comparison with the classification based on the coupling of irradiance and CBH measurements simultaneously proposed this year by Ylivinkka et al. (2020). Thus, the Validation in Appendix B was conducted in two steps: the first step was carried out comparing the present automatized cloud classification with a visual cloud classification based on sky images collected during 1 month of wintertime field campaign; the second validation step was carried out comparing the present automatized cloud classification with the one discussed by Ylivinkka et al., (2020). The overall balanced accuracy was 80% for the visual validation and 90% for the intercomparison with the Ylivinkka et al., (2020) methodology underlying the reliability of the classification algorithm allowing to study the impact of clouds on LAA HR with a sufficient grade of certainty.

~~2.3.3 Average photon energy~~

~~The relative distribution of energy over the solar spectrum in the measured range of the MRI was also investigated for each cloud type calculating the average photon energy (APE) which describes the spectral characteristics of direct and diffuse radiation modulated by clouds. In fact APE quantifies the spectral shape of solar irradiance and represents the average energy of photons impinging upon a target, in this case the aerosol layer close to the surface. Thus, single APE can identify a unique spectral irradiance distribution which describes the light available for absorption in different spectral regions. APE (expressed in eV) is calculated dividing the total energy in a spectrum by the total number of photons it contains (Norton et al., 2015), i.e.:~~

~~= (7)~~

~~where q represents the electron charge,~~ $F_{n,\lambda}$ ~~is the n^th^ type (direct, diffuse) radiation at wavelength λ (W m^-2^ nm^-1^), and~~ Φ_{λ} ~~(photons m^-2^ s^-1^ nm^-1^) is the photon flux density at wavelength λ determined using the Plank-Einstein equation:~~

~~= (8)~~

~~where~~ h ~~is the Plank constant and~~ c ~~the speed of light.~~

~~From Eq. (8) it follows that APE is normalized for the total amount of radiation, becoming thus independent from the absolute intensity of light at each λ and indicating only the average distribution of light across the spectrum. Particularly, higher APE values describe the shift of a radiation spectrum towards UV-blue region (Figure S4). It has to be noted that the APE index depends on the range of the investigated spectrum (lower and upper limits of the integral), which in our case relate to the MRI measurements (350 – 1000 nm), thus for any absolute APE comparison with other studies, the spectrum range should be taken into account.~~

~~Characteristic APE values of diffuse~~ ~~(APE_{diff}) and direct (APE_{dir})~~ ~~irradiance measured from U9 site for different sky condition are presented in Section 3.4 together with a discussion concerning the relationship between APE and HR.~~

3 Results and Discussion

~~HR values considered in this study were~~Data measured over Milan from November 2015 to March 2016 ~~are, as~~(this period covers the simultaneous presence of radiation, lidar and absorption information necessary for the analysis)~~measurements fundamental for the analysis presented here (section 2).~~ ~~)~~; ~~These data~~ are presented in Section 3.1. The role of cloudiness and cloud type ~~its influence~~ on the~~-~~ total HR is discussed in section 3.2 while ~~section 3.3 describes the impact of each cloud type on the HR. In S~~in section 3.~~4~~3, the clouds impact on the HR is discussed with respect to the light absorbing aerosol species: BC and BrC. All the data are reported ~~everywhere~~ as mean±95% confidence interval.

3.1 ~~HR,~~ eBC, ~~and~~ irradiance~~tion~~ HR and cloud data presentation

High time resolution data (5 minutes) of eBC, F_{glo}, CBH, cloudiness (oktas) and resulting HR are shown in Figure 5; their ~~M~~monthly averaged values ~~of eBC and HR~~ are presented in Figure ~~5a~~ 6a ~~while~~ and ~~the corresponding~~

~~numerical values of these and additional parameters (e.g. ADRE, b_{abs}) are also~~ summarized in Table 2. ~~Corresponding high time resolution data (5 minutes) are shown in Figure S5.~~

The lowest eBC values (1.54±0.04 μg m^{-3}) were recorded in March while, as expected, the~~The~~ highest values of eBC (and $b_{abs(880nm)}$) were found~~, as expected,~~ in the middle of ~~the~~ winter, in December (6.29±0.09 μg m^{-3} and 31.1±0.5 Mm^{-1}, respectively) with a maximum value of 27.44 μg m^{-3} (135.7 Mm^{-1}) when strong emissions in the Po Valley are released into the stable boundary layer (Sandrini et al., 2014; Ferrero et al., 2011b; Barnaba et al., 2010). In ~~fact, in~~ this month the average PM_{10} and $PM_{2.5}$ were also at their maximum, with 73.1±0.6 and 69.3±0.6 μg m^{-3}, respectively (source: Milan Environmental Protection Agency, ARPA Lombardia) and~~.~~ the ~~Thus,~~ eBC accounted for ~10% of PM mass concentration~~n,~~.~~resulting in the absorption of shortwave radiative power (ADRE) of 20.7±0.7 mW m^{-3} which was responsible for an HR of 1.43±0.05 K day^{-1}. The lowest HR (monthly average) was recorded in spring (March) with a value of 0.54±0.02 K day^{-1} related to an amount of eBC of 1.54±0.04 μg m^{-3}.~~

These high wintertime values of eBC~~, HR and ADRE~~ agree with those observed previously in the Po Valley due to the low atmospheric mixing conditions (Ferrero et al., 2014, 2018) and confirm that eBC ~~is the main~~can be an important driver for the ~~behavior of~~atmospheric heating ~~HR and ADRE on the seasonal time scale~~. ~~However, in agreement with Eq. 1 (section 2.1), the interaction of absorbing aerosol with the impinging radiation cannot be neglected as heating rate varies differently than anticipated from the concentrations alone. In fact, d~~Concerning the radiation, during the investigated period, the lowest monthly irradiance value was observed in December (F_{glo}: 141±4 W m^{-2}; Table 2) while the highest in March (F_{glo}: 310±7 W m^{-2}). As a result of eq. 3 the highest monthly average HR was recorded December (1.43±0.05 K day^{-1}) while the lowest one was recorded in March with a value of 0.54±0.02 K day^{-1} (Figure 6a, Table 2). Even the HR monthly behavior followed the eBC trend (Table 2; R^2=0.82, not shown) it is also useful to compare the maximum to minimum ratio of eBC monthly mean (December to March, eBC ratio: 4.10±0.12) to the same for the HR (2.65±0.16). ~~the ratio between maximum and minimum eBC monthly mean concentration (December to March, eBC ratio: 4.10±0.12) was higher than that of HR (2.65±0.16)~~. This ratio is higher for eBC~~This is~~ because the incoming ~~radiation~~ irradiance was lower in December (F_{glo}: 141±4 W m^{-2}; Figures ~~5b~~ 6b~~and S5~~) with respect to March (F_{glo}: 310±7 W m^{-2}, ratio of 0.45±0.02), partially compensating the marked wintertime increase of eBC.

This is due to the interaction of LAA with F_{dir}. In fact, once F_{dir} is scaled by $cos(\theta_z)$ (eq. 3, section 2.2, Figure S5) it is quite constant along the year (and perfectly constant only in clear sky conditions). Conversely, the diffuse and reflected irradiance (Figure S5), under the isotropic and Lambertian assumptions (eq. 3), remain seasonally modulated (Figure S5).

~~This is mainly due to the interaction of light absorbing aerosol with F_{dir}. In fact, once F_{dir} is scaled by μ (eq. 1, section 2.1, Figure S6) it is quite constant along the year (and perfectly constant only in clear sky conditions). Conversely, the diffuse and reflected radiation (Figure S6), even when scaled by μ (under the isotropic and Lambertian assumptions), linearly follow the behavior of irradiance F_{dif} and F_{ref} thus being seasonally modulated (Figure S6). A detailed discussion about this explanation is reported in Ferrero et al. (2018).~~These observations introduce the importance of both amount and kind (direct, diffuse and reflected) of radiation that interacts with LAA. In brief, any process able to influence the total amount and the kind of impinging irradiance (e.g. presence/absence of clouds, cloudiness and cloud type) will result in a different HR, even keeping constant LAA levels. The investigation of this aspect is the main focus and added value of this study. High resolution data (Figure

5 and Figure S5) provided a first hint on the importance of cloud presence on HR; a sharp global irradiance decrease was observed in cloudy conditions especially in presence of low level clouds (low CBH) and high cloud cover (7-8 oktas).

Cloudiness and cloud type were thus determined carefully as detailed in sections 2.3.1 and 2.3.2. Overall, along the whole campaign, the average cloudiness was 3.58±0.04 oktas with the highest monthly value in February (4.56±0.07 oktas) and the lowest in November (2.91±0.06 oktas). These data are in line with the mean cloudiness over Europe (~5.5 oktas; Stjern et al., 2009) and over Italy (~4 oktas; Maugeri et al., 2001). Moreover, during the campaign, clear sky (CS) conditions were only present 23% of the time, the remaining time (77%) being characterized by partially cloudy (35%, 1-6 oktas) to totally cloudy (42%, 7-8 oktas) conditions. ~~This is relevant as it was found that c~~Cloudy conditions are therefore dominant in terms of frequency. ~~Here we will further investigate the clouds-HR relationships by exploring the effect of different types of clouds on this relationship.~~ The cloud-type resolved frequency concurring to the overall 77% of cloudy conditions is given in Figure 7a. ~~Figure 7a shows how the overall 77% of cloudy conditions encountered during the observational period was composed by the different cloud types, revealing that these were mainly~~The dominating cloud class was that of St (42%), followed by S~~tCu~~c (13%) Ci, C~~iCu~~c-C~~iSt~~s (7% and 5%, respectively). The contribution of each cloud type to the cloudiness ~~(expressed in oktas) of the sky~~ is reported in Figure 7b.~~ This clearly shows that, w~~While St were mostly responsible of overcast situations (oktas=7-8, frequency: 87 and 96%), Sc~~StCu~~ dominated the intermediate cloudiness conditions (oktas=5-6, frequency: 47 and 66%)~~;~~ and the transition from Cc-Cs to Sc determined moderate cloudiness (oktas=3-4); finally, ~~were mostly due to a transition from CiCu-CiSt to StCu while~~ low cloudiness (oktas=1-2) were mostly dominated by Ci and Cu (frequency: 59 and 40%, respectively). As mentioned (section 2.3.2 and Figure 4) low level clouds (<2 km) include Stratus (St), Cumulus (Cu) and Stratocumulus (Sc), mid-altitude clouds (2-7 km) include Altostratus (As), and Altocumulus (Ac) and high-altitude clouds (>7 km) include Cirrus (Ci), Cirrocumulus and Cirrostratus (Cc-Cs). Thus, it is clear that, as a general pattern, the higher cloud cover (higher oktas) is due to a higher frequency of low-mid altitude clouds. This is evident in Figure 7b which reports the average CBH for each oktas. CBH was related with oktas (Figure S6a, Supplemental material) underling the linkage (together with Figure 7b) between the fraction of sky covered by clouds and the cloud type responsible for it, at least at the measuring site. Indeed the cloudiness (oktas) is a non-linear function of the cloud type, as cloud type are related to the meteorological patterns: e.g. cirrus clouds are associated mostly with a synoptic sunny weather (especially in transition with clear sky) with higher winds than the opposite situation in which highly persistent stratiform clouds generate cloudy weather in lower windy conditions. Figure 8 summarizes the average cloudiness associated with different cloud type showing oktas rise from cirrus clouds (0.51±0.05 oktas) till stratus clouds (7.20±0.04 oktas) dominated conditions. This is in agreement with a recent work of Bartoszek et al. (2020) who associated higher cloudiness level with the presence of stratiform clouds. A deeper analysis of the relationship between oktas, CBH in our dataset is provided in Figure S7a, while the possible role of wind on cloud type is explored in Figure S8.

~~These considerations introduce the importance of both amount and kind (direct, diffuse and reflected) of the radiation that interacts with light absorbing aerosol. In brief, any process able to influence the total amount and the kind of impinging radiation (e.g. presence/absence of clouds, cloudiness and cloud type) will result in a different HR, even keeping constant eBC levels. The investigation of this aspect is the main focus and added value of this study and is reported in the next sections.~~

3.2 Cloud ~~fraction~~ impact on the hating rate

3.2.1 The role of cloudiness

Figure 6a already provided t~~T~~he first indication of the important role played by clouds on the total HR. In fact, it shows ~~can be derived from~~ the magnitude of the absolute (and relative) contribution of the diffuse component (HR_{dif}) with respect to the total HR revealing that on a monthly basis, ~~to the HR (HR_{dif}) as reported in Figure 5a. It shows the monthly average values of HR, HR_{dir}, HR_{dif} and HR_{ref} revealing that~~ the diffuse contribution accounted ~~for~~ on average 40±1% of the total HR. In most cases this is~~. On a monthly basis, this was~~ comparable or even higher than HR_{dir}. The only exception was in November 2015 ~~were~~ when ~~a~~ the lowest~~r~~ fraction of both HR_{dif} (Figure 6a) and F_{dif} ~~diffuse radiation was~~(Figure 6b) ~~–~~ were measured ~~(Figure 5b) compared to the other months~~(30.4±1.4% and 34.3±2.6%, respectively) this also being the month with the lowest average cloudiness~~. In fact, in November, the average okta value was~~(-2.91±0.06 oktas~~,~~) ~~lower than that observed in the other months (3.75±0.03), due to the highest frequency of clear sky conditions~~. The aforementioned data demonstrate the importance of the diffuse component of radiation. Therefore, the absolute values of the HR and its components were firstly investigated as a function of cloudiness (clear sky and complete overcast situations) in Figure 9a (seasonal averages). In the wintertime clear sky, the direct component of the HR (HR_{dir}) was higher than HR_{dif} and HR_{ref} accounting for 1.35±0.04 K day^{-1} and explaining on average 60±5% of the total HR; similarly, in the springtime clear sky HR_{dir} was 0.47±0.01 K day^{-1} again higher than HR_{dif} and HR_{ref}. Conversely, in complete overcast conditions (Oktas=7-8), HR_{dif} alone (84±1% of total HR) accounted for 0.33±0.01 and for 0.19±0.01 K day^{-1} during both winter and spring.

I~~ and thus of cloudy days in determining the HR induced by the absorbing aerosol. I~~n order to deeper investigate the role of cloudiness, it is necessary to decouple the variability of the HR induced by radiation from that due to LAA ~~eBC~~ concentrations. ~~In Figure 6 we thus show how fast a volume of air containing a specific BC mass heats due to the absorption of the impinging radiation — that is,~~ Thus, the HR values and that of its components (HR_{dir}, HR_{dif} and HR_{ref}) were normalized to the unit mass of eBC (K m^3 day^{-1} µg^{-1}) —and reported as a function of ~~oktas~~ cloudiness in Figure 9a together with ~~and further differentiate its components (HR_{dir}/eBC, HR_{dif}/eBC) as well as~~ the measured ~~radiation~~ irradiance (F_{glo}, F_{dir}, ~~and~~ F_{dif}) and F_{ref}~~)~~). Overall, Figure 9a shows the general decease of HR/eBC for increasing cloud cover, a pattern also observed for both HR_{dir}/eBC and HR_{ref}/eBC which follows the relevant decrease of direct and reflected irradiance. Note that at oktas ~~HR_{dir}/eBC decreased constantly from clear sky conditions (okta=0) to complete overcast situation (oktas=7-8) following the decreasing amount of the incoming solar F_{dir}. At oktas~~ values of 7-8, ~~the~~ $HR_{dir/eBC}$ reached values close to 0 (due to the suppression of F_{dir} by clouds) while HR_{ref}/eBC was 0.03±3*10^{-4} K m^3 day^{-1} µg^{-1} due to the presence of surficial albedo effect on the diffuse irradiance (F_{dif}). Conversely,— HR_{dif}/eBC increased ~~with~~ while increasing cloudiness, but not ~~continuously~~monotonically~~.~~; ~~In fact,~~ HR_{dif}/eBC ~~showed~~ reached a maximum peak (0.16±0.01 K m^3 day^{-1} µg^{-1}) at intermediate cloudiness conditions (5-6 oktas), in line with the behavior of the diffuse irradiance ~~when also the diffuse radiation peaked reaching F_{dif}:~~: maximum of 147±6 W m^{-2}, doubling the ~~relevant~~ value in ~~completely~~ overcast conditions (74±3 W m^{-2}; 7-8 oktas) and exceeding 150% of that in clear sky (91±2 W m^{-2}). In overcast situations (oktas=7-8) both HR_{dif}/eBC and the diffuse ~~radiation~~ irradiance reached their minimum due to the capability of clouds to effectively attenuate the whole radiation; however,~~.~~ ~~Yet~~in these conditions, ~~differently from~~

~~the direct radiation, the~~ HR$_{dif}$ /eBC ~~is~~ was still not null (0.08±0.01 K m^3 day^{-1} µg^{-1}) becoming the highest contributor of the total atmospheric HR, with a percentage of 84±1%.

HR/eBC and cloudiness data were linearly related showing a high level of correlation (R^2=0.935, Figure S6b); thus, in a first insight cloudiness could be used as good predictor (in modelling activity) for the HR/eBC.

As from Figure S6a (section 3.1), the CBH appeared related with the cloudiness, an additional linear correlation was tested between HR/eBC and CBH (Figure S6c; R^2=0.857); this relationship is is weaker than that between HR/eBC and cloudiness as the cloudiness, describing the fraction of sky covered by clouds, is a better predictor of the capability to suppress the incoming radiation (and thus the HR promoted by LAA). ~~-~~The relationship between CBH and cloudiness should be also investigated in other monitoring site around the world to unravel the possibility to use CBH (together with cloudiness) as a promising prognostic variable for the HR of LAA in future studies.

~~The absolute values of the HR and its components as a function of cloudiness is shown in Figure 6b. We show seasonally averaged (winter: NDJ, spring: FM) HR in clear sky (oktas=0) and complete overcast situation (oktas=7-8). In clear sky, the direct component of the HR (HR$_{dir}$) was higher than HR$_{dif}$ and HR$_{ref}$ accounting for 1.35±0.04 K day^{-1} and explaining on average 60±5% of the total HR during winter. Similarly, in clear sky springtime conditions, HR$_{dir}$ was 0.47±0.01 K day^{-1} again higher than HR$_{dif}$ and HR$_{ref}$. Conversely, in complete overcast conditions (Oktas=7-8), HR$_{dif}$ alone (84±1% of total HR) accounted for 0.33±0.01 and for 0.19±0.01 K day^{-1} during winter and spring, in agreement with Figure 5a.~~

These results clearly highlight that clouds are responsible for an important feedback on the aerosol HR that needs to be carefully quantified, pointing to the need to correctly include and model cloudy conditions in radiative transfer calculations aimed at evaluating~~of~~ the ~~'~~real ~~world'~~ contribution of aerosol ~~DRE~~ forcing on the atmospheric ~~and the~~ HR on a global scale.

~~Experimental~~ Our experimental HR ~~measurements at high time resolution hence~~data enabled us to estimate the degree of error introduced by improperly assuming clear-sky conditions in radiative transfer calculations. Particularly, we found that he simplified assumption of clear-sky conditions leads to overestimate the LAA-induced ~~by incorrectly assuming clear-sky conditions the~~ HR ~~of light absorbing aerosol can be overestimated~~ by ~~the following~~a factor~~s:~~ ranging from 50 to 470% (50% in low cloudiness, oktas=1-2~~)~~, 109% ~~(~~in moderate cloudiness, oktas=3-4~~)~~, 148% ~~(~~in intermediate cloudiness, oktas=5-6~~)~~, and 470% in cloudy conditions ~~(~~oktas=7-8). ~~Note that, during the campaign, clear sky conditions were present only 23% of the time, the remaining time (77%) being characterized by partially cloudy (35%, 1-6 oktas) to totally cloudy (42%, 7-8 oktas) conditions.~~

3.2.2 Cloudiness and diurnal pattern of HR

The presence of clouds can also alter the HR diurnal pattern. Figure 10a-d shows the mean diurnal pattern of eBC, wind speed, F_{glo}, and HR in both clear sky (oktas=0) and cloudy conditions (oktas=7-8). In clear sky, the eBC peaked at 8:00 LST (6.41±0.31 µg m^{-3}) during the rush hour (Figure 10a); then eBC decreased until its minimum in the early afternoon (1.07±0.10 µg m^{-3}) when the wind speed reached its maximum (1.5±0.1 m s^{-1}, Figure 10b). The incoming F_{glo} in clear sky peaked as expected at midday with 497±10 W m^{-2} (Figure 10c). This caused an asymmetric HR diurnal pattern, being characterized by a fast increase to the maximum at 10:00 LST (3.60±0.18 K day^{-1}) and a subsequent slower decrease till sunset (Figure 10d). This pattern was not present in cloudy conditions (Figure 10d). First, eBC showed a moderate peak at 10:00 LST (4.09±0.20 µg m^{-3}) being quite stable during afternoon – remaining above 3 µg m^{-3} until 16:00 LST (Figure 10a). The eBC behavior was consistent with that of wind speed which only slightly rose during the day, however being always below 1 m s^{-1} (on average 0.64±0.03 m s^{-1}, Figure 10b). The incoming F_{glo} in cloudy conditions peaked again as expected at midday with 103±4 W m^{-2} with a much slower increase during the day (Figure 10c). The supplemental material (section: Wind speed, cloudiness and clouds) and Figure 7b show that cloudy conditions were mostly associated to stratus and very low windy conditions (0.64±0.02 m s^{-1}), explaining the flat diurnal behavior of eBC differing from the clear sky case. Moreover, the absence of any direct irradiance in cloudy conditions (Figure 9b; section 3.1) determines that F_{glo} was essentially due to the diffuse irradiance whose symmetrical bell shape curve drove the HR behavior (Figure 10d), peaking at midday with a value of 0.74±0.01 K day^{-1} (much lower than in CS).

As a conclusion, in different cloudiness conditions, not only the absolute magnitude of the HR is different, but also its diurnal pattern. This also changes the related atmospheric feedbacks, such as the influence on the liquid water content (Jacobson et al., 2002), planetary boundary layer dynamics (Ferrero et al., 2014; Wang et al., 2018), regional circulation systems (Ramanathan and Carmichael, 2008; Ramanathan and Feng, 2009), and finally on the cloud dynamic and evolution itself (Koren et al., 2008; Bond et al., 2013). Thus, an inappropriate use of clear sky assumption in models will also reflect on the modelled HR-triggered feedbacks. These results also acquire relevance in the context of the counterintuitive semi-direct effect proposed by Perlwitz and Miller (2010) and referred to in Section 1: the atmospheric heating induced by tropospheric absorbing aerosol could lead to a cloud cover increase (especially low-level clouds). Such a feedback stresses the need for a proper inclusion of sky conditions into radiative transfer calculations.

3.2.3 The role of cloud type

The previous section showed the ~~importance~~ effect of cloudiness ~~in determining both the kind of the active radiation and the suppression~~ on the total LAA~~of~~ HR~~ with increasing the cloud cover.~~ . ~~This is relevant as it was found that cloudy conditions are dominant in terms of frequency. Here we will further investigate the clouds-HR relationships by exploring the effect of different types of clouds on this relationship. Figure 7a shows how the overall 77% of cloudy conditions encountered during the observational period was composed by the different cloud types, revealing that these were mainly St (42%), followed by StCu (13%) Ci, CiCu-CiSt (7% and 5%, respectively). The contribution of each cloud type to the cloudiness (expressed in oktas) of the sky is reported in Figure 7b. This clearly shows that, while St were mostly responsible of overcast situations (oktas=7-8, frequency: 87 and 96%), StCu dominated the intermediate cloudiness conditions (oktas=5-6, frequency: 47 and 66%); moderate cloudiness (oktas=3-4) were mostly due to a transition from CiCu-CiSt to StCu while low cloudiness (oktas=1-2) were mostly dominated by Ci and Cu (frequency: 59 and 40%, respectively).~~

The impact of each cloud type on the HR is addressed here as not all clouds have the same effect on irradiance (Tapakis and Charalambides, 2013).

As done in the previous section, we refer to HR values normalized to eBC unit mass (HR/eBC) to decouple radiation and aerosol effects. Figure 11a-d shows the total HR/eBC and F_{glo}~~,~~ together with the corresponding components (HR$_{dir}$/eBC and F_{dir}; HR$_{dif}$/eBC and F_{dif} ; HR$_{ref}$/eBC and F_{ref}; Figure 11b-d). ~~together with the corresponding components (HR$_{dir}$/eBC and F_{dir}; HR$_{dif}$/eBC and F_{dif} ; HR$_{ref}$/eBC and F_{ref}) is reported in Figure 8a-d.~~ The figure shows a prefect agreement between cloud type, irradiance and ~~radiation suppression of different cloud types and the consequent~~the corresponding HR/eBC~~ decrease~~ (R^2>0.93; not shown). It also highlights how critical is, for radiative transfer calculations and HR determination, to ~~conduct a proper simulation taking~~take into account the role of each cloud type. ~~We see that roughly, all different cloud types reduce HR/eBC differently, while~~Only the~~eir~~ cloud influence on the ~~diffuse component~~ HR$_{dif}$/eBC is ~~less~~ diverse from the other components. In terms of absolute values (not normalized for eBC), Figure ~~9~~ 12 reveals that the HR$_{dir}$~~HR due to direct radiation~~ was only dominant during CS and Ci conditions (HR$_{dir}$: 1.11±0.04 and 0.92±0.05 K day^{-1}, respectively), explaining 66±3 and 57±4% of the total atmospheric HR~~ of light absorbing aerosol (LAA)~~. In the other cloudy cases (St, As~~lSt~~ and ~~StCu~~Sc) HR$_{dif}$ dominates, reaching the highest absolute contribution of 84.4±3.8, 83.0±10.7 and 76±4% (HR$_{dif}$: 0.25±0.01, 0.34±0.03 and 0.66±0.02 K day^{-1}), respectively.

Given the aforementioned impact of cloud type, the capability of cloudiness to be a good predictor for the HR (as detailed in section 3.2.1) and the linkage (over the investigated site) between cloudiness and cloud type (section 3.1, Figure 7b), the synergic impact of cloudiness and cloud type on HR was investigated and presented in Figure 13. In the figure, we summarize the HR results in terms of percent difference from the clear sky (CS) case by averaging the cloudiness (in oktas) for each cloud type (as detected in section 3.3). Overall, the derived linear regression indicates a HR decrease of about 12% per okta; the R^2 (0.963) was slightly higher than that reported in Figure S6b (R^2=0.935; relationship with the cloudiness only) suggesting the need (for precise calculations) to account for the cloud types responsible for any sky coverage in agreement with a recent work of Bartoszek et al. (2020). ~~Exploring the relationship between cloud type and HR, we found a strong linear relationship between the mean cloudiness (in oktas) and the percent decrease of HR due to each cloud type with respect to the clear sky (CS) case (Figure 10). These results were obtained by averaging the cloudiness (in oktas) for each cloud type (as detected in section 3.3) and computing the cloud type resolved percentage decrease of LAA HR with respect to clear sky conditions. Overall, the derived linear regression (R^2=0.96) indicates a HR decrease of about 12% per okta.~~ Figure 13 ~~Knowledge of the dominant cloud types associated to the different cloud cover also~~ allow~~ed~~s us to associate ~~this~~ the HR decrease to each specific cloud type~~s~~. ~~(Figure 10). In particular~~Particulalry, Ci ~~are~~ were found to produce a modest impact on cloudiness (0.50±0.05 oktas) decreasing the HR by ~3%, while Cu (1.76±0.09 oktas) decrease the ~~LAA~~ HR by -26±8%. ~~CiCu~~Cc-~~CiSt~~ Cs (oktas of 3.56±0.14) were responsible for a -49±6 decrease of the HR. Their impact was comparable to that of ~~StCu~~ Sc (4.68±0.10 oktas, -48±4% of HR). ~~AlCu~~ Ac (4.11±0.18 oxtas) had a higher impact, decreasing the HR ~~of~~ by -59±6%. The highest impact was ~~given by~~due to ~~AlSt~~ As (6.57±0.15 oktas; -76±4% of HR) and~~ finally~~ by St (oktas: 7.19±0.04) that suppressed the ~~LAA~~ HR by a factor of -83±4%.

~~It is also worth to mention that not only the absolute value of the HR changes as a function of clouds in the atmosphere, but the presence of clouds also alters its diurnal pattern. In fact, as introduced in section 3.1, F_{dir} is scaled by μ in Eq. 1 (section 2.1) and thus it is perfectly constant along the day only in clear sky conditions. Conversely, even when scaled by μ, the diffuse and reflected radiation linearly follow the behavior of irradiance F_{dif} and F_{ref} (under the assumption of isotropic and Lambertian surface, Ferrero et al., 2018).~~

~~Thus any influence of clouds on F_{dir}, F_{dif} and F_{ref} will reflect into the interaction between the radiation itself and the absorbing aerosol, changing the HR diurnal pattern . To illustrate this effect, Figure 11 shows the average diurnal pattern of the HR in both clear sky (blue) and cloudy conditions (red; oktas=7-8, dominated exclusively by St and AlSt). This clearly shows that, while in clear sky conditions the HR exhibits an asymmetric diurnal pattern with a maximum around 10:00 LST, in cloudy conditions it shows a bell shape curve similar to that of F_{glo} (which is driven by the diffuse only component, which peaks at midday). As explained in more detail in Ferrero et al. (2018), the presence of the asymmetrical peak in clear sky conditions is due to the coupling between the eBC~~

~~daily pattern (characterized by a morning rush hour peak) and that of F_{dir}/μ, that is constant in CS. This is not the case in cloudy conditions when the most important radiation is F_{dif}.~~

~~A further important consequence of that change in the diurnal pattern of HR is that it reflects into related atmospheric feedbacks, such as the influence on the liquid water content (Jacobson et al., 2002), planetary boundary layer dynamics (Ferrero et al., 2014; Wang et al., 2018), regional circulation systems (Ramanathan and Carmichael, 2008; Ramanathan and Feng, 2009) and finally on the cloud dynamic and evolution itself (Koren et al., 2008; Bond et al., 2013). Thus, any inappropriate use of clear sky assumption in models will also reflect on the modelled HR-triggered feedbacks.~~

3.3 The impact of clouds on the ~~absolute and relative~~ BC and BrC heating rates

In this last part of the work we focus on the HR of the two main absorbing aerosol species: BC and BrC (obtained as detailed in section 2.1.1). The monthly averaged values of HR of BC and BrC (HR_{BC} and HR_{BrC}) are reported in Figure 14. The highest HR_{BC} and HR_{BrC} values were recorded in December (1.24±0.03 K day^{-1} and 0.19±0.01 K day^{-1}) while the lowest were recorded in March (0.46±0.01 K day^{-1} and 0.07±0.01 K day^{-1}). Overall, HR_{BrC} accounted for 13.7±0.2% of the total HR.

The variability of total HR_{BC} and HR_{BrC} as a function of cloudiness is reported in Figure 15a, with panels b-d showing their direct ($HR_{BC,dir}$ and $HR_{BrC,dir}$), diffuse ($HR_{BC,dif}$ and $HR_{BrC,dif}$) and reflected ($HR_{BC,ref}$ and $HR_{BrC,ref}$) components. Figure 15a shows that both HR_{BC} and HR_{BrC} decreased with increasing cloudiness, going from the CS maxima (HR_{BC} and HR_{BrC}: 1.14±0.03 and 0.20±0.01 K day^{-1}) to the completely overcast conditions (oktas=8) minima of 0.16±0.01 and 0.02±10^{-3} K day^{-1} (mainly due to St and As clouds; see Figure 7b). As shown in Figures 9a, the change of irradiance magnitude with cloudiness was different for direct, diffuse and reflected components affecting the corresponding direct, diffuse and reflected components of HR_{BC} and of HR_{BrC} (Figure 15b-d). $HR_{BC,dir}$ and $HR_{BrC,dir}$ (Figure 15b) decreased as a function of cloudiness from 0.74±0.03 and 0.11±0.01 K day^{-1} (oktas=0) to negligible levels (HR<10^{-4} K day^{-1}) in completely overcast conditions. $HR_{BC,dif}$ and $HR_{BrC,dif}$ (Figure 15c) increased with cloudiness, reaching their maximum in partially cloudy conditions (at oktas=6, 0.51±0.01 and 0.09±0.01 K day^{-1}). Further increasing cloudiness reduced their values to minimum values (0.13±0.01 and 0.02±0.01 K day^{-1}). $HR_{BC,ref}$ and $HR_{BrC,ref}$ (Figure 15d) behave similarly to the total HR_{BC} and HR_{BrC}, since the reflected irradiance is dominated by the global irradiance impinging on the ground (see Figure 9b for a comparison); $HR_{BC,ref}$ and $HR_{BrC,ref}$ decreased with increasing oktas from maximum values in clear sky ($HR_{BC,ref}$ and $HR_{BrC,ref}$: 0.17±4*10^{-3} and 0.03±1*10^{-3} K day^{-1}) down to overcast minimum ($HR_{BC,ref}$ and $HR_{BrC,ref}$ 0.02±10^{-3} and 3*10^{-3}±10^{-3} K day^{-1}). Figure 15a-d also shows that HR_{BC} was always greater (in absolute values) than HR_{BrC}, as expected. The relative decrease of HR_{BrC} from CS to complete overcast conditions was 12±6% larger with respect to that of HR_{BC}. At a first glance, Figure 15a-d could give the impression that BrC is more efficient in heating the surrounding atmosphere (with respect to BC) in CS conditions. However, any change of both BC and BrC $b_{abs}(\lambda)$ in different sky conditions has to be taken into account to avoid any misinterpretation of the results. While the variability of BC $b_{abs}(\lambda)$ with cloudiness was limited (Figure S8a), this was not the case for BrC. In fact, $b_{abs}(\lambda)$ BrC values in high cloudiness were statistically lower than the ones in CS (at oktas=8, $b_{abs}(\lambda)$ of BrC was -23±3% lower than in CS, Figure S8b). The relative decrease of the HR_{BrC} with cloudiness was therefore higher compared to that of HR_{BC}. Understanding of the reason behind the observation of higher $b_{abs}(\lambda)$ values for BrC in

CS is beyond the aim of the present paper (we can speculate it could be related to the formation of secondary BrC at high radiation levels, e.g., Kumar et al., 2018).

Here we focus on the fact that the magnitude of $b_{abs(\lambda)}$ of BC and BrC changed differently with cloudiness. Thus, in order to decouple the variability of the HR induced by the varying incoming irradiance from that due to changes in $b_{abs}(\lambda)$, both HR_{BC} and HR_{BrC} were normalized to the dimensionless integral of the $b_{abs}(\lambda)$ over the whole aethalometer spectrum. In this way, the magnitude of $b_{abs}(\lambda)$ is accounted for along the whole spectrum avoiding the choice of an arbitrary wavelength as a reference for the normalization. Similarly to section 3.2.2 for the total of LAA HR, the variability of the normalized HR_{BC} and HR_{BrC} was investigated with respect to cloudiness and cloud type. Figure 16a shows the decrease of normalized HR_{BC} and HR_{BrC} as a function of average cloudiness for each cloud type. We found a strong linear relationship between the decrease of both normalized HR_{BC} and HR_{BrC} (relative to CS) and the mean cloudiness (in okta) for each cloud type. Focusing on the cloud type, Ci were found to produce a statistically negligible impact on cloudiness (0.50±0.05 oktas) decreasing the HR_{BC} and HR_{BrC} by ~1-6%, respectively. Cu (1.76±0.09 oktas) decreased the HR_{BC} and HR_{BrC} by -31±12% and -26±7%, respectively. Cc-Cc featured oktas of 3.56±0.14, and were responsible for a -60±8% and -54±4% decrease of the HR_{BC} and HR_{BrC}. Their impact was comparable to that of Ac (4.11±0.18 oktas): -60±6% and -46±4% decrease of the HR_{BC} and HR_{BrC}. Sc (4.68±0.10 oktas) had a higher impact, decreasing HR_{BC} and HR_{BrC} of -63±6% and -58±4%. The highest impact was given by As (6.57±0.15 oktas; -78±5% and -73±4% of HR_{BC} and HR_{BrC}) and by St (oktas: 7.19±0.04) suppressing the HR_{BC} and HR_{BrC} by -85±5% and -83±3%, respectively.

Overall, the derived linear regressions indicate a decrease of ~12% per oktas for both HR_{BC} and HR_{BrC} (with high R^2: 0.958 and 0.963, respectively). In details, the respective decreases of HR_{BC} and HR_{BrC} were -11.8±1.2% and -12.6±1.4% per okta, these values not being statistically different. We show that, while BC and BrC have different optical properties and wavelength dependence of absorption, their HR normalized to absorption, changed without any statistical difference as a function of cloudiness and cloud type. This simplifies the models and reduces the number of details needed to be considered: once HR_{BC} and HR_{BrC} are determined in clear sky conditions, their dependence on the cloudiness can be determined from the simple reduction of the HR normalized to the absorption coefficient (about 12% for both species, once dominant cloud type is known).

However, it noteworthy that normalized HR_{BrC} values in Figure 16 were always greater or equal to the corresponding ones of BC (even if 95% confidence interval bands overlapped). A possible explanation can be the synergic effect between the different spectral absorption of BC and BrC and the influence of clouds on the energy of the impinging radiation; this is detailed in the Supplement (section: The role of average photon energy on the HR of BC and BrC). This feature needs further investigation in other seasons and elsewhere the world where the prevailing clouds type and the light absorption by BrC might be different.

~~As mentioned in the introduction, one of the key uncertain factors in climate change evaluations is the role played by different species of absorbing aerosol, the two most important species being BC and BrC. In this work we thus investigate the contribution of these two species to the HR at our measuring site. In the previous sections we discussed the absolute intensity of~~ ~~HR_{BC}~~ ~~and~~ ~~HR_{BrC}~~~~. They varyis function of four main variables, namely: 1) the absolute absorption coefficient values (~~~~$b_{abs(\lambda)}$~~~~) of both BC and BrC, 2) the absolute magnitude of the impinging radiation (~~~~$F_{n(\lambda,\theta)}$~~~~), 3) the different spectral absorption of BC and BrC, described by their AAE, and 4) the spectral features of the impinging radiation (~~~~$F_{n(\lambda,\theta)}$~~~~) described by the APE (section 2.3.3). Among these factors, the first~~

~~two are the dominant ones. However, the presence of clouds influences both the absolute magnitude and the spectral feature of the impinging radiation (sections 3.2 and 3.3).~~

~~We first present the impact of cloudiness and cloud type on both HR_{BC} and HR_{BrC} considering the absolute values of $b_{abs(\lambda)}$ and $F_{n(\lambda,\theta)}$ measured during the campaign (section 3.4.1). Then, in Section 3.4.2, we discuss the influence of different sky conditions and cloud type on HR due to both BC and BrC, focusing on the radiation APE through a HR_{BC} and HR_{BrC} data normalization with respect to the absolute magnitude of the $b_{abs(\lambda)}$ of both species.~~

~~3.3.1 The role of cloudiness~~

~~To complement the results in Figure 5a, the contribution of BC and BrC to the monthly averaged HR is reported in Figure 12. On average, the HR_{BrC} accounted for 13.7±0.2% of the total HR, the BrC being characterized by an AAE of 3.49±0.01, thus fully within ranges previously observed in other studies (e.g., Yang et al, 2009; Massabò et al., 2015; Ferrero et al., 2018). In Figure 13, HR_{BC} and HR_{BrC} are reported as a function of the oktas (total HR in Figure 13a and the contribution of direct, diffuse and reflected HR in panels b-d, respectively). As expected, Figure 13a shows that both HR_{BC} and HR_{BrC} decreased with increasing oktas, going from the clear sky maxima (HR_{BC} and HR_{BrC}: 1.14±0.03 and 0.20±0.01 K day^{-1}) to the overcast conditions minima (mainly due to St and AlSt clouds; see Figure 7b) of 0.16±0.01 and 0.02±10^{-3} K day^{-1}, respectively. This change is an important result related to the decrease of the absolute magnitude of impinging radiation, as described in sections 3.2 and 3.3. In fact, during the campaign, clear sky conditions were present only 23% of the time, the remaining time (77%) being characterized by partially cloudy (35%, 1-6 oktas) to totally cloudy (42%, 7-8 oktas) conditions. Moreover, as reported in the same sections (3.2 and 3.3) and shown in Figures 5 and 6, the change of radiation magnitude with cloudiness was different for direct, diffuse and reflected radiation. This behavior affected the corresponding direct, diffuse and reflected radiation components of HR_{BC} and of HR_{BrC} (Figure 13 b-d). For the direct radiation, Figure 13b shows both $HR_{BC,dir}$ and $HR_{BrC,dir}$ to decrease as a function of cloudiness to negligible levels (HR<10^{-4} K day^{-1}) in overcast conditions. Conversely, $HR_{BC,dif}$ and $HR_{BrC,dif}$ increased for increasing oktas (Figure 13c), reaching their maximum in partially cloudy conditions (at oktas=6, 0.51±0.01 and 0.09±0.01 K day^{-1}) when also the maximum of F_{dif} was registered (section 3.2 and Figure 6a). Then, for further increasing cloudiness, they dropped down to minimum values (0.13±0.01 and 0.02±0.01 K day^{-1}). Finally, $HR_{BC,ref}$ and $HR_{BrC,ref}$ (Figure 13d) behave similarly to the total HR_{BC} and HR_{BrC}, being the reflected radiation dominated by the total radiation impinging on the ground (see Figures 8a and 8d for a comparison). In this respect, $HR_{BC,ref}$ and $HR_{BrC,ref}$ decreased with increasing oktas from maximum values in clear sky ($HR_{BC,ref}$ and $HR_{BrC,ref}$: 0.17±4*10^{-3} and 0.03±1*10^{-3} K day^{-1}) down to overcast minimum ($HR_{BC,ref}$ and $HR_{BrC,ref}$ 0.02±10^{-3} and 3*10^{-3}±10^{-3} K day^{-1}).~~

~~Figure 13 also clearly shows that HR_{BC} is always greater than HR_{BrC}, as expected. However, a deeper investigation of the data reported in Figure 13 allows us to better describe the interaction between radiation and LAA in heating the surrounding atmosphere. To this purpose, it is particularly useful to compare the relative decrease of HR_{BrC} from clear sky to complete overcast situation to that of HR_{BC}. The clouds, going from 0 to 8 oktas, decrease the HR_{BrC} 12±6% more compared to HR_{BC}. The same happened to $HR_{BC,dir}$ and $HR_{BrC,dir}$. The diffuse component of the HR behaves differently: the clouds decrease $HR_{BrC,dif}$ 38±6% more compared to $HR_{BC,dif}$.~~

~~At a first glance, Figure 13 could give the impression that BrC is more efficient in heating the surrounding atmosphere (with respect to BC) in clear sky conditions, compared to cloudy ones. Note however that, as stated at~~

~~the beginning of this section, any change of both BC and BrC $b_{abs(\lambda)}$ in different sky conditions has to be accounted for to avoid any misinterpretation of the results.~~

~~In fact, we observed that at all wavelengths and for both BC and BrC, $b_{abs(\lambda)}$ was not constant during periods with different cloudy conditions (Figure S7). However, while the variability of $b_{abs(\lambda)}$ BC with varying oktas was limited, this was not the case for BrC (Figure S7a).Values of $b_{abs(\lambda)}$ BrC in high cloud cover conditions were statistically lower than the one in clear sky/moderate cloudy conditions (at oktas=8 the $b_{abs(\lambda)}$ of BrC was on average -23±3% lower than in clear sky, Figure S7b). The full understanding of this behavior, perhaps linked to the formation of secondary BrC at high radiation in clear sky compared to cloudy ones (Kumar et al., 2018), is beyond the aim of the present paper. Here we focus the attention on the fact that the magnitude of $b_{abs(\lambda)}$ of BC and BrC changed differently with cloudiness. This behavior explains why, at a first glance, the relative decrease of the HR_{BrC}, from 0 to 8 oktas, was higher compared to that of HR_{BC}. At the same time, the fact that the diffuse component of the HR_{BrC} ($HR_{BrC,dif}$) experienced a higher relative decrease (from clear sky situation to overcast ones) than those observed for the total HR_{BrC} asks for further investigation. Some insights into this behavior are given in the next Section.~~

~~3.3.2 The role of the average photon energy and cloud type~~

~~In order to decouple the variability of the HR induced by radiation from that due to $b_{abs(\lambda)}$, both HR_{BC} and HR_{BrC} were normalized for the adimensional integral of the $b_{abs(\lambda)}$ over the whole aethalometer spectrum. In this way, the magnitude of $b_{abs(\lambda)}$ is accounted for along the whole spectrum avoiding the choice of an arbitrary λ as a reference for the normalization. Figure S8 reports the same data present in Figure 13a after the normalization for $b_{abs(\lambda)}$ and for the corresponding CS HR_{BC} and HR_{BrC} values. Results first show that the relative decrease of the HR_{BrC}, from 0 to 8 oktas, was 12±6% lower compared to that of HR_{BC}, or, in other words, it was the decrease the HR_{BC} that was 12±6% higher compared to that of HR_{BrC} A counter-intuitive consequence of this analysis is that, compared to CS, cloudy This means that cloudiness and clouds not only affect absolute values of both HR_{BC} and HR_{BrC} but they markedly affect their ratio.~~~~Also in this case, the variability of the HR induced by radiation was decoupled from that due to $b_{abs(\lambda)}$ by normalizing HR_{BC} and HR_{BrC} for the adimensional integral of $b_{abs(\lambda)}$ over the whole aethalometer spectrum. We found a strong linear relationship between the mean cloudiness (in oktas) and the percent decrease of both (BC and BrC) HRs with respect to those in clear sky conditions (Figure 15). These results were obtained by averaging the cloudiness (in oktas) for each cloud type (as detected in section 3.3) and combining them with percentage decrease of HR_{BC} and HR_{BrC} (again averaged for each cloud type) with respect to clear sky conditions. Overall, the derived linear regression indicates for both HR_{BC} and HR_{BrC} a decrease of about 12% per oktas (with high R^2). Knowledge of the dominant cloud types associated to the different cloud cover also allows us to associate this decrease to specific cloud types. In particular, Ci were found to produce a modest impact on cloudiness (0.50±0.05 oktas) decreasing the HR_{BC} and HR_{BrC} by ~1-6%, respectively. Instead, Cu (1.76±0.09 oktas) decreased the HR_{BC} and HR_{BrC} by -31±12% and -26±7%, respectively. CiCu-CiSt were associated to an averaged oktas of 3.56±0.14, and were responsible for a -60±8% and -54±4% decrease of the HR_{BC} and HR_{BrC}. Their impact was comparable to that of AlCu (4.11±0.18 oktas): -60±6% and -46±4% decrease of the HR_{BC} and HR_{BrC}. StCu (4.68±0.10 oktas) had a higher impact, decrasing HR_{BC} and HR_{BrC} of -63±6% and -58±4%. The highest impact was given by AlSt (6.57±0.15 oktas; -78±5% and -73±4% of HR_{BC} and HR_{BrC}) and finally by St (oktas: 7.19±0.04) that suppressed the HR_{BC} and HR_{BrC} by a factor of -85±5% and -83±3%, respectively.These results confirm that, on average, the HR_{BC} is more affected by cloudy conditions than HR_{BrC}, further proving that~~

~~the presence of different cloud types in different proportions in the sky can bring to inaccurate HR_{BC} and HR_{BrC} estimations if clear sky assumptions are improperly used to model the aerosol DRE. Particularly, if clear sky is assumed improperly, HR_{BC} and HR_{BrC} can be overestimated up to a factor of ~6 in highly cloudy St conditions. Thus, the aerosol DRE and related HR has to be properly calculated in the presence of clouds for correct future scenario of our climate system.~~

~~1~~

~~nconditions suppress much more the HR_{BC} with respect to HR_{BrC}. The diffuse component of the HR was the only one that kept an opposite behavior after the normalization for $b_{abs(\lambda)}$. The decrease of $HR_{BrC,dif}$ was 21±6% higher compared to that of $HR_{BC,dif}$ (from clear sky situation to overcast ones); however this value is lower than the 38±6% reported in section 3.4.1 before the normalization for $b_{abs(\lambda)}$ meaning that, even at equal absorption, the diffuse component of radiation plays a role in affecting the BrC response. This means that cloudiness and clouds not only affect absolute values of both HR_{BC} and HR_{BrC} but they markedly affect their ratio.~~

~~The role of the average photon energy and cloud type~~

~~This pattern can be related to the different APE (section 2.3.3) that the direct and diffuse radiations feature in different sky conditions (Figure 14). Higher APE values describe the shift of a radiation spectrum towards UV-blue region and vice versa (section 2.3.3). Figure 14 shows that while APE_{dir} slightly increases towards overcast conditions, APE_{dif} strongly decreases going from clear sky to 8 oktas. The $APE_{dif,dir}$ behavior can easily be explained considering the features of the direct and diffuse radiation spectra (Figure S9). In fact, in clear sky conditions, the diffuse radiation is characterized by a high density in the UV-blue high energy region with respect to the direct radiation, which indeed is depleted in that region by the molecular Rayleigh scattering. APE_{dir} in clear sky conditions is in fact 1.89±0.01 eV, lower than the 2.20±0.01 eV of APE_{dif} (Figure 14). Conversely, in cloudy conditions (Figure 14 and Figure S9) $F_{dif,\lambda}$ and $F_{dir,\lambda}$ behave similarly and the APE_{dif} values equals that of APE_{dir}: 1.99±0.01 eV. The BrC has the capacity to absorb much more radiation in the UV-blue region (featuring higher AAE of 3.49±0.01, compared to ~1 of BC). It follows that, depending on sky conditions, different parts of the absorption spectra are important for BrC relative to BC. In this respect, ΔAPE_{dir} (cloudy-CS) was $0.11\pm3*10^{-3}$ eV while ΔAPE_{dif} was 2 times higher ($0.22\pm2*10^{-3}$ eV). This explains the behavior of $HR_{BC,dir}$ and $HR_{BrC,dir}$ and of $HR_{BC,dif}$ and $HR_{BrC,dif}$ after the normalization for $b_{abs(\lambda)}$. However, they do not explain the behavior of the total HR_{BC} and HR_{BrC} with respect to cloudiness: the absolute amount of direct and diffuse radiation F_{dir}, F_{dif} (and not only their spectral feature) has to be accounted for. Thus, the APE for the total sky radiation was determined as a weighted average with respect to the absolute amount of F_{dir} and F_{dif} in function of cloudiness expressed in oktas; results are reported in Figure 14 and clearly show an increasing APE_{tot} from clear sky to cloudy conditions, approaching APE_{dif} at okta=8. This APE_{tot} feature explain the counter-intuitive property that cloudy conditions suppress much more the HR_{BC} with respect to HR_{BrC}, as shown above.~~

~~We have shown that different cloud types are responsible for the different cloudiness (Section 3.3 and Figure 7b). It is worth to explore the relationship between cloud type and both HR_{BC} and HR_{BrC} as previously done for the total LAA HR (Figure 10). Also in this case, the variability of the HR induced by radiation was decoupled from that due to $b_{abs(\lambda)}$ by normalizing HR_{BC} and HR_{BrC} for the adimensional integral of $b_{abs(\lambda)}$ over the whole aethalometer spectrum. We found a strong linear relationship between the mean cloudiness (in oktas) and the percent decrease of both (BC and BrC) HRs with respect to those in clear sky conditions (Figure 15). These results were obtained by averaging the cloudiness (in oktas) for each cloud type (as detected in section 3.3) and combining~~

~~them with percentage decrease of HR$_{BC}$ and HR$_{BrC}$ (again averaged for each cloud type) with respect to clear sky conditions. Overall, the derived linear regression indicates for both HR$_{BC}$ and HR$_{BrC}$ a decrease of about 12% per oktas (with high R^2). Knowledge of the dominant cloud types associated to the different cloud cover also allows us to associate this decrease to specific cloud types. In particular, Ci were found to produce a modest impact on cloudiness (0.50±0.05 oktas) decreasing the HR$_{BC}$ and HR$_{BrC}$ by ~1-6%, respectively. Instead, Cu (1.76±0.09 oktas) decreased the HR$_{BC}$ and HR$_{BrC}$ by -31±12% and -26±7%, respectively. CiCu-CiSt were associated to an averaged oktas of 3.56±0.14, and were responsible for a -60±8% and -54±4% decrease of the HR$_{BC}$ and HR$_{BrC}$. Their impact was comparable to that of AlCu (4.11±0.18 oktas): -60±6% and -46±4% decrease of the HR$_{BC}$ and HR$_{BrC}$. StCu (4.68±0.10 oktas) had a higher impact, decrasing HR$_{BC}$ and HR$_{BrC}$ of -63±6% and -58±4%. The highest impact was given by AlSt (6.57±0.15 oktas; -78±5% and -73±4% of HR$_{BC}$ and HR$_{BrC}$) and finally by St (oktas: 7.19±0.04) that suppressed the HR$_{BC}$ and HR$_{BrC}$ by a factor of -85±5% and -83±3%, respectively.~~

~~These results confirm that, on average, the HR$_{BC}$ is more affected by cloudy conditions than HR$_{BrC}$, further proving that the presence of different cloud types in different proportions in the sky can bring to inaccurate HR$_{BC}$ and HR$_{BrC}$ estimations if clear sky assumptions are improperly used to model the aerosol DRE. Particularly, if clear sky is assumed improperly, HR$_{BC}$ and HR$_{BrC}$ can be overestimated up to a factor of ~6 in highly cloudy St conditions. Thus, the aerosol DRE and related HR has to be properly calculated in the presence of clouds for correct future scenario of our climate system.~~

Summary and c~~C~~onclusions

The heating rates (HR) associated to the two major LAA species, i.e., Black Carbon (BC) and Brown Carbon (BrC) (HR$_{BC}$ and HR$_{BrC}$) were experimentally determined based on~~at~~ high time resolution ~~(5-minutes)~~ radiation and aerosol measurements in the Po Valley. The total HR was firstly ~~and further~~ examined in relation to sky conditions to determine the impact of cloud-aerosol-radiation interactions on the atmospheric heating. Results showed a constant decrease of LAA HR with increasing cloudiness of the atmosphere. Our real-atmosphere, all-sky, measurement-based results suggest that using a simplified assumption of clear sky in radiative transfer calculations might produce HR overestimated by over~~From the obtained results, the error (in %) associated to HR radiative transfer calculations in case of a simplified but incorrect assumption of clear sky was calculated as a function of the real (observed) cloudiness showing overestimations up to 470~~400%. The effect of different cloud types on the HR was also investigated. While cirrus were characterized by a modest impact cumulus, cirrocumulus-cirrostratus and Altocumulus~~:~~ suppressed the HR of both BC and BrC by a factor of ~2. Stratocumulus, altostratus stratus suppressed the HR$_{BC}$ and HR$_{BrC}$ up to 80%. The cloudiness also changed the diurnal pattern of HR with possible feedbacks on planetary boundary layer dynamics and/or regional circulation systems.

~~Thus, any inappropriate use of clear sky assumption in models will also reflect on the modelled HR-triggered feedbacks.~~

~~Finally, the cloud impact on the solar radiation spectrum affected more, on average, the HR$_{BC}$ than HR$_{BrC}$. This means that cloudiness and clouds type not only affect absolute values of both HR$_{BC}$ and HR$_{BrC}$ but they markedly affect their ratio~~ Total HR, HR$_{BC}$ and HR$_{BrC}$ are affected by both cloudiness and cloud type so that inaccurate HR$_{BC}$ and HR$_{BrC}$ estimations can be derived from simulations if presence of clouds is ignored and cloud type is not taken into account. Most important, the coupling between the cloud impact on the solar radiation spectrum (and its direct, diffuse and reflected components) and the spectral absorption properties of BC and BrC showed that the absolute HR_{BC} and HR_{BrC} vary differently with cloudiness (especially the diffuse component), but feature a very similar normalized (to the absorption coefficient) dependence on the cloudiness. This simplifies the models and reduces the number of details that need to be considered: once HR_{BC} and HR_{BrC} are determined in clear sky conditions, their dependence on the cloudiness can be determined from the simple reduction of the HR normalized to the absorption coefficient (about 12% for both species) and the respective absorption coefficients. These data acquire importance when discussed in the context of the counterintuitive semi-direct effect proposed by Perlwitz and Miller (2010): the atmospheric heating induced by tropospheric absorbing aerosol could lead to a cloud cover increase stressing the needs for a proper determination and simulation of sky conditions during radiative transfer calculations.

Acknowledgements

This paper is an output of the GEMMA center in the framework of the MIUR project "Dipartimenti di Eccellenza 2018-2022". The authors want to acknowledge the COST action COLOSSAL CA16109, Aerosol d.o.o and LSI-Lastem for the cooperation during the campaign.

Data Availability

Data will be available upon request.

Author contribution

Conceptualization, L. Ferrero, E. Bolzacchini, Grisa Mocnik, Martin Rigler and A. Gregoric; Methodology, L. Ferrero, A. Gregoric, S. Cogliati, N. Losi, F. Barnaba, L. Di Liberto, G.P. Gobbi; Data Investigation, L. Ferrero, A. Gregoric, S. Cogliati, F. Barnaba, G. Mocnik, M. Rigler; Resources, E. Bolzacchini, M. Rigler; Original Draft Preparation, L. Ferrero; Writing-Review & Editing, L. Ferrero, A. Gregoric, G. Mocnik and F. Barnaba; Supervision, G. Mocnik, Martin Rigler, F. Barnaba, E. Bolzacchini.

Conflict of interest

The authors declare no conflict of interest. The funders had no role in the design of the study; in the collection, analyses, or interpretation of data; in the writing of the manuscript, and in the decision to publish the results.

Appendix A: Nomenclature

Nomenclature	
Aerosol Acronyms	
AAE	Absorption Angstrom Exponent
AAE_{BC}	Absorption Angstrom Exponent of Black Carbon
AAE_{BrC}	Absorption Angstrom Exponent of Brown Carbon
ADRE	Absorptive Direct Raditive Effect
$b_{abs(\lambda)}$	wavelength dependent aerosol absorption coefficient
BC	Black Carbon

BrC	Brown Carbon
eBC	equivalent Black Carbon concentration
LAA	Light Absorbing Aerosol
HR	Heating Rate
HR_{BC}	Heating Rate of Black Carbon
HR_{BrC}	Heating Rate of Brown Carbon

Cloud/Sky Acronyms

As	Altostratus
Ac	AltoCumulus
Ci	Cirrus
Cc-Cs	Cirrocumulus-Cirrostratus
Cu	Cumulus
CS	Clear Sky
St	Stratus
Sc	Stratocumulus
CBH	Cloud Base Height (km)
N	numer of oktas (0-8)
R	ratio (R) between observed global irradiance (Fglo) and the modelled clear sky irradiance (GHI)
SD	standard deviation of the measured F_{glo} in 20 minute time intervals
SZA	Solar Zenith Angle

Other Symbols/Acronyms

ϕ	Azimuth angle
Φ_λ	photon flux density at wavelength λ
λ	Wavelength
ρ	Air Density
θ	angle of the impinging radiation
a	empirical coefficient from Ehnberg and Bollen (2005); Table S1
a_0	empirical coefficient from Ehnberg and Bollen (2005); Table S1
a_1	empirical coefficient from Ehnberg and Bollen (2005); Table S1
a_3	empirical coefficient from Ehnberg and Bollen (2005); Table S1
APE	Average Photon Energy
APE_{dif}	Average Photon Energy for diffuse radiation
APE_{dir}	Average Photon Energy for direct radiation
APE_{ref}	Average Photon Energy for reflected radiation
c	speed of light (m s^{-1})
C_p	Isobaric specific heat of dry air (1005 J kg^{-1} K^{-1})
dif	diffuse
dir	direct

F_{glo}	Global Irradiance; $F_{glo}= F_{dir} + F_{dif}$
F_{dif}	Diffuse Irradiance
F_{dir}	Direct Irradiance
F_{ref}	Reflected Irradiance
$F_{dir,dif,ref(\lambda)}$	Spectral irradiance in function of λ
h	Plank constant (J s)
ref	reflected
L	empirical coefficient from Ehnberg and Bollen (2005); Table S1
q	Electron charge
$R(\lambda,\theta,\phi)$	Radiance at wavelength λ from zenith and azimuth angles θ and ϕ

Appendix B: Cloud type validation

The validation was conducted in two subsequent steps. In the first step the automatized cloud classification (based on Duchon and O'Malley, 1999 including lidar cloud base height) was compared to the visual cloud classification based on sky images collected during 1 month of field campaign.

The second validation step involved the recently published method discussed by Ylivinkka et al. (2020) which is based on the same methodological approach used in this study: the application of Duchon and O'Malley (1999) classification improved by the knowledge of the CBH. Thus, the aim of the second step was to determine the degree of consistency between the two approaches that were developed simultaneously and independently in two different regions of the globe.

Both the two validations were evaluated by means of a confusion matrix, a special kind of contingency table, with two dimensions and identical sets of "classes" in both of them. From the confusion matrix the balanced accuracy was computed as follows:

$$Balanced\ Accuracy = \frac{Sensitivity+Specificity}{2} \tag{B1}$$

where the *Sensitivity* describes the true positive rate (the number of correct positive predictions divided by the total number of positives) and the *Specificity* describes the true negative rate (the number of correct negative predictions divided by the total number of negatives). The balanced accuracy is especially useful when the investigated classes are imbalanced, i.e. one of the classes appears a lot more often than the other, a condition useful for cloud classification (García et al., 2009).

Appendix B1: visual cloud classification

Sky images were collected during 1 month (13 February – 9 March 2017) using a sky view camera (GoPro Hero4 Session installed on the U9 roof) characterized by a field of view of 95x123°; the camera was oriented south each day manually with the same declination of the shadow band applied to DPA154 global radiometer for diffuse broadband irradiance measurements (section 2.1.2); sky images were taken with 1 minute time resolution. Visual classification of sky images, based on the principles of cloud classification published in Cloud Atlas (WMO). Figure B1 reports an example of SD-R diagram (section 2.3.2) with CBH for each sky/cloud conditions with the corresponding image.

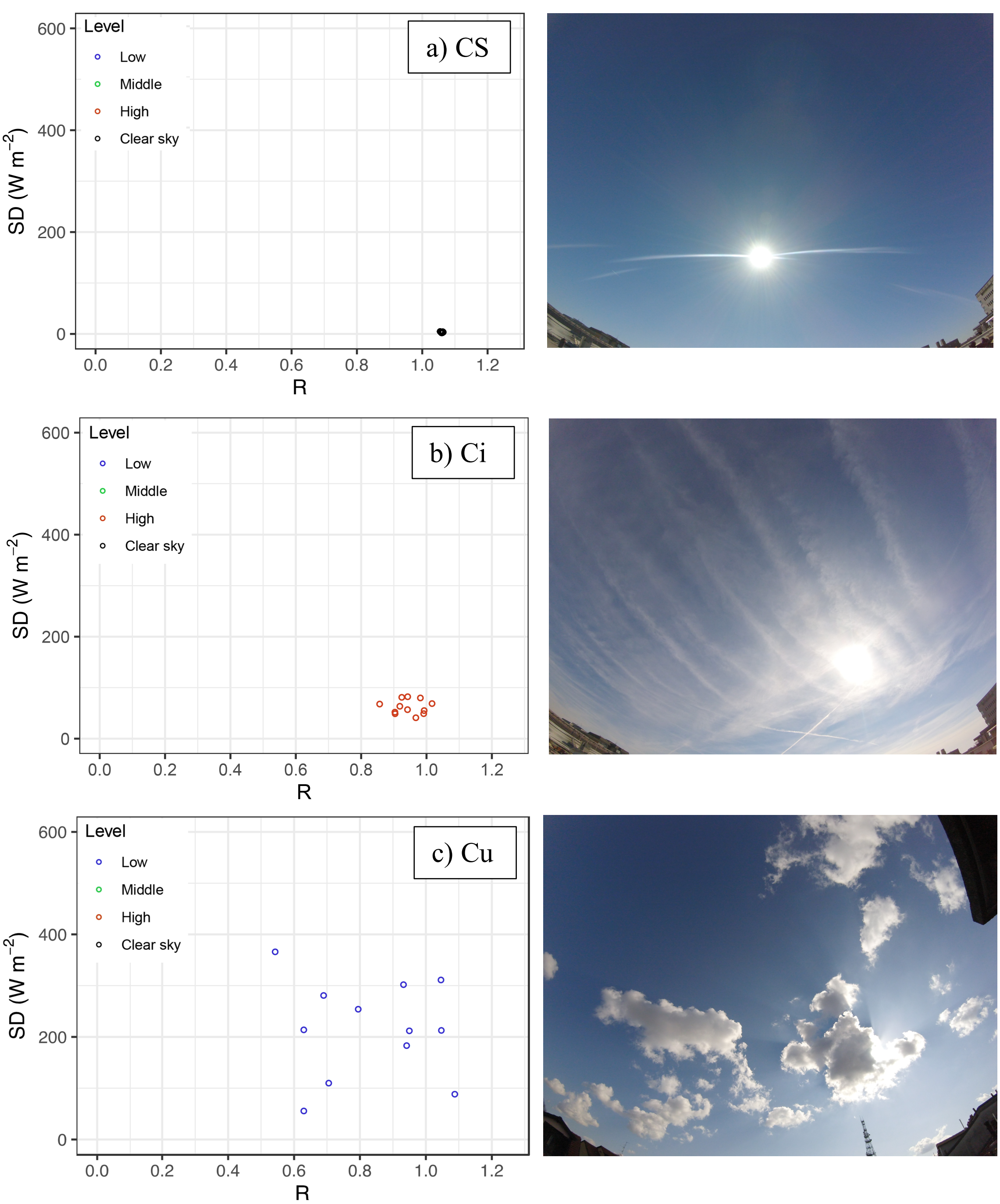
a) CS
b) Ci
c) Cu
Level
Low
Middle
High
Clear sky
SD (W m^{-2})
R
0
200
400
600
0.0
0.2
0.4
0.6
0.8
1.0
1.2

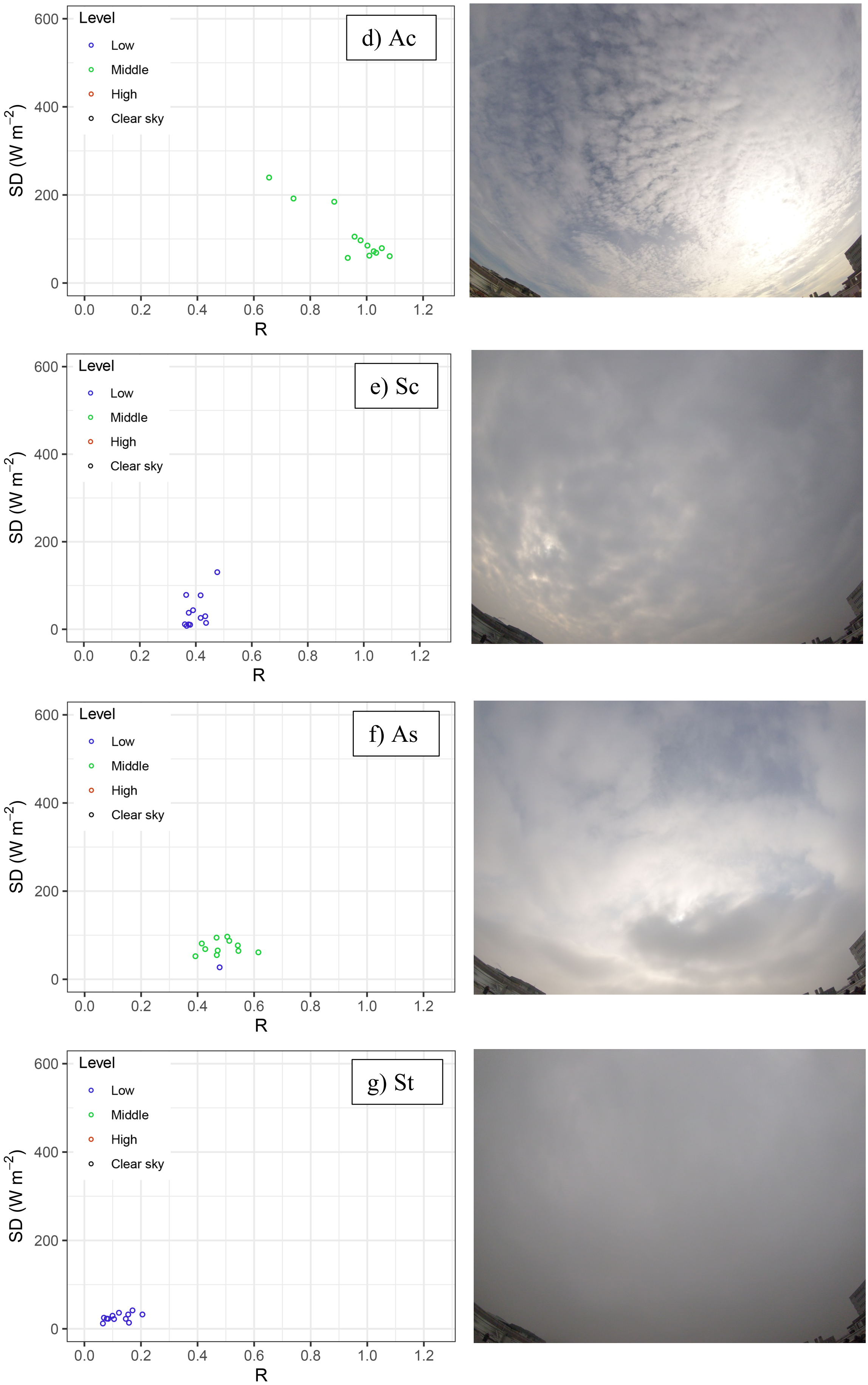

d) Ac
e) Sc
f) As
g) St
Level
Low
Middle
High
Clear sky
SD (W m^{-2})
R
0
200
400
600
0.0
0.2
0.4
0.6
0.8
1.0
1.2

Figure B1. SD-R diagram (left panel) and the corresponding sky images for the February-March 2017 field campaign: a) CS case, b) Ci clouds case, c) Cu clouds case, d) Ac clouds case, e) Sc clouds case, f) As clouds case and g) St clouds case.

To test the performance, 869 sky images were analyzed, and the cloud type was determined through visual inspection. From the visual classification and the automatized one (Table 1) the following confusion matrix (Table B1) was created. The highest balanced accuracy was found for St data (9495%) while the lowest (50%) for mixed cloud types (Cc-Cs) whose absolute number of cases, however, was ~0.6% of the total, probably biasing the obtained accuracy; the same happened for Cu and Ac. Overall, five classes over eight were above 68% of balanced accuracy while the overall balanced accuracy was 80%, underlying the reliability of the classification algorithm allowing to study the impact of clouds on LAA HR with a sufficient grade of certainty.

Table B1. Confusion matrix and balanced accuracy for each cloud type classified visually and following the algorithm reported in Table 1 within the present work.

Appendix B2: intercomparison with Ylivinkka et al. (2020)

The second validation step involved the recently published method discussed by Ylivinkka et al. (2020), which is based on the same logical approach followed in our work: the application of Duchon and O'Malley (1999) classification improved by the knowledge of the CBH. At this purpose, the classification scheme of Ylivinkka et al. (2020) is resumed in Table B2 following the nomenclature used in the present work. It is necessary to underline that the cloud classes determined in the work Ylivinkka et al. (2020) differ from those reported in the present work. Particularly, while both approaches enabled the Cu, St, Sc classification, some of the cloud classes were merged in the Ylivinkka et al. (2020) study: CS and Ci (CS+Ci), Ac and As (Ac+As) and mixed situation composed by Ci, Cc, Cs (Ci+Cc+Cs). In addition they introduced the classes Cu+GRE and Ci+GRE to account for global radiation enhancement (GRE) due to this cloud types; a possible explanation for such difference with respect to present work could be hidden in the different latitude at which the two algorithms were developed, a parameter able to affect the solar zenith angle and the sun light interaction with clouds. A detailed investigation of this difference is beyond the aim of the present work. However, it is necessary to account for the classification differences in order to properly merge cloud classes with similar features to finally perform a comparison between the two methods. The cloud classes homogenization is summarized in Table B3 while the final intercomparison is reported in Table B4. The confusion matrix (Table B4) revealed a global balanced accuracy of 90% making the two methods comparable, despite the aforementioned differences. The highest accuracy (100%) was obtained for CS followed by Ac+As (99%); Cu, St and Sc reached values of 94, 93 and 86%, respectively. The lowest performance was reached for Ns whose presence cannot be detected in the present study generating a false positive signal in the Ac+As class; however, due to the very low number of Ns cases (1.8%), its impact on the cloud classification can be neglected. Overall, also the second validation step pointed out the reliability of the results obtained in the present work.

Cloud type	CBH (m)	R	SD (W/m2)	N of cloud layers
Cu	< 2000	0.6 – 0.85 & Rmax > 1	>= 200	1
	< 2000	> 0.85 & Rmax > 1	0 – 200	1
St	< 2000	< 0.6	< 100	1
Sc	< 2000	0.1 – 0.6	>= 100	1
Ns	2000 - 3000	< 0.3	< 100	1
Ac+As	2000 - 5000	>=0.3	< 500	1
Ci+Cc+Cs	>= 4000	0.85 – 1.1	50 - 400	1
	>= 4000	0.5 – 0.85	< 400	1
CS+Ci	NaN	0.85 – 1.05	< 50	1
Cu+GRE	< 2000	> 1 & Rmax > 1	>= 200	1
Ci+GRE	>=4000	> 1	< 400	1

Table B2. Final criteria adopted for cloud classification in Ylivinkka et al. (2020). Ns here represents Nimbostratus while GRE global enhancement radiation.

This study	Cu	St	Sc	/	Ac, As	Ci Cc-Cs	CS
Ylivinkka et al., 2020	Cu, Cu+GRE	St	Sc	Ns	Ac+As	Ci+Cc+Cs Ci+GRE	CS+Ci
Merged Cloud type	Cu	St	Sc	Ns	Ac+As	Ci+Cc+Cs	CS+Ci

Table B3. Cloud classes homogenization adopted for comparison purposes between the present study cloud classification and the one reported in Ylivinkka et al. (2020).

Cloud type classification		Ylivinkka et al. (2020)							Balanced accuracy
		Cu	St	Sc	Ns	Ac+As	Ci+Cc+Cs	CS+Ci	
This study	Cu	**80**							94%
	St		**3853**	58		1			93%
	Sc	11	596	**231**					86%
	Ns				**0**				50%
	Ac+As				153	**383**	51		99%
	Ci+Cc+Cs						**846**		97%
	CS+Ci							**2142**	100%

Table B4. Confusion matrix and balanced accuracy for each cloud type classified using the algorithm reported in the present study and the one reported in Ylivinkka et al. (2020).

References

Andreae, M., Ramanathan, V.: Climate's Dark Forcings. Science, 340 (2002), 280–281, 2013.

Bikkina, S., Sarin, M.M.: Light absorbing organic aerosols (brown carbon) over the tropical Indian Ocean: impact of biomass burning emissions. Environ. Res. Lett., 8 (4), 044042, 2013.

Barnaba, F. and Gobbi, G. P.: Aerosol seasonal variability over the Mediterranean region and relative impact of maritime, continental and Saharan dust particles over the basin from MODIS data in the year 2001, Atmospheric Chemistry and Physics, 4(9/10), 2367–2391, doi:10.5194/acp-4-2367-2004, 2004.

Barnaba, F., Putaud, J.P., Gruening, C., Dell'Acqua, A., Dos Santos, S., 2010. Annual cycle in co-located in situ, total-column, and height- resolved aerosol observations in the Po Valley (Italy): Implications for ground-level particulate matter mass concentration estimation from remote sensing. J. Geophys. Res., 115, D19209, doi:10.1029/2009JD013002.

Bartoszek, K., Matuszko, D. and Soroka, J.: Relationships between cloudiness, aerosol optical thickness, and sunshine duration in Poland, Atmospheric Research, 245(April), 105097, doi:10.1016/j.atmosres.2020.105097, 2020.

Boers, R., de Haij, M. J., Wauben, W., Baltink, H. K., van Ulft, L. H., Savenije, M., & Long, C. N.: Optimized fractional cloudiness determination from five ground-based remote sensing techniques. Journal of Geophysical Research, 115, D24116. https://doi.org/10.1029/ 2010JD014661, 2010.

Bond, T. C., Doherty, S. J., Fahey, D. W., Forster, P. M., Berntsen, T., Deangelo, B. J., Flanner, M. G., Ghan, S., Kärcher, B., Koch, D., Kinne, S., Kondo, Y. and Quinn, P. K.: Bounding the role of black carbon in the climate system : A scientific assessment, J. Geophys. Res., 118, 1–173, doi:10.1002/jgrd.50171, 2013.

Bond, T. C. and Bergstrom, R. W.: Light Absorption by Carbonaceous Particles: An Investigative Review, Aerosol Sci. Tech., 40, 27–67, doi:10.1080/02786820500421521, 2006.

Calbo´ , J., Gonza´ lez, J.A., Page` s, D., 2001. A method for sky-condition classification from ground-based solar radiation measurements. Jour- nal of Applied Meteorology 40, 2193–2199.

Calbó, J., Pagès, D., and González, J.-A.: Empirical studies of cloud effects on UV radiation: A review, Reviews of Geophysics, 43, n/a-n/a, 10.1029/2004RG000155, 2005.

Carbone, C., Decesari, S., Mircea, M., Giulianelli, L., Finessi, E., Rinaldi, M., Fuzzi, S., Marinoni, A., Duchi, R., Perrino, C., Sargolini, T., Vardè, M., Sprovieri, F., Gobbi, G. P., An- gelini, F., and Facchini, M. C.: Size-resolved aerosol chemical composition over the Italian Peninsula during typical summer and winter conditions, Atmos. Environ., 44, 5269–5278, doi:10.1016/j.atmosenv.2010.08.008, 2010.

Campbell, J.R., Lolli, S., Lewis, J.R., Gu, Y., and Welton, E. J.: Daytime Cirrus Cloud Top-of-the-Atmosphere Radiative Forcing Properties at a Midlatitude Site and Their Global Consequences. J. Appl. Meteorol. Climatol., 55, 1667–1679, 2016.

Chung, C. E., Ramanathan, V., Decremer, D. Observationally constrained estimates of carbonaceous aerosol radiative forcing. Proceedings of the National Academy of Sciences of the United States of America, 109 (29), 11624–11629, 2012.

Collaud Coen M., Weingartner E., Apituley A., Ceburnis D., Fierz-Schmidhauser R., Flentje H., Henzing J.S., Jennings S.G., Moerman M., Petzold A., Schmid O., and Baltensperger U. Minimizing light absorption measurement artifacts of the Aethalometer: evaluation of five correction algorithms. Atmos. Meas. Tech., 3, 457–474, 2010.

Costabile, F., Barnaba, F., Angelini, F. and Gobbi, G. P.: Identification of key aerosol populations through their size and composition resolved spectral scattering and absorption, Atmospheric Chemistry and Physics, 13(5), 2455–2470, doi:10.5194/acp-13-2455-2013, 2013.

Croke, M. S., Cess, R. D. and Hameed, S.: Regional cloud cover change associated with global climate change: Case studies for three regions of the United States, Journal of Climate, 12(7), 2128–2134, 1999.

Diémoz, H., Barnaba, F., Magri, T., Pession, G., Dionisi, D., Pittavino, S., Tombolato, I.K.F., Campanelli, M., Della Ceca, L., Hervo, M., Di Liberto, L., Ferrero, L., Gobbi, G.P.: Transport of Po Valley aerosol pollution to the northwestern Alps. Part 1: phenomenology, Atmos. Chem. Phys., 19, 3065–3095, https://doi.org/10.5194/acp-19-3065-2019, 2019a.

Diémoz, H., Gobbi, G.P., Magri, T., Pession, G., Pittavino, S., Tombolato, I.K.F., Campanelli, M., Barnaba, F.: Transport of Po Valley aerosol pollution to the northwestern Alps. Part 2: Long-term impact on ari quality, Atmos. Chem. Phys., 19, 10129–10160, 2019 https://doi.org/10.5194/acp-19-10129-2019 2019b.

Dionisi, D., Barnaba, F., Diémoz, H., Di Liberto, L. and Gobbi, G. P.: A multiwavelength numerical model in support of quantitative retrievals of aerosol properties from automated lidar ceilometers and test applications for AOT and PM10 estimation, Atmospheric Measurement Techniques, 11(11), 6013–6042, doi:10.5194/amt-11-6013-2018, 2018.

~~IPCC, 2013: Climate Change 2013: The Physical Science Basis. Cambridge University Press, Cambridge, United Kingdom and New York, USA, 2013.~~

Duchon, C.E., O'Malley, M.: Estimating Cloud Type from Pyranometer Observations. J. App. Meteorology, 38, 132–141, 1999.

Eleftheriadis, K., Vratolis, S. and Nyeki, S.: Aerosol black carbon in the European Arctic: Measurements at Zeppelin station, Ny-Ålesund, Svalbard from 1998-2007, Geophysical Research Letters, 36(2), doi:10.1029/2008GL035741, 2009.

Ehnberg, J. S. G. and Bollen, M. H. J.: Simulation of global solar radiation based on cloud observations, Solar Energy, 78(2), 157–162, doi:10.1016/j.solener.2004.08.016, 2005.

Feister, U., Cabrol, N., and Häder, D.: UV Irradiance Enhancements by Scattering of Solar Radiation from Clouds, Atmosphere, 6, 1211-1228, 10.3390/atmos6081211, 2015.

Ferrero, L., Riccio, A., Perrone, M. G., Sangiorgi, G., Ferrini, B. S., and Bolzacchini, E.: Mixing height determination by teth- ered balloon-based particle soundings and modeling simulations, Atmos. Res, 102, 145–156, doi:10.1016/j.atmosres.2011.06.016, 2011a.

Ferrero, L., Mocnik, G., Ferrini, B. S., Perrone, M. G., Sangiorgi, G. and Bolzacchini, E.: Vertical profiles of aerosol absorption coefficient from micro-Aethalometer data and Mie calculation over Milan., Sci. Total Environ., 409(14), 2824–37, doi:10.1016/j.scitotenv.2011.04.022, 2011b.

Ferrero, L., Cappelletti, D., Moroni, B., Sangiorgi, G., Perrone, M. G., Crocchianti, S. and Bolzacchini, E.: Wintertime aerosol dynamics and chemical composition across the mixing layer over basin valleys, Atmos. Environ., 56, 143–153, doi:10.1016/j.atmosenv.2012.03.071, 2012.

Ferrero, L., Castelli, M., Ferrini, B.S., Moscatelli, M., Perrone, M.G., Sangiorgi, G., Rovelli, G., D'Angelo, L., Moroni, B., Scardazza, F., Mocnik, G., Bolzacchini, E., Petitta, M., Cappelletti, D.: Impact of Black Carbon Aerosol over Italian basin valleys: high resolution measurements along vertical profiles, radiative forcing and heating rate. Atmos. Chem. Phys., 14, 9641–9664, 2014.

Ferrero, L., Cappelletti, D., Busetto, M., Mazzola, M., Lupi, A., Lanconelli, C., Becagli, S., Traversi, R., Caiazzo, L., Giardi, F., Moroni, B., Crocchianti, S., Fierz, M., Mocnik, G., Sangiorgi, G., Perrone, M.G., Maturilli, M., Vitale, V., Udisti, R., Bolzacchini, E.: Vertical profiles of aerosol and black carbon in the Arctic: a seasonal phenomenology along 2 years (2011–2012) of field campaigns, Atmos. Chem. Phys., 16(19), 12601–12629, https://doi.org/10.5194/acp-16-12601-2016, 2016.

Ferrero L., Močnik G., Cogliati S., Gregorič A., Colombo R., Bolzacchini E.: Heating Rate of Light Absorbing Aerosols: Time-Resolved Measurements, the Role of Clouds, and Source Identification. Environ. Sci. Tech., 52, 3546−3555, DOI: 10.1021/acs.est.7b04320, 2018.

Ferrero, L., Sangiorgi, G., Perrone, M.G., Rizzi, C., Cataldi, M., Markuszewski, P., Pakszys, P., Makuch, P., Petelski, T., Becagli, S., Traversi, R., Bolzacchini, E., Zielinski, T.: Chemical Composition of Aerosol over the Arctic Ocean from Summer ARctic EXpedition (AREX) 2011 – 2012 Cruises: Ions, Amines, Elemental Carbon, Organic Matter, Polycyclic Aromatic Hydrocarbons, n-Alkanes, Metals, and Rare Earth Elements. Atmosphere 10, 54, 1-32, doi:10.3390/atmos10020054, 2019°.

Ferrero, L., Ritter, C., Cappelletti, D., Moroni, B., Močnik, G., Mazzola, M., Lupi, A., Becagli, S., Traversi, R., Cataldi, M., Neuber, R., Vitale, V., Bolzacchini, E: Aerosol optical properties in the Arctic: the role of aerosol chemistry and dust composition in a closure experiment between Lidar and tethered balloon vertical profiles. Sci. Tot. Environ., 686, 452–467, doi.org/10.1016/j.scitotenv.2019.05.399, 2019b.

Feudale, L. and Manzato, A.: Cloud-to-ground lightning distribution and its relationship with orography and anthropogenic emissions in the Po Valley, Journal of Applied Meteorology and Climatology, 53(12), 2651–2670, doi:10.1175/JAMC-D-14-0037.1, 2014.

~~Duchon, C. E. and O'Malley, M. S.: Estimating cloud type from pyranometer observations, Journal of Applied Meteorology, 38(1), 132–141, doi:10.1175/1520-0450, 1999.~~

Galli, C., Nardino, M., Levizzani, V., Rizzi, R. and Georgiadis, T.: Radiative energy partition and cloud radiative forcing at a Po valley site, Atmospheric Research, 72(1–4), 329–351, doi:10.1016/j.atmosres.2004.03.022, 2004.

Gao, R. S., Hall, S. R., Swartz, W. H., Schwarz, J. P., Spackman, J. R., Watts, L. A., Fahey, D. W., Aikin, K. C., Shetter, R. E. and Bui, T. P.: Calculations of solar shortwave heating rates due to black carbon and ozone absorption using in situ measurements, Journal of Geophysical Research Atmospheres, 113(14), 14–19, doi:10.1029/2007JD009358, 2008.

García V., Mollineda R.A., Sánchez J.S.: Index of Balanced Accuracy: A Performance Measure for Skewed Class Distributions. In: Araujo H., Mendonça A.M., Pinho A.J., Torres M.I. (eds) Pattern Recognition and Image Analysis. IbPRIA 2009. Lecture Notes in Computer Science, vol 5524. Springer, Berlin, Heidelberg. https://doi.org/10.1007/978-3-642-02172-5_57, 2009.

Harrison, R. G., Chalmers, N. and Hogan, R. J.: Retrospective cloud determinations from surface solar radiation measurements, Atmospheric Research, 90(1), 54–62, doi:10.1016/j.atmosres.2008.04.001, 2008.

IPCC, 2013: Climate Change 2013: The Physical Science Basis. Cambridge University Press, Cambridge, United Kingdom and New York, USA, 2013.

Jacobson, M. Z. Control of fossil-fuel particulate black carbon and organic matter, possibly the most effective method of slowing global warming. J. Geophys. Res., 107 (D19), 4410, 2002.

Jacobson, M.Z.: Short-term effects of controlling fossil-fuel soot, biofuel soot and gases, and methane on climate, arctic ice, and air pollution health, J. Geophys. Res., 115, D14209, doi:10.1029/2009JD013795, 2010.

Junker, C., Jennings, S. G., and Cachier, H. Aerosol light absorption in the North Atlantic: trends and seasonal characteristics during the period 1989 to 2003. Atmos. Chem. Phys., 6, 1913– 1925, 2006.

Kaufman, Y.J., Tanré, D., Boucher, O.: A satellite view of aerosols in the climate system. Nature 419, 215–223, 2002.

Koch, D., Schulz, M., Kinne, S., McNaughton, C., Spackman, J. R., Balkanski, Y., Bauer, S., Berntsen, T., Bond, T. C., Boucher, O., Chin, M., Clarke, A., De Luca, N., Dentener, F., Diehl, T., Dubovik, O., Easter, R., Fahey, D. W., Feichter, J., Fillmore, D., Freitag, S., Ghan, S., Ginoux, P., Gong, S., Horowitz, L., Iversen, T., Kirkevåg, A., Klimont, Z., Kondo, Y., Krol, M., Liu, X., Miller, R., Montanaro, V., Moteki, N., Myhre, G., Penner, J. E., Perlwitz, J., Pitari, G., Reddy, S., Sahu, L., Sakamoto, H., Schuster, G., Schwarz, J. P., Seland, Ø., Stier, P., Takegawa, N., Takemura, T., Textor, C., van Aardenne, J. A., Zhao, Y.: Evaluation of black carbon estimations in global aerosol models. Atmos. Chem. Phys., 9, 9001–9026, 2009, doi:10.5194/acp-9-9001-2009.

Koch, D., Del Genio, A.D.: Black carbon semi-direct effects on cloud cover: review and synthesis. Atmos. Chem. Phys. 10, 7685–7696, 2010, doi:10.5194/acp-10-7685-2010.

Koren, I., Kaufman, Y.J., Remer, L.A., Martins, J.V.: Measurments of the effect of amazon smoke on inhibition of cloud formation. Science, 303, 1342-1345, 2004.

Koren, I., Martins, J.V., Remer, L.A., Afargan, H.: Smoke invigoration versus inhibition of clouds over the amazon, Science, 321, 946-949, 2008.

Kumar, N. K., Corbin, J. C., Bruns, E. A., Massabó, D., Slowik, J. G., Drinovec, L., Močnik, G., Prati, P., Vlachou, A., Baltensperger, U., Gysel, M., El-Haddad, I., and Prévôt, A. S. H.: Production of particulate brown carbon during atmospheric aging of residential wood-burning emissions, Atmos. Chem. Phys., 18, 17843–17861, https://doi.org/10.5194/acp-18-17843-2018, 2018.

Liou K.N.: An Introduction to Atmospheric Radiation, Second Edition. INTERNATIONAL GEOPHYSICS SERIES, Volume 84, Academic Press, 2007.

Lolli, S., Madonna, F., Rosoldi, M., Campbell, J.R., Welton, E.J., Lewis, J.R., Gu, Y., Pappalardo G.: Impact of varying lidar measurement and data processing techniques in evaluating cirrus cloud and aerosol direct radiative effects. Atmos. Meas. Tech., 11, 1639–1651, 2018, https://doi.org/10.5194/amt-11-1639-2018.

López, M. L., Palancar, G. G., and Toselli, B. M.: Effect of different types of clouds on surface UV-B and total solar irradiance at southern mid-latitudes: CMF determinations at Córdoba, Argentina, Atmos. Environ., 43, 3130-3136, http://dx.doi.org/10.1016/j.atmosenv.2009.02.065, 2009.

Madonna, F., Amato, F., Vande Hey, J., and Pappalardo, G.: Ceilometer aerosol profiling versus Raman lidar in the frame of the INTERACT campaign of ACTRIS, Atmos. Meas. Tech., 8, 2207–2223, https://doi.org/10.5194/amt-8-2207-2015, 2015.

Martucci, G., Milroy, C., & O'Dowd, C. D.: Detection of cloud-base height using Jenoptik CHM15K and Vaisala CL31 ceilometers. Journal of Atmospheric and Oceanic Technology, 27, 305–318. https://doi.org/10.1175/2009JTECHA1326.1, 2010.

Mims, F. E., and Frederick, J. E.: Cumulus clouds and UV-B, Nature, 371, 291, 1994.

Myhre, G., Samset, B. H., Schulz, M., Balkanski, Y., Bauer, S., Berntsen, T. K., Bian, H., Bellouin, N., Chin, M., Diehl, T., Easter, R. C., Feichter, J., Ghan, S. J., Hauglustaine, D., Iversen, T., Kinne, S., Kirkevåg, A., Lamarque, J. F., Lin, G., Liu, X., Lund, M. T., Luo, G., Ma, X., Van Noije, T., Penner, J. E., Rasch, P. J., Ruiz, A., Seland, Skeie, R. B., Stier, P., Takemura, T., Tsigaridis, K., Wang, P., Wang, Z., Xu, L., Yu, H., Yu, F., Yoon, J. H., Zhang, K., Zhang, H. and Zhou, C.: Radiative forcing of the direct aerosol effect from AeroCom Phase II simulations, Atmospheric Chemistry and Physics, 13(4), 1853–1877, doi:10.5194/acp-13-1853-2013, 2013.

Massabò, D., Caponi, L., Bernardoni, V., Bove, M.C., Brotto, P., Calzolai,, G., Cassola, F., Chiari, M., Fedi, M.E., Fermo, P., Giannoni, M., Lucarelli, F., Nava, S., Piazzalunga, A., Valli, G., Vecchi, R., Prati, P.: Multi-wavelength optical determination of black and brown carbon in atmospheric aerosols, Atmos. Environ., 108, 1-12, 2015.

Maugeri, M., Bagnati, Z., Brunetti, M. and Nanni, T.: Trends in Italian total cloud amount, 1951-1996, Geophysical Research Letters, 28(24), 4551–4554, doi:10.1029/2001GL013754, 2001.

Moosmüller, H., Chakrabarty, R. K., Ehlers, K. M. and Arnott, W. P.: Absorption Ångström coefficient, brown carbon, and aerosols: Basic concepts, bulk matter, and spherical particles, Atmospheric Chemistry and Physics, 11(3), 1217–1225, doi:10.5194/acp-11-1217-2011, 2011.

Moroni, B., Cappelletti, D., Marmottini, F., Scardazza, F., Ferrero, L., and Bolzacchini, E.: Integrated single particle-bulk chemical approach for the characterization of local and long range sources of particulate pollutants, Atmos. Environ., 50, 267–277, doi:10.1016/j.atmosenv.2011.12.022, 2012.

Moroni, B., Ferrero, L., Crocchianti, S., Perrone, M. G., Sangiorgi, G., Bolzacchini, E., and Cappelletti, D.: Aerosol dynamics upon Terni basin (Central Italy): results of integrated vertical profile measurements and electron microscopy analyses, Rend. Lincei, 24, 319–328, doi:10.1007/s12210-013-0230-8, 2013.

~~Mims, F. E., and Frederick, J. E.: Cumulus clouds and UV-B, Nature, 371, 291, 1994.~~

Myhre, G., Samset, B. H., Schulz, M., Balkanski, Y., Bauer, S., Berntsen, T. K., Bian, H., Bellouin, N., Chin, M., Diehl, T., Easter, R. C., Feichter, J., Ghan, S. J., Hauglustaine, D., Iversen, T., Kinne, S., Kirkevåg, A., Lamarque, J. F., Lin, G., Liu, X., Lund, M. T., Luo, G., Ma, X., Van Noije, T., Penner, J. E., Rasch, P. J., Ruiz, A., Seland, Skeie, R. B., Stier, P., Takemura, T., Tsigaridis, K., Wang, P., Wang, Z., Xu, L., Yu, H., Yu, F., Yoon, J. H., Zhang, K., Zhang, H. and Zhou, C.: Radiative forcing of the direct aerosol effect from AeroCom Phase II simulations. Atmos. Chem. Phys., 13(4), 1853–1877, doi:10.5194/acp-13-1853-2013, 2013.

Nielsen, L., Prahm, L., Berkowicz, R., Conradsen, K.: Net incoming radiation estimated from hourly global radiation and/or cloud observations. J. Climatol., 1 ,255– 272, 1981.

Nordmann, S., Cheng, Y. F., Carmichael, G. R., M. Yu, M., Denier van der Gon, H. A. C., Zhang, Q., Saide, P. E., Pöschl, U., Su, H., Birmili, W., Wiedensohler, A. Atmospheric black carbon and warming effects influenced by the source and absorption enhancement in central Europe. *Atmos. Chem. Phys.* **2014**, *14*, 12683–12699, doi:10.5194/acp-14-12683-2014.

Orsini, A., Tomas, C., Calzolari, F., Nardino, M., Cacciari, A., Georgi- adis, T., 2002. Cloud cover classification through simultaneous ground-based measurements of solar and infrared radiation. Atmo- spheric Research 61, 251–275.

Perlwitz, J. and Miller, R. L.: Cloud cover increase with increasing aerosol absorptivity: A counterexample to the conventional semidirect aerosol effect, Journal of Geophysical Research Atmospheres, 115(8), 1–23, doi:10.1029/2009JD012637, 2010.

Petzold, A., Schloesser, H., Sheridan, P.J., Arnott, W.P., Ogren, J.A., Virkkula, A.: Evaluation of Multiangle Absorption Photometry for Measuring Aerosol Light Absorption. Aerosol Science and Technology, 39, 40–51, 2005.

Ramana, M. V, Ramanathan, V., Kim, D., Roberts, G. C. and Corrigan, C. E.: Albedo , atmospheric solar absorption and heating rate measurements with stacked UAVs, , 1931, 1913–1931, doi:10.1002/qj, 2007.

Ramanathan, V., Carmichael, G.: Global and regional climate changes due to black carbon. Nat. Geosci., 1, 221–227, 2008.

Ramanathan, V. and Feng, Y.: Air pollution, greenhouse gases and climate change: Global and regional perspectives, Atmos. Environ., 43(1), 37–50, doi:10.1016/j.atmosenv.2008.09.063, 2009.

Rodríguez, S., Van Dingenen, R., Putaud, J.-P., Dell'Acqua, A., Pey, J., Querol, X., Alastuey, A., Chenery, S., Ho, K.-F., Harrison, R., Tardivo, R., Scarnato, B., and Gemelli, V.: A study on the relationship between mass concentrations, chemistry and number size distribution of urban fine aerosols in Milan, Barcelona and London, Atmos. Chem. Phys., 7, 2217–2232, doi:10.5194/acp-7- 2217-2007, 2007.

Sandradewi J., Prevot A.S.H., Szidat S., Perron N., Alfarra M.R., Lanz V.A., Weingartner E., and Baltensperger U.: Using Aerosol Light Absorption Measurements for the Quantitative Determination of Wood Burning and Traffic Emission Contributions to Particulate Matter. Environ. Sci. Technol., 42, 3316–3323, 2008a.

Sandradewi, J., Prevot, A.S.H., Weingartner, E., Schmidhauser, R., Gysel, M., Baltensperger, U. A study of wood burning and traffic aerosols in an Alpine valley using a multi-wavelength Aethalometer. Atmos. Environ, 42, 101–112, 2008b.

Schwarz, J. P., Spackman, J. R., Gao, R. S., Watts, L. A., Stier, P., Schulz, M., Davis, S. M., Wofsy, S. C., and Fahey, D. W.: Global-scale black carbon profiles observed in the remote atmosphere and compared to models, Geophys. Res. Lett., 37, L18812, doi:10.1029/2010GL044372, 2010.

Shamjad, P. M., Tripathi, S. N., Pathak, R., Hallquist, M., Arola, A., Bergin, M. H.: Contribution of Brown Carbon to Direct Radiative Forcing over the Indo-Gangetic Plain. Environ. Sci. Technol., 49 (17), 10474–10481, 2015.

Stjern, C.W., Kristjansson J.E., Hansen A.W.: Global dimming and global brightening – an analysis of surface radiation and cloud cover data in northern Europe. Int. J. Climatol., 29, 643–653, 2009.

Sun, H., Biedermann, L. and Bond, T. C.: Color of brown carbon: A model for ultraviolet and visible light absorption by organic carbon aerosol, Geophysical Research Letters, 34(17), 1–5, doi:10.1029/2007GL029797, 2007.

Tapakis, R. and Charalambides, A. G.: Equipment and methodologies for cloud detection and classification: A review, Solar Energy, 95, 392–430, doi:10.1016/j.solener.2012.11.015, 2013.

Thiel, S., Ammannato, L., Bais, A., Bandy, B., Blumthaler, M., Bohn, B., Engelsen, O., Gobbi, G. P., Gröbner, J., Jäkel, E., Junkermann, W., Kazadzis, S., Kift, R., Kjeldstad, B., Kouremeti, N., Kylling, A., Mayer, B., Monks, P. S., Reeves, C. E., Schallhart, B., Scheirer, R., Schmidt, S., Schmitt, R., Schreder, J., Silbernagl, R., Topaloglou, C., Thorseth, T. M., Webb, A. R., Wendisch, M., and Werle, P.: Influence of clouds on the spectral actinic flux density in the lower troposphere (INSPECTRO): overview of the field campaigns, Atmos. Chem. Phys., 8, 1789–1812, https://doi.org/10.5194/acp-8-1789-2008, 2008.

Tian, P., Liu, D., Zhao, D., Yu, C., Liu, Q., Huang, M., Deng, Z., Ran, L., Wu, Y., Ding, S., Hu, K., Zhao, G., Zhao, C. and Ding, D.: In-situ vertical characteristics of optical properties and heating rates of aerosol over Beijing, Atmospheric Chemistry and Physics Discussions, 1–33, doi:10.5194/acp-2019-780, 2019.

Tosca, M.G., Campbell, J., Garay, M., Lolli, S., Seidel, F.C., Marquis, J., Kalashnikova, O.: Attributing accelerated summertime warming in the southeast united states to recent reductions in aerosol burden: Indications from vertically-resolved observations. Remote Sens., 9, 674, https://doi.org/10.3390/rs9070674, 2017.

Virkkula, A.: Correction of the Calibration of the 3-wavelength Particle Soot Absorption Photometer (3PSAP). Aerosol Science and Technology, 44, 706–712, 2010.

Wang, Z., Huang, X., and Ding, A.: Dome effect of black carbon and its key influencing factors: a one-dimensional modelling study, Atmos. Chem. Phys., 18, 2821-2834, 10.5194/acp-18-2821-2018, 2018.

Weingartner, E., Saathoff, H., Schnaiter, M., Streit, N., Bitnar, B., Baltensperger, U.: Absorption of light by soot particles: determination of the absorption coefficient by means of aethalometers. Journal of Aerosol Science, 34 (10), 1445–1463, 2003.

Wiegner, M. and Geiß, A.: Aerosol profiling with the Jenoptik ceilometer CHM15kx, Atmos. Meas. Tech., 5, 1953–1964, doi:10.5194/amt-5-1953-2012, 2012.

Wofsy, S. C., the HIPPO Science Team and Cooperating Modellers and Satellite Teams: HIAPER Pole-to-Pole Observations (HIPPO): fine grained, global-scale measurements of climatically important atmospheric gases and aerosols, Philos. T. R. Soc., 369, 2073–2086, 2011.

WMO/GAW Aerosol Measurement Procedures, Guidelines and Recommendations 2nd Edition, GAW Report 227, World Meteorological Organization, Geneva, 2016.

Yang, M., Howell, S.G., Zhuang, J., Huebert, B.J.: Attribution of aerosol light absorption to black carbon, brown carbon, and dust in China and interpretations of atmospheric measurements during EAST-AIRE. Atmos. Chem. Phys., 9, 2035-2050, 2009.

Ylivinkka, I., Kaupinmäki, S., Virman, M., Peltola, M., Taipale, D., Petäjä, T., Kerminen, V. M., Kulmala, M. and Ezhova, E.: Clouds over Hyytiälä, Finland: An algorithm to classify clouds based on solar radiation and cloud base height measurements, Atmospheric Measurement Techniques, 13(10), 5595–5619, doi:10.5194/amt-13-5595-2020, 2020.

Zotter, P., Herich, H., Gysel, M., El-Haddad, I., Zhang, Y., Mocnik,G., Hüglin,C., Baltensperger,U., Szidat,S., Prevôt,A.S.H.: Evaluation of the absorption Ångström exponents for traffic and wood burning in the Aethalometer-based source apportionment using radiocarbon measurements of ambient aerosol. Atmos. Chem. Phys., 17, 4229−4249, 2017.

Level	Cloud type	SD	*R*	cloud layer
Low (<2 km)	Stratus (St)	<120	0.0-0.4	1
	Cumulus (Cu)	/	0.8-1.1	1
	Stratocumulus (Sc~~t~~~~Cu~~)	/	0.4-0.8	1
Middle (2-7 km)	Altostratus (As~~lSt~~)	<120	0.0-0.4	1
	Altocumulus (Ac~~lCu~~)	>120	0.4-0.8	1
High (>7 km)	Cirrus (Ci)	/	0.8-1.1	1
	Cirrocumulus-Cirrostratus (Cc-Cs~~iCu-CiSt~~)	/	0.0-0.8	1
	Clear Sky (CS)	/	/	0

Table 1. Final criteria adopted for cloud classification. SD represents the standard deviation of the measured global irradiance with respect to the theoretical behaviour in clear sky conditions; R represents the ratio between observed global irradiance (F_{glo}) and the modelled irradiance (F_{glo_CS}) in clear sky conditions; cloud layer: is the number of cloud layers detected by the lidar.

Month	Metric	T	P	eBC*	b_{abs}*	ADRE	$ADRE_{dir}$	$ADRE_{dif}$	$ADRE_{ref}$	HR	HR_{dir}	HR_{dif}	HR_{ref}	F_{glo}	F_{dir}	F_{dif}	F_{ref}
		°C	hPa	ng m^{-3}	Mm^{-1}	mW m^{-3}	mW m^{-3}	mW m^{-3}	mW m^{-3}	K day^{-1}	K day^{-1}	K day^{-1}	K day^{-1}	W m^{-2}	W m^{-2}	W m^{-2}	W m^{-2}
Nov-15	**mean**	12.8	1003.8	4288	21.2	18.42	10.17	5.62	2.64	1.30	0.72	0.40	0.19	200	131	69	51
	CI 95%	0.2	0.3	96	0.5	0.61	0.44	0.18	0.08	0.04	0.03	0.01	0.01	5	1	5	1
Dec-15	**mean**	8.4	1012.8	6289	31.1	20.70	9.29	8.64	2.77	1.43	0.64	0.59	0.19	141	66	75	34
	CI 95%	0.1	0.1	97	0.5	0.68	0.48	0.24	0.08	0.05	0.03	0.02	0.01	4	2	3	1
Jan-16	**mean**	7.2	997.4	4198	20.8	12.57	5.53	5.26	1.79	0.87	0.38	0.36	0.12	150	85	65	36
	CI 95%	0.2	0.4	106	0.5	0.55	0.36	0.23	0.07	0.04	0.02	0.02	0.01	5	2	5	1
Feb-16	**mean**	9.2	995.5	2851	14.1	8.62	3.50	3.81	1.31	0.61	0.25	0.27	0.09	191	104	87	46
	CI 95%	0.1	0.3	74	0.4	0.35	0.23	0.14	0.05	0.02	0.02	0.01	0.00	6	3	6	2
Mar-16	**mean**	12.6	996.2	1535	7.6	7.58	2.96	3.28	1.34	0.54	0.21	0.23	0.10	310	174	136	77
	CI 95%	0.1	0.2	36	0.2	0.22	0.14	0.08	0.04	0.02	0.01	0.01	0.00	7	3	7	2

Table 2. Monthly averaged data and confidence interval at 95% of temperature (T), pressure (P), equivalent black carbon (eBC), absorption coefficient (b_{abs}), absorptive direct radiative effect (ADRE) together with the heating rate (HR) divided into their direct (dir), diffuse (dif) and reflected (ref) components and, finally, global (F_{glo}), direct (F_{dir}), diffuse (F_{dif}) and reflected (F_{ref}) irradiances. * denotes Aethalometer data referred to λ=880 nm.